SYNTHESIS, CHARACTERIZATION AND CATALYTIC ACTIVITY OF METAL CONTAINING MCM-41 AND HMS

THESIS

SUBMITTED TO THE

UNIVERSITY OF PUNE

FOR THE DEGREE OF

DOCTOR OF PHOLOSOPHY

IN CHEMISTRY

BY

SHRIKANT S. BHOWARE
(Research Student)

Dr. A. P. SINGH
(Research Guide)

CATALYSIS DIVISION

NATIONAL CHEMICAL LABORATORY

PUNE - 411008

INDIA

SEPTEMBER 2007

CERTIFICATE

Certified that the work incorporated in the thesis "**Synthesis, characterization and catalytic activity of metal containing MCM-41 and HMS**" submitted by Mr. Shrikant S. Bhoware, for the Degree of Doctor of Philosophy was carried out by the candidate under my supervision at Catalysis Division, National Chemical Laboratory, Pune-411 008, India. Such material as has been obtained from other sources has been duly acknowledged in the thesis.

Dr. A. P. Singh

(Research Supervisor)

DECLARATION BY RESEARCH SCHOLAR

I hereby declare that the thesis entitled "**Synthesis, characterization and catalytic activity of metal containing MCM-41 and HMS**" submitted for the Degree of Doctor of Philosophy to the University of Pune, has been carried out by me at Catalysis Division, National Chemical Laboratory, Pune 411 008, India, under the supervision of Dr. A. P. Singh. The work is original and has not been submitted in part or full by me for any other degree or diploma to this or any other University.

Shrikant S. Bhoware

ACKNOWLEDGEMENTS

I find it difficult to write something in short to acknowledge my research supervisor, Dr. A. P. Singh. His constant inspiration, invaluable guidance and constructive criticism helped me a lot to focus my views in the proper perspective. I take this opportunity to express my intense reverence towards him for the extensive scientific discussions and for giving me the freedom in research. My deepest personal regards are due for him forever for his timely helps and for being a strong support, both scientific and personal, on all stages of my research period.

I am indebted to Dr. Rajeev Kumar, Head, Catalysis Division and Dr. S. Sivasankar, former Head of Catalysis Division, for allowing me to use all the available facilities in the division, for the stimulating discussions, valuable suggestions and for the constant encouragement and support. My heartfull thanks are due to Dr. S. B. Halligudi, Dr. K. R. Kamble, Dr. P. N. Joshi, Dr. S. Deshpande, Dr. Belhekar, Dr. Nalini Jacob, Mr. R. K. Jha, Ms. Violet Samuel and all other scientific and non-scientific staff of the division and NCL for their valuable help and cooperation during my tenure as a research student.

With much appreciation, I would like to mention the crucial role of my labmates Vandana, Venkatesh, Shylesh, Chidambaram, Surendran, Selvakumar, Prinson, Balasaheb, Shital, Rajeesh, for their helping hands, splendid companionship and for making the lab feel like a family. Special thanks to Ankur, Mahesh, Pranjal, Atul, Amit, Sahoo, Sachine, Daboo, Rohit, Shanbag, Biju, Rajendra, Vasudev and all other research scholars of catalysis division for such a friendly and cheerful working atmosphere, for their constant support, love and care throughout my stay in NCL. I sincerely thank all of them for their incessant moral support, kind cooperation, love, respect, appreciation and for the scientific discussions.

I take this opportunity to express my earnest respect to my schoolteachers, graduation tutors for their way of teaching that build up my research career in science.

I am forever indebted to my parents and brother for their love, understanding and encouragement throughout my life.

Finally, my thanks are due to Council of Scientific and Industrial Research, Government of India, for awarding the junior and senior research fellowships and Dr. S. Sivaram and Dr. B. D. Kulkarni, Deputy Director, National Chemical Laboratory to carry out my research works, extending all infrastructural facilities and to submit this work in the form of a thesis for the award of Ph. D degree.

S. S. Bhoware

Dedicated

To my

Grandparents, Parents &

Teachers

CONTENTS

List of Figures

List of Tables

List of Schemes

mechanism.

List of Abbreviations

APTS	3-aminopropyl triethoxysilane
BE	Binding Energy
BET	Braunauer-Emmett-Teller
BJH	Barrett-Joyner-Halenda
CMC	Critical Micelle Concentration
CTMABr	Cetyl trimethyl ammonium bromide
DR UV-Vis	Diffuse Reflectance Ultraviolet-Visible
FTIR	Fourier Transform Infrared
GC	Gas Chromatography
HMS	Hexagonal Mesoporous Silica
TEM	Transmission Electron Microscopy
LCT	Liquid Crystal Template
MCM	Mobil Composition of Matter
SBA	Santa Barbara Amorphous
SEM	Scanning Electron Microscopy
SLC	Silicatropic Liquid Crystal
TBHP	*tert*-Butyl Hydroperoxide
TEM	Transmission Electron Microscopy
TEOS	Tetraethyl Orthosilicate
XPS	X-Ray Photoelectron Spectroscopy
XRD	X-Ray Diffraction

1.1. GENERAL BACKGROUND

Jons Jakob Berzelius coined the term 'catalysis' (which means loosening down in Greek) in 1835 to refer certain chemicals that speed up reaction [1]. However, long before chemists recognized the existence of catalysts. Ordinary people had been using the catalytic process for number of purposes like making soap, fermenting wine to create venegar, leavening bread etc. [2]. The art of producing alcohol from sugar, by fermentation, has ancient roots and the origins of this process are too remote to trace [3]. In the early nineteenth century, scientists began to take note of this phenomenon. In 1812, Russian chemist Gottlieb Kirchhof was studying the conversion of starch to sugar in the presence of strong acids [3,4]. During the same time, English chemist Sir Humphry Davy noticed that in certain organic reactions, platinum acted to speed the reaction without undergoing any change [5,6]. Later, Michael Faraday demonstrated the ability of platinum to recombine hydrogen and oxygen that had been separated by the electrolysis of water.

Catalyst is defined as "**substance that increases the rate of chemical attainment of chemical equilibrium without itself undergoing chemical change**". But, it follows from this definition that if the rate of forward reaction is speeded up in presence of particular catalyst, the reverse reaction will likewise be facilitated to the same degree. Catalysts generally react with one or more reactants to form a chemical intermediate that subsequently reacts to form the final reaction product while regenerating the catalyst.

Catalysts can either be heterogeneous or homogeneous. Heterogeneous catalysts are present in different phases from the reactants (e. g. solid catalyst in liquid

reaction mixture), whereas homogeneous catalysts are in the same phase (e. g. dissolved catalyst in liquid reaction mixture). Heterogeneous catalysts provide surface on which the reactants (or substrates) temporarily become adsorbed. Bonds in the substrate become weakened sufficiently for new bonds to be created. The bonds between the products and the catalyst are weaker, so the products formation takes place. Active sites on the metal allow partial weak bonding to the reactant gases, which are adsorbed onto the metal surface. As a result, the bond within the molecule of a reactant is weakened and the reactant molecules are held in close proximity to each other. In this way the particularly strong triple bond in nitrogen is weakened and the hydrogen and nitrogen molecules are brought closer together in the gas phase, so the rate of reaction increases.

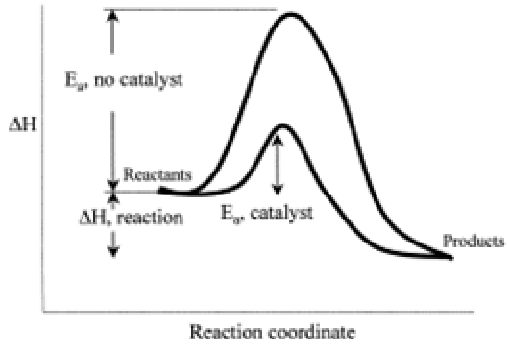

Fig. 1.1. Energy profile diagram of chemical reaction with catalyst and without catalyst [2].

Fig. 1 shows the energy profile diagram of the hypothetical chemical reaction when carried out with catalyst and without catalyst. The catalysed reaction pathway, despite having lower activation energy, produces the same final result. Uncatalysed reaction pathway needs more energy of activation than catalysed pathway. Catalysts

work by providing (alternative) mechanism involving a different transition state and lower activation energy. The effect of this is that more molecular collisions have the energy needed to reach the transition state. Hence, catalysts can perform reactions that, although thermodynamically feasible, would not run without the presence of a catalyst, or perform them much faster, more specific, or at lower temperatures. This means that catalysts reduce the amount of energy needed to start a chemical reaction. Catalysts cannot have effect on chemical equilibrium of a reaction because the rate of both the forward and the reverse reaction are equally affected [8]. The net free energy change of a reaction is the same whether a catalyst is used or not; the catalyst just makes it easier to activate. Energy is an important component in the chemical reaction because a certain threshold, called the activation energy (E_a), must be crossed before the reaction occurs. A temperature increase raises the energy of the collisions, increasing the chance that the activation-energy threshold will be crossed, resulting in the breaking of molecular bonds.

More than 90 % of the chemical manufacturing processes in use throughout the world utilize catalysts. Catalysis is of paramount importance in the chemical industry. The production of most industrially important chemicals involves catalysis. The earliest commercial processes are the Haber process for ammonia synthesis and the Fischer-Tropsch synthesis. Research into catalysis is a major field in applied science, and involves many fields of chemistry, notably in organometallic chemistry, and physics. Catalysis is important in many aspects of environmental science, from the catalytic converter in automobiles to the causes of the ozone hole. Catalytic, rather

than stoichiometric reactions are preferred in environmentally friendly green chemistry due to the reduced amount of waste generated.

Porous materials have been extensively studied with regard to technical applications as catalysts and catalyst supports. According to the IUPAC definition, porous materials are divided into three classes: microporous (pore size < 2 nm), mesoporous (2-50 nm), and macroporous (>50 nm) materials [9]. In addition, also the term 'nanoporous' is increasingly being used. Many kinds of porous materials such as (pillared) clays, anodic alumina, carbon nanotubes and related porous carbons and so on, have been extensively described in the literature [10].

McBain introduced the term 'molecular sieve' in 1932 to define porous solid materials (mainly activated carbons and zeolites) that act as sieves at a molecular level. Zeolites are crystalline molecular sieves of microporous hydrated aluminosilicates. They are highly useful catalysts in oil refining and petrochemicals. More recently attention has been focused on their use in the manufacture of fine chemicals. The synthetic utility of zeolites and related molecular sieves has been considerably extended by the incorporation of redox metals into their frameworks. The resulting redox molecular sieves catalyze a variety of selective oxidations under mild conditions in the liquid phase. Among the family of microporous materials, the best-known members are zeolites, which have a narrow and uniform micropore size distribution due to their crystallographically defined pore system. In recent years, environmental and economic considerations have raised strong interest to redesign commercially important processes so that the use of harmful substances and the generation of toxic waste could be avoided. In this respect, heterogeneous catalysis

plays key role in the development of environmentally benign processes in petroleum chemistry and in the production of chemicals, for instance by substitution of liquid acid catalysts by solid materials. Especially, zeolites have attracted strong attention as such acids, base and redox catalysts. However, zeolites present severe limitations when large reactant molecules are involved, especially in liquid-phase systems, as found in the synthesis of fine chemicals, due to the fact that mass transfer limitations are very severe for microporous solids. Attempts to improve the diffusion of reactants to the catalytic sites have so far focused on increasing the zeolite pore sizes [11], on decreasing zeolite crystal size [12], or on providing an additional mesopore system within the microporous crystals [13]. An important line of research has focused on the enlargement of the pore sizes into the mesopore range, allowing larger molecules to enter the pore system, to be processed there and to leave the pore system again.

The first synthesis of an ordered mesoporous material was described in the patent literature in 1969. However, due to a lack of analysis, the remarkable features of this product were not recognized [14]. In 1992, a similar material was synthesized by scientist at Mobil Oil Corporation who discovered the remarkable features of this novel type of silica and opened up research in this field [15]. MCM-41 (Mobil Composition of Matter No. 41) shows a highly ordered hexagonal array of unidimensional pores with a very narrow pore size distribution [16]. The walls, however, very much resemble amorphous silica. Other related phases such as MCM-48 and MCM-50, which have a cubic and lamellar mesostructure, respectively, were reported in these early publications as well. At the same time, Yanagisawa et al. described less versatile approach to mesoporous materials [17]. Kanemite, a layered

silicate, serves as a silica source, the pathway leading to the ordered mesoporous material is thought to proceed via surfactant intercalation into the silicate sheets, distorting of the sheets and transformation to the hexagonally packed material. Modifying and optimizing the reaction conditions yielded highly ordered mesoporous silicates and aluminosilicate [18]. The obtained materials are designated as FSM-n, Folded Sheet mesoporous. Materials-n, here n is the number of carbon atoms in the surfactant alkyl chain used to synthesize the material. Since these early discoveries, research effort has been emphasized in the synthesis and characterization of a variety of different, although related materials. Many reviews hade been published covering various aspects of ordered mesoporous materials, such as their synthesis, surface modification, application as host materials and in catalysis [18,19-22]. It has been possible to synthesize stable non-silica mesoporous materials [23].

1.2. SYNTHESIS AND MECHANISM OF FORMATION OF MESOPOROUS SILICA

1.2.1. Liquid Crystal Templating (LCT) Mechanism

The researchers of Mobil Corporation proposed 'liquid crystal templating' (LCT) mechanism to explain the formation of M41S type mesoporous materials [16]. It was based on the similarity between liquid crystalline surfactant assemblies (i.e. lyotropic phases) and M41S [16,24]. The mesostructure formation depends on the hydrocarbon chain length of the surfactant tail group, [25] the effect of variation of the surfactant concentration and the additional organic swelling agents. The lowest

concentration at which surfactant molecules aggregate to form spherical isotropic micelles is called critical micelle concentration (CMC_1). Further increase in the surfactant concentration initiates aggregation of spherical into cylindrical or rod-like micelles (CMC_2). There are three main liquid crystalline phases with hexagonal, cubic and lamellar structures. The hexagonal phase is the result of hexagonal packing of cylindrical micelles, the lamellar phase corresponds to the formation of surfactant bilayers and the cubic phase may be regarded as a bi continuous structure. The Mobil researchers proposed two synthesis mechanisms [16b]. In the first route, the $C_nH_{2n+1}(CH_3)_3N^+$ surfactant species organize into lyotropic liquid crystal phase, which can serve as template for the formation of hexagonal MCM-41 structure.

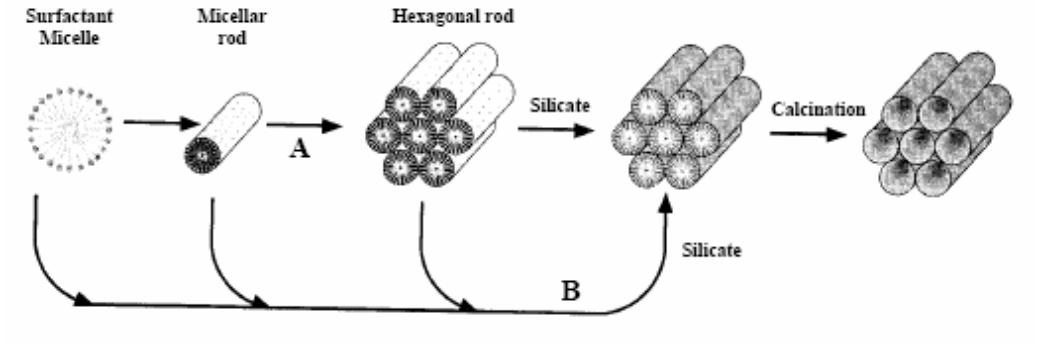

Scheme 1.1. Liquid crystal templating (LCT) mechanism proposed for the formation of MCM-41; (A) liquid crystal phase initiated and (B) silicate anion initiated [Ref. 16b].

Firstly, the surfactant micelles aggregate into a hexagonal array of rods followed by interaction of silicate or aluminate anions present in the reaction mixture with the surfactant cationic head groups. Thereafter condensation of the silicate

species occurs, leading to the formation of an inorganic polymeric species. After combusting off the surfactant template by calcination, hexagonally arranged inorganic hollow cylinders are produced (Scheme 1.1).

However, the drawbacks of this synthesis pathway was pointed out by Cheng et al. [26], according to whom the hexagonal liquid-crystal phase does not form below 40 % of surfactant concentration. It is known that MCM-41 may be formed at low surfactant concentrations (1 wt %) with respect to water content, and in situ ^{15}N NMR spectra indicated that the hexagonal liquid crystalline phase was not present anytime during formation of MCM-41.

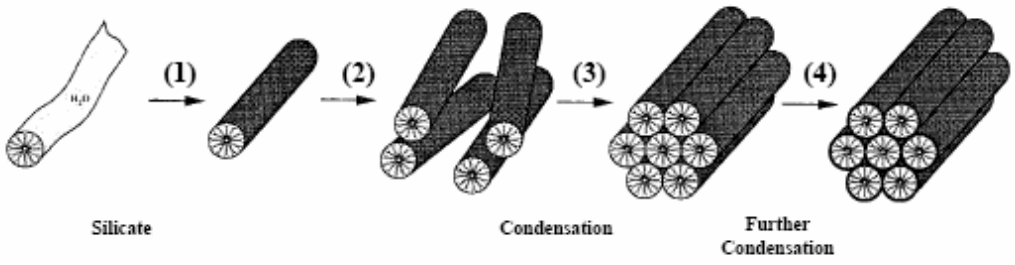

Scheme 1.2. Silicate rod assembly proposed for the formation of MCM-41; (1) and (2) random ordering of rod-like micelles and interaction with silicate species, (3) spontaneous packing of the rods, and (4) remaining condensation of silicate species on further heating [Ref. 25].

In the second route, the hexagonal ordering is initiated by the presence of silicate species in the reaction mixture [16]. Chen et al. explained that randomly distributed surfactant micelles with rod-like morphology form initially, and their interaction with silicate oligomers generate randomly oriented surfactant micelles

surrounded by two or three silica monolayers [25]. The presence of rod-like micelles in solution was supported by isotropic in situ ^{14}N NMR [25]. Further condensation between silicate species on adjacent rods occurs on heating, initiating the long-range hexagonal ordering (Scheme 1.2).

1.2.2. Charge Density Matching and Folded Sheet Mechanism

Both the charge density matching and folded sheet mechanistic models are based on the transformation of lamellar phase to hexagonal phases. The 'charge density matching' model proposed by Stucky et al. suggested that condensation occurs between initially formed silicate species by the electrostatic interactions between the anionic silicates and the cationic surfactant head groups [27,28,18a]. This eventually reduces the charge density and therefore, curvature was introduced into the layers to maintain the charge density balance with the surfactant head groups, which leads to transformation of the lamellar mesostructure into the hexagonal one (Scheme 1.3A).

The 'folded-sheet mechanism' postulated by Inagaki et al. indicated the presence of intercalated silicate phases in the synthesis medium of the reaction products [18a]. The flexible silicate layers of kanemite fold around the surfactant cations and cross-linking of the interlayer occurs by condensation of silanol groups on adjacent silicate sheets. This folding and cross-linking process is facilitated by the flexibility of the single-layered kanemite sheets. On increase of pH, the amount of occluded alkyltrimethylammonium cations in kanemite increases and as a result the interlayers of kanemite expand to form a regular hexagonal structure called FSM-16.

The undissolved portion of kanemite converts to FSM-16 materials whereas the dissolved species yield amorphous silica (Scheme 1.3B).

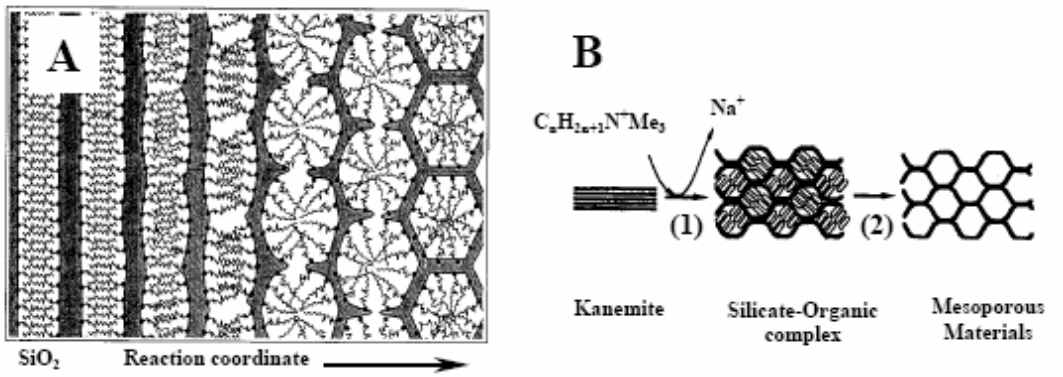

Scheme 1.3. Mechanisms proposed for the transformation of surfactant-silicate systems from lamellar to hexagonal mesophases: (A) Hexagonal mesophases obtained by charge density matching and (B) folding of kanemite silicate sheets around intercalated surfactant molecules [Ref. 27, 28].

1.2.3. Silicatropic Liquid Crystals

Firouzi et al. have developed a model based on cooperative organization of inorganic and organic molecular species into three-dimensional structured arrays [29]. According to this model, the physicochemical properties of a particular system were not determined by the organic arrays having long-range pre-organized order, but by the dynamic interplay among ion-pair inorganic and organic species, so that different phases can be readily obtained through small variation of controllable synthesis parameters. The silicate anions exchanged with the surfactant halide counter ions formed the 'silicatropic liquid crystal' (SLC) phase, which exhibited very similar

behavior to that of typical lyotropic systems and finally condensed irreversibly into MCM-41 (Scheme 1.4).

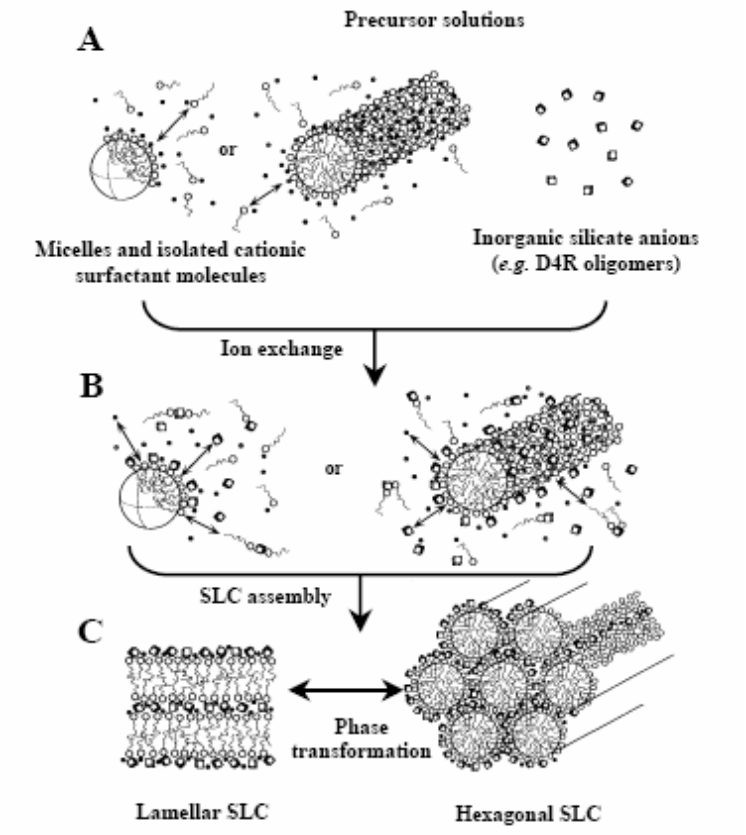

Scheme 1.4. Cooperative organization for the formation of silicatropic liquid crystal phase/silicate-surfactant mesophases: (A) organic and inorganic precursor solutions, (B) preliminary interaction of the two precursor solutions after mixing (C) multidentae interaction of oligomeric silicate units with the surfactants [ref. 23].

1.2.4. Generalized Liquid Crystal Templating Mechanism

Many researchers have tried to explain the possible ways by which a surfactant species interacts with the silica species under various synthesis conditions for the development of mesoporous materials having interesting textual and structural properties. In all cases, a favorable interaction between the surfactant and silicate

species is reported, unless results in disordered materials with any ordered pore structures. A brief summary of the possible interactions between surfactant and silicate species is discussed in this section and a summary of the various synthesis opted under different pathways are depicted in Table 1.1.

Table 1.1. Synthesis of various mesoporous materials under different reaction conditions

Interaction	Template source	Pathway	Examples
Strong electrostatic interactions			
Direct interaction	Ammonium surfactant	S^+I^-	MCM-41, KIT-1
Anion mediated interaction	Ammonium surfactant	$S^+X^-I^+$	MCM-48, FSM-16, SBA-1,2,3
	Triblock Copolymers	$(S^oH^+)X^-I^+$	SBA-15,16
Weak Van der Waals interaction			
Hydrogen bonding interaction	Amine surfactant	S^oI^o	HMS
Hydrogen bonding interaction	Non-ionic Ethylene oxides	N^oI^o	MSU-n

1.2.4.1. Ionic Route (Electrostatic Interaction)

Huo et al. proposed a generalized mechanism for the formation of mesostructures, which was based on specific types of electrostatic interaction between an inorganic precursor (I^o) and a surfactant head group (S^o). In this concept, four different approaches were proposed to synthesize transition metal oxide mesostructures [30]. The first route involves the charge density matching between surfactant cations and inorganic anions (S^+I^-). The second route deals with the charge-

reversed situation, i.e. anionic surfactant and cationic inorganic species (S^-I^+). Both the third and fourth routes are counter ionmediated pathways. The third one demonstrates the assembly of cationic species *via* halide ions ($S^-X^+I^-$), while the fourth one depicts the assembly of anionic species *via* alkali metal ions ($S^+X^-\ I^+$). These synthesis strategies are acceptable for the formation of a wide variety of hexagonal, cubic or lamellar mesophases, but a common problem encountered was the instability of the inorganic framework after the removal of template.

1.2.4.2. Neutral Templating Route (Hydrogen Bonding Interaction)

Tanev and Pinnavaia proposed another route to synthesize hexagonal mesoporous silicas (HMS) having thicker pore wall, high thermal stability and smaller crystallite size [31,32]. This route is essentially based on hydrogen bonding between neutral primary amines (S^o) and neutral inorganic precursors (I^o), wherein hydrolysis of tetraethyl orthosilicate (TEOS) in an aqueous solution of dodecylamine yields neutral inorganic precursor. However, these materials lacked long range ordering of pores and have broader pore size distribution and higher amounts of interparticle mesoporosity than MCM-41 materials. Using the same approach, porous lamellar silicas with vesicular particle morphology (MSU-V) have been synthesized with the help of double headed alkyl amines linked by a hydrophobic alkyl chain (α,ω-dialkyl amine). Bagshaw et al. used nonionic polyethylene oxide surfactants (PEO) to prepare mesoporous materials (MSU) having pore size in the range 20-60 Å. An advantage of this method endows the low cost, non-toxic and biodegradable nature of surfactants and the facile recovery of the templates [31]

1.2.4.3. Ligand-Assisted Templating Route (Covalent Interaction)

Antonelli and Ying proposed a ligand-assisted templating mechanism for the synthesis of hexagonally packed mesoporous metal oxides [32]. In a typical synthesis, the surfactant was dissolved in the metal alkoxide precursor, before addition of water, to form metal-ligated surfactants by nitrogen–metal covalent bond formation between the surfactant head group and the metal alkoxide precursor. The existence of this covalent interaction was confirmed by ^{15}N NMR spectroscopic studies. In this approach, the structure of the mesophases can be controlled by adjustment of the metal/surfactant ratio, which led to a new class of mesoporous transition metal oxides analogous to the M41S family.

1.3. SURFACE MODIFICATIONS OF MESOPOROUS SILICA

The applications of siliceous mesoporous materials itself is restricted because of the limitations in the active sites and have to be modified according to the requirements. Hence, in order to utilize the unique properties of the mesoporous material for specific applications in catalysis, sorption, sensor, ion exchange, etc. introduction of reactive organic functional groups by the incorporation of organic components as part of the silicate walls or trapped within the channels to form organic-inorganic hybrid materials remains the key issues [34]. The advantages of organic-inorganic hybrid materials arise from the fact that inorganic components can provide mechanical, thermal or structural stability, while the organic features can be readily modified for various specific applications [35]. Further, organic modification of the silicates permits precise control over the surface properties and pore sizes of the

mesoporous sieves and at the same time stabilizing the materials towards hydrolysis. Through the development of organic-inorganic hybrid mesoporous solids, much progress has been made in the last few years towards application of mesoporous solids in a variety of fields. Mesoporous solids have been functionalised at specific sites and were demonstrated to exhibit improved activity, selectivity, and stability in a large number of catalytic reactions and sorption processes [36]. The synthesis procedures developed so far effectively utilized the large amount of silanol groups resting in the surface of M41S related materials. Another advantage of these materials is that the hydrophilic hydrophobic properties can be tailored by the judicious choice of the organo alkoxy silanes [37]. This section briefly highlights the possible ways of surface modifications over mesoporous materials for the formation of organic-inorganic hybrid mesoporous materials.

1.3.1. Grafting Methods

Grafting refers to post synthesis modification of the inner surface of a mesoporous support, where the organic functional groups are introduced as the terminal groups of organic monolayers, usually after surfactant removal (Scheme 1.5) [38]. Mesoporous silicas possess surface silanol groups (Si-OH) in high concentration and, like in amorphous silica; it can act as convenient anchoring points for organic functionalisation. Silylation generally occurs on free (≡Si–OH) and geminal silanol (=$Si(OH)_2$) groups, while hydrogen-bonded silanol groups are less accessible to modification because they form hydrophilic networks among themselves [39]. The original structure of the mesoporous support is usually maintained after grafting.

However, if a high surface coverage of organic functional groups is required, it is important to maintain a large number of surface silanol groups, after the removal of surfactants. Surfactant removal is usually carried out either by calcination or by appropriate solvent extraction methods. Since calcinations at higher temperatures can lead to the condensation of silanol groups, a decrease in the density of silanol groups is often obtained than the solvent extraction process (e.g. with acid/alcohol mixtures for cationic surfactants or with alcohols for neutral surfactants).

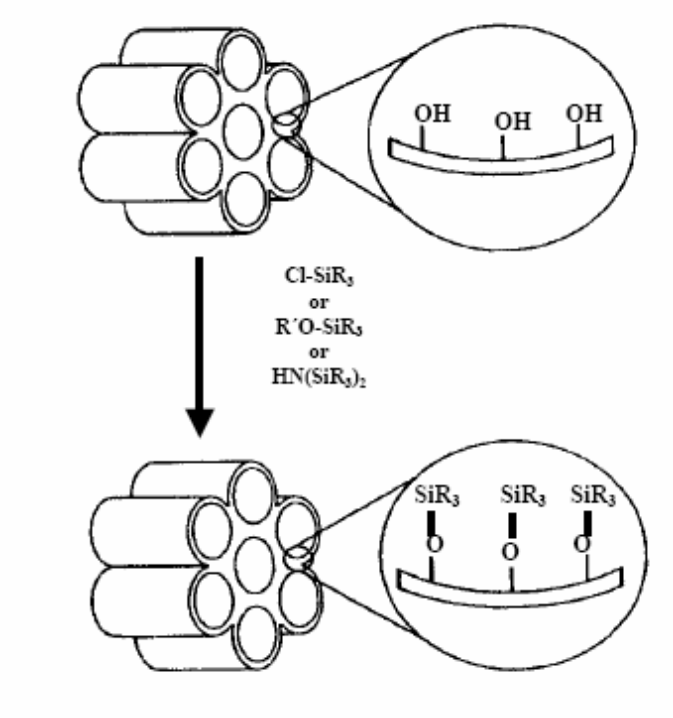

Scheme 1.5. Synthesis of organic-inorganic hybrid mesoporous silicates by grafting reactions [Ref. 40].

In order to retain high-density silanol groups for the anchoring of large concentration of organic groups, the calcined mesoporous silica will be treated with boiling water [41] or steam [42] or by the acid hydrolysis [43]. Recently, supercritical

fluids have been used as a reaction medium to anchor the siloxane to the mesopore channels. This method is particularly suitable for small pore materials due to the low density, viscosity, surface tension and the high diffusivity of the supercritical fluids like CO_2. It was also observed that when this technique was applied to mesoporous silica a high degree of cross-linking was observed, resulting in a higher hydrothermal stability for the materials [44].

1.3.1.1. Grafting with Passive Surface Groups

Organic functional groups with lower reactivity could be grafted to enhance the hydrophobicity of the surface and protecting the material towards hydrolysis. Further, the pore diameter of mesoporous materials can also be adjusted by varying the alkyl chain length of the silylating agent or by increasing the quantity of the silylating agent [45]. The commonly used surface modifying agents are the trimethyl chlorosilane (Me_3SiCl), trimethyl ethoxysilane ($Me_3Si(OC_2H_5)$) and hexamethyldisilazane ($(Me_3Si)_2NH$) [46]. Hexamethyldisilazane functionalization was widely used to quantify the number of surface silanols, to passivate the surface silanols and also to depolarize the surface for selective adsorption experiments [47].

1.3.1.2. Grafting with Reactive Surface Groups

Grafting of the mesoporous silica surfaces with organic units containing reactive functional groups like olefin, cyanide, thiol, amide, halide, etc. permits further functionalization of the surface as their terminal end contains a reactive functional group. For instance, modification of these reactive materials includes hydroboration

[48] and bromination of olefins [49], (vinyl-terminated materials), hydrolysis of cyanide to carboxylic acids [50], oxidation of thiols to sulphonic acids [51], nucleophilic substitution of amines and halides [52]. After, modification of these materials with the desired functionalities, catalytically active homogenous transition metal complexes as well as organometallic complexes can be anchored over these organic-inorganic hybrid materials. For instance, the functionalization of Mn (III) schiff base salen complex to surface-modified MCM-41 containing 3-chloro propyl silane (3-CPTS) is feasible by the nucleophilic replacement of the halogen atom [53].

1.3.1.3. Site-Selective Grafting

The external surface silanols of the mesoporous materials are kinetically more accessible than the internal surface silanols. Hence, in order to minimize the grafting of reactive surface sites on the external surface and thereby to utilize the inner pore channels, it is necessary to passivate the external silanol groups before functionalizing on the internal surfaces [54]. Shepherd et al. had passivated the external surface of the MCM-41 surface with dichloro diphenyl silane (Ph_2SiCl_2) first and then 3-aminopropyl triethoxy silane (3-APTS) was grafted over the internal channels for the heterogenization of an active ruthenium cluster. The existence of amine functional groups in the inner pore channels of MCM-41 was confirmed by the high-resolution transmission electron microscopy (HRTEM) [55]. Another approach effectively utilized was the template ion exchange property, for the grafting of Me_3SiCl, without removing the surfactants from the pore channels. The advantage of this method is that this procedure avoids the two-step synthesis procedure and that the grafting

exclusively occurs in the external surfaces due to the steric constraint of the surfactants [56]. Following solvent extraction, for the removal of surfactant groups, the internal surface of the materials is free for further modifications while the external surface is passivated. In another way, Antochshuk and Jaroniec carried out simultaneous grafting and extraction of template molecules by modification of uncalcined MCM-41 with trialkylchlorosilanes. As-synthesized MCM-41 was refluxed in neat trialkylchlorosilane, first by itself, and then with added anhydrous pyridine, followed by multiple washing with different solvents, leading to surfactant-free mesoporous products [57]. The loading of surface organic groups exceeded on calcined supports that were otherwise treated in a similar way. The advantages of this method include the increased concentration of surface hydroxyl groups and the decreased reduction in pore size of the materials, as this procedure avoids the high temperature calcination process for the removal of surfactant groups.

1.3.2. Co-condensation Reactions

Organic-inorganic hybrid mesoporous materials can be also prepared at room temperature or at higher temperatures by the one-step co-condensation method between tetraalkoxy silanes [$Si(OR)_4$, R = Et, Me] with one or more organoalkoxy silanes [RSi(OR)3, R = Et, Me], through the sol-gel process in presence of a structure orientor [58]. Depending on the nature of the R groups, a variety of organofunctionalized mesoporous materials attached covalently with the silica surface can be synthesized. The advantages of this method than the grafting procedures include the stability of the inorganic framework even at higher organic loadings,

homogenous distribution of the organic groups in the pore channels as well as the single step preparation procedures [59]. Solvent extraction of the as-synthesized materials in an acidic-alcohol mixture helps to remove the occluded surfactants from the pore channels and to obtain the organofunctionalized ordered mesoporous material (Scheme 1.6). Several research groups had employed this co-condensation procedure for the synthesis of organic-inorganic hybrid mesoporous materials under S+I-, $S^{+}X^{-}I^{+}$, $S^{o}I^{o}$ and $N^{o}I^{o}$ pathways [61].

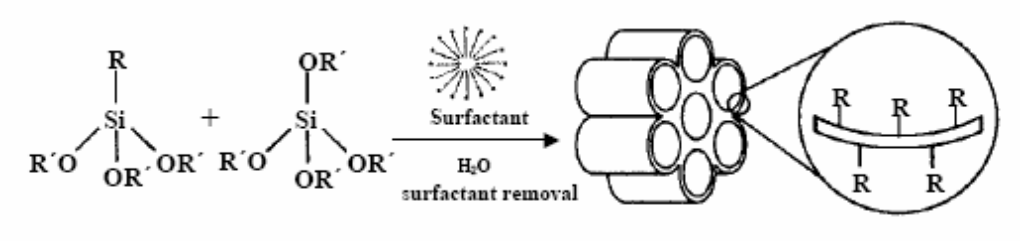

Scheme 1.6. Synthesis of organic-inorganic hybrid mesoporous silicates by cocondensation reactions. [60].

1.4. METAL-SUBSTITUTED MESOPOROUS MOLECULAR SIEVES

The advantages of using ordered mesoporous solids in catalysis are due to the relatively large pores, which facilitate mass transfer, and the very high surface area, which allows a high concentration of active sites per mass of material [62]. Although mesoporous materials posses unique textual as well as morphological features, siliceous M41S materials show limited catalytic activity in various organic transformations and hence ample modifications are necessary to make them as suitable candidates for various catalytic organic transformations. The incorporation of

heteroatoms into the inert framework or walls of pure siliceous mesoporous materials is an important route to modify the nature of the framework. In fact, the first catalytic studies with mesoporous molecular sieves were focused on metal-substituted MCM-41 materials, in which the active species were incorporated into the silicate matrix [63]. However, since the wall structure of mesoporous silica resembles more to amorphous silica, incorporation of heteroatoms does not lead to the formation of defined sites as in zeolites, but as a rather wide variety of different sites with different local environments. Therefore, the catalytic properties of such materials resemble more to metal-containing amorphous silica rather than the framework-substituted zeolites [64]. Modification of the framework composition of mesoporous materials is possible by the direct synthesis i.e. from mixtures containing both silicon and the hetero element to be incorporated or by post synthesis treatment of an initially prepared mesoporous material. The direct method usually results in a homogeneous incorporation of the hetero element while post synthesis methods help in an increased concentration of heteroatoms on the surface. Various heteroatoms are incorporated into the pore channels of mesoporous supports and it is generally observed that apart from the synthesis conditions, viz. gel pH, temperature and time, the degree of metal incorporation as well as coordination of metal sites in the mesopore structure is dependant on the nature of metal precursor used [65]. Thus, the incorporation of trivalent metal ions such as B, Al, Ga, etc. in the silica frame walls produces framework negative charges that can be compensated by protons providing acid sites and hence serve as important materials in acid catalysis. The substitution of various transition metals like Ti, V, Cr, Mn, Fe, etc. helps in the development of mesoporous

materials with redox catalytic properties. Although the chemical elaboration of the surfactant templated mesoporous materials has been extensively applied to catalysis, the Si-MCM-41 type mesoporous materials potentially suffers from a plumbing problem. Since the periodic porosity is one-dimensional and nanoscopic in MCM-41, any internal blockage can shutoff the catalyzed walls from reaction [66]. However, the three dimensionally channel oriented mesoporous architectures, like the hexagonal mesoporous silica (HMS) materials, with continuous but periodically porous network offer new transport routes and has less diffusion limitations and are reported to be catalytically more active than the M41S materials. For instance, Tanev e*t al* had shown that Ti-HMS catalyst shows improved catalytic activity than Ti-MCM-41 catalysts in the oxidation reaction of 2,6-DTBP, MMA and styrene [67]. Even though, the catalytic transformations of bulky organic molecules can be carried out in the 'nanoreactors' of the mesoporous materials, there exist significant differences between metal-substituted zeolites and mesoporous silica materials. A comparison of metal incorporated zeolitic molecular sieves with mesoporous materials shows that the activity and heterogenity of the zeolitic catalysts lie far ahead than the mesoporous molecular sieves [68]. Hence, an important question arise that what causes for the much lower activity observed on the M-MCM-41 samples than the zeolitic metallosilicates, even though they share almost similar metal local environments. Obviously, diffusion limitations and steric constraints due to reactants or transition-state intermediates are not the only factors that govern the activity of metal sites in molecular sieves. The crucial difference in the structure of M41S and zeolite is that the M41S materials have no long-range order and the pore walls are essentially

amorphous. Thus, the Si-O-M bonds sitting in the amorphous environment of M41S are supposed to be connected by more comfortable bond angles and are thermodynamically more stable than those of metal incorporated silicates, which had crystalline frameworks. Therefore, the Si-O-M bonds in mesoporous materials should be less reactive and have lower redox potential than those in zeolite samples. Further, since a part of active metal sites can be located inside the walls in mesoporous materials, these sites are not accessible for the reactants and this property was commonly observed when the metal precursor was introduced together with the silica source during the synthesis [69]. Another difference with zeolite concerns the nature of framework itself. In zeolites the number of defect groups like silanols is low, as they are located on the outer surface of the crystals. Hence, zeolites have a relatively high hydrophobic character, well suited for oxidation reactions in aqueous medium [70]. In contrast, mesoporous silica contain large amounts of internal silanol groups, capable of hydrogen bonding with water molecules, which will affect their performance in aqueous catalytic reactions. The catalytic activity of metal-containing mesoporous materials is strongly influenced by the hydrophobic properties of the support surface, the local environment and the stability of the metal introduced. Hence, bifunctional organic-inorganic hybrid mesoporous materials containing heteroatoms like titanium and organic groups such as methyl silanes were prepared in a one step co-condensation method in order to improve the hydrophobic features of the metal-containing periodic mesoporous silica materials [71]. The methyl-tethered Ti-MCM-41 showed better epoxidation activity than the nonmodified Ti-MCM-41, in the epoxidation reaction of cyclohexene. Bhaumik and Tatsumi synthesized a wide range

of organically modified Ti-MCM-41 samples by cocondensation of TEOS, organo-triethoxy silanes like methyl, vinyl, allyl, 3-chloropropyl, pentyl, phenyl and titanium tetrabutoxide [72]. Higher titanium incorporation as well as enhanced epoxide selectivity was observed in presence of organic groups than in their absence and were attributed to the improved hydrophobicity of the organo-modified mesoporous surface. Akin to periodic mesoporous silicas, periodic mesoporous organosilicas also offer advantages for various surface modifications due to the presence of T^2 type silanol sites [73]. For instance, titanium-containing PMO materials show exceptional catalytic activity and oxime selectivity in the ammoxidation reaction of ketones, whereas the conventional Ti-MCM-41 catalysts are not active for the same reaction [74]. Among the reasons put forward to explain this dependence was the hydrophobicity of the matrix; as the more hydrophobic the surface, the higher the reaction rate because of the increased concentration of the organic substrate at the active titanium site. One of the major drawbacks of metal-containing M41S materials is the decreased hydrothermal stability. However, because of the presence of organic fragments, especially ethane groups, in the frame wall positions the PMO materials show better hydrothermal stability than the M41S materials [75]. Thus the presence of hydrophobic organic groups, integrated inside the frame wall positions, improved the catalytic activity and overall structural stability of the mesoporous materials.

1.5. MESOPOROUS SILICA AS SUPPORT OR HOST FOR THE HETEROGENIZATION OF HOMOGENEOUS CATALYSTS

Materials with well-defined pores belong to the most interesting class of compounds, because they can be converted into organic-inorganic hybrid nanocomposites by various surface modifications. The microporous and organized mesoporous materials obtained after the hydrothermal synthesis are in fact a nonporous organic-inorganic hybrid since the organic structure director (template or surfactant) is usually trapped in the cavities of the solid. Hence, to obtain completely porous solid and to introduce reactive organic functional groups inside the channels of ordered materials, it is necessary to remove the entrapped organic species from the as-synthesized samples. The commonly employed method for the removal of surfactant consist of calcining the materials, in a flow of air, typically >400 ^{o}C. However, the high-cost template reactant is destroyed and such treatments further cause damage to the porous materials, since during calcination high local temperature and water formation may occur, and therefore extra framework sites may be formed [76]. An alternative method involves the removal of the template by mild treatments such as liquid extraction using acidic solutions, alcohols or a mixture of both [77]. This method is especially effective for mesoporous materials where the framework-surfactant interactions are weak (electrostatic, van der Waals or hydrogen bonding interactions) and because of the larger pore sizes. An added advantage of this method is that under acidic extraction conditions, exchange of sodium ions for protons is also achieved simultaneously with the removal of surfactants. Moreover, the mild routes for the removal of templates helps in the reuse of the organic templates for a

subsequent synthesis with similar textual properties [78]. The materials obtained after the removal of surfactant groups contains ordered pore channels with abundant silanol sites. These mesoporous hosts can be utilized for the synthesis of organic-inorganic hybrid mesoporous materials having reactive functional groups and have stimulated fundamental research interests in the inclusion of metals and metal complexes inside the mesoporous channels [79]. During the last few years, organic-inorganic hybrid mesoporous materials constitutes an emerging area in the field of materials science and had shown its impact in a wide range of heterogeneous catalysis reactions [80]. However, the main problem encountered in heterogenized catalysts is that the bonds between metal and ligand are often broken and reformed during catalytic reactions, leading to leaching of the metal from the catalyst in the product, thus decreasing the reaction rate and activity [81]. Hence the nature of interaction between the homogenous catalyst and the support surface decides the overall stability and reusability of the heterogenized catalysts and in general, if the anchoring is covalent, it can be robust enough to withstand the harsh conditions of the catalytic reactions. The most common immobilization techniques used for this purpose include grafting or tethering, physical entrapment, ship-in-a-bottle synthesis and supported liquid phase catalysis [82]. Earlier, the supports used to tether the homogeneous catalyst are the organic polymers, which are soluble in the reaction media. The advantage of this support is that the active sites are distributed through out the reaction solution and hence the catalyst architecture is similar to that of the homogeneous catalyst that it is trying to mimic [83]. Insoluble supports are preferable than the homogeneous supports because of several reasons i.e. they are readily recovered, they have potential

applications in flow process and they do not need extra solvents for precipitation. Insoluble organic polymers are effective supports, but the polymer had to be carefully chosen and tuned so as to avoid swelling and to ensure that the homogeneous complex catalyst is tightly bound with the support not merely occluded inside. In contrast to the insoluble organic polymers, inorganic silica materials like amorphous silica gels or mesoporous silicas did not swell or dissolve in organic solvents. However, because of the lack of ordered pore channels, amorphous silica gels are unable to provide the size/shape specificity properties. Hence the immobilization of various homogeneous metal catalysts over solid organic-inorganic hybrid mesoporous supports as a mean of 'heterogenization' has particular significance. Heterogenization of useful homogenous catalysts or active centers will improve the overall efficiency of the catalytic process due to: (i) it is easier to separate the catalyst from the liquid by simple filtration, where the homogenous catalyst often leads to complicated and laborious extraction or distillation requirements, (ii) often the catalysts can be regenerated and recycled, (iii) confinement of the catalyst in the mesopores provides a means of introducing the size/shape selectivity and thus a greater specificity to a desired reaction. Moreover, if the functional groups or the catalytic active site was attached firmly to the solid support, the leaching problem, usually encountered in liquid phase reactions, can be greatly reduced.

1.6. PHYSICOCHEMICAL CHARACTERIZATION

Understanding the structural and electronic properties of the catalyst by spectroscopic techniques is one of the major goals in catalysis research because they

can provide fundamental information about catalytic structures and surface reaction intermediates under controlled environments and also gives insight into the relation between physical and chemical properties of the catalyst and its activity. In catalytic research, a number of techniques will be used to characterize a sample and a summation of all characterization techniques will reveal the active sites in a catalyst and these in turn will help in the design of a new catalyst or to improve the catalytic performances. The commonly used characterization techniques, their principles, advantages and limitations are briefly described in this section.

1.6.1. X-Ray Diffraction (XRD)

XRD has been applied as the most important tool to determine the structure of the materials characterized by long-range ordering, to identify bulk phases, to monitor the kinetics of bulk transformations and to estimate particle sizes [84]. The XRD method involves the interaction between the incident monochromatized X-rays (like Cu K_α or Mo K_α source) with the atoms of a periodic lattice. X-rays scattered by atoms in an ordered lattice interfere constructively in directions given by Bragg's law: $n\lambda = 2d\sin\theta$, where, λ is the wavelength of the X-rays, d is the distance between two lattice planes, θ is the angle between the incoming X-rays and the normal to the reflecting lattice plane and n is an integer known as the order of reflection [85]. Bragg peaks are measured by observing the intensity of the scattered radiation as a function of scattering angle 2θ. The angles of maximum intensity enable one to calculate the spacings between the lattice planes and allow phase identifications while the width of diffraction peaks carries information on the dimensions of the reflecting planes. The

width of the diffraction lines can be further used to estimate the crystal size by the Debye-Scherrer formula: $D_{hkl} = k\lambda/\beta\cos\theta$, where D_{hkl}, λ, β and θ are the volume averaged particle diameter, X-ray wavelength, full width at half maximum (FWHM) and diffraction angle, respectively, and *k* is a constant, often taken as unity [86]. Isomorphous substitution of heteroatoms in the framework of molecular sieves can be calculated from the changes in the unit cell parameters and unit cell volume. Unit cell parameter (a_o) of a hexagonal lattice can be calculated from, $a_o = 2d_{100}/\sqrt{3}$ and a cubic lattice can be determined by the following equation: $a_o = d_{211}/\sqrt{6}$. The unit cell dimension determined by XRD is also used to calculate the frame wall thickness (FWT) of the channels of the mesoporous materials. A major limitation of XRD is that this technique requires samples, which possess sufficient long-range order. Amorphous phases and small particles give either broad and weak diffraction lines or no diffraction at all, which makes them virtually invisible for XRD.

1.6.2. Porosity Measurements by N_2 Adsorption Method

The most common method of measuring surface area and textural characteristics of catalytic materials is that based on the theory developed by Brunauer, Emmett and Teller (BET), considering the multilayer adsorption. The BET equation can be represented as: $P/V(P_0-P) = 1/cV_m + [(c-1)/cV_m]\ (P/P_0)$, where P is adsorption equilibrium pressure, P_0 is saturation vapor pressure of the adsorbate at the experimental temperature, V is volume of N_2 adsorbed at pressure P, V_m is volume of adsorbate required for monolayer coverage and c, a constant that is related to the heat of adsorption and liquefaction [87]. A linear relationship between $P/V(P_0-P)$ and P/P_0

is required to obtain the quantity of nitrogen adsorbed. The monolayer volume, V_m is given by 1/(S+I), where *S* is the slope and is equal to (c-1)/cV_m and I is the intercept equal to 1/cV_m. The surface area of the catalyst (S_{BET}) is related to V_m, by the equation, S_{BET} =(V_m/22414) $N_a\sigma$, where N_a is Avogadro number and σ is mean cross sectional area covered by one adsorbate molecule. The σ value generally accepted for N_2 is 0.162 nm. Several computational procedures are available for the derivation of pore size distribution of mesoporous samples from physisorption isotherms. Most popular among them is the Barrett-Joyner-Halenda (BJH) model, which is based on speculative emptying of the pores by a stepwise reduction of P/P_0, and allowance being made for the contraction of the multilayer in those pores already emptied by the condensate [88]. The mesopore size distribution is usually expressed as a plot of $\Delta V_p/\Delta r_p$ versus r_p, where V_p is the pore volume, and r_p is the pore radius.

1.6.3. Scanning Electron Microscopy (SEM)

Scanning electron microscopy is a straightforward technique to probe the morphological features of mesoporous molecular sieve materials. SEM scans over a sample surface with a probe of electrons (5-50 eV) and detects the yield of either secondary or back-scattered electrons as a function of the position of the primary beam. Contrast is generally caused by the orientation that parts of the surface facing the detector appear brighter than parts of the surface with their surface normal pointing away from the detector. The interaction between the electron beam and the sample produces different types of signals providing detailed information about the surface structure and morphology of the sample [89]. When an electron from the beam

encounters a nucleus in the sample, the resultant Coulombic attraction leads to a deflection in the electrons path, known as Rutherford elastic scattering. A fraction of these electrons will be completely backscattered, re-emerging from the incident surface of the sample. Since the scattering angle depends on the atomic number of the nucleus, the primary electrons arriving at a given detector position can be used to produce images containing topological and compositional information [90]. A major advantage of SEM is that bulk samples can also be directly studied by this technique.

1.6.4. Transmission Electron Microscopy (TEM)

Transmission electron microscopy is typically used for high resolution imaging of thin films of a solid sample for micro structural and compositional analysis. The technique involves: (i) irradiation of a very thin sample by a high-energy electron beam, which is diffracted by the lattices of a crystalline or semi crystalline material and propagated along different directions, (ii) imaging and angular distribution analysis of the forward scattered electrons (unlike SEM where backscattered electrons are detected) and (iii) energy analysis of the emitted X-rays [91]. In detail, a primary electron beam of high energy and high intensity passes through a condenser to produce parallel rays, which impinge on the sample. As the attenuation of the beam depends on the density and the thickness, the transmitted electrons forms a two-dimensional projection of the sample mass, which is subsequently magnified by the electron optics to produce the so-called bright field image. The dark field image is obtained from the diffracted electron beams, which are slightly off angle from the transmitted beam. Typical operating conditions for TEM instruments are 100-200 keV electrons, 10-6

mbar vacuum, 0.5 nm resolution and a magnification of 105 to 106. The topographic information obtained by TEM in the vicinity of atomic resolution can be utilized for structural characterization and identification of various phases of mesoporous materials viz. hexagonal, cubic or lamellar [92]

1.6.5. Fourier Transform Infrared Spectroscopy (FT-IR)

Infrared spectroscopy (IR) can be considered as the first and the most important of the modern spectroscopic techniques that has found profound applications in the field of catalysis. This is primarily due to the fact that IR provides actual information on the structure, geometry and orientation of practically all molecules that are present in the reaction mixture, irrespective of the physical state, temperature or pressure. IR is therefore a feasible tool to identify phases that are present in the catalyst or its precursor stages, the adsorbed species, adsorption sites and the way in which the adsorbed species are chemisorbed on the surface of the catalyst [93]. Infrared spectroscopy is the common form of vibrational spectroscopy and it depends on the excitation of vibrations in molecules or in solid lattices by the absorption of photons. Absorption of an infrared photon occurs only if a dipole moment changes during the vibration. However, it is not necessary that the molecule possess a permanent dipole, it is sufficient if a dipole moment changes during the vibrations. The intensity of the infrared band is proportional to the change in the dipole moment. Although this statement is of little practical value, as the magnitude of dipole moments during the vibrations are not known, it explains why species with polar bonds such as CO, NO and OH exhibit strong IR bands, where as covalent bonds

such as C-C absorb infrared light only weakly and molecules such as H_2, N_2 are not infrared active at all. A variety of IR techniques have been used to attain information on the surface chemistry of different solids. A great advantage of infrared spectroscopy is that the technique can be used to study catalysts in situ. In case of porous silicates, the FTIR spectra in the 1300-400 cm^{-1} region provides information about the structural details, whereas the bands in the 4000-3000 cm^{-1} region allows to determine different Brønsted and Lewis acid sites and silanol groups of the material [94]. The band at 980-960 cm^{-1} in the framework region is very important in metal-containing molecular sieves, as this region provides information about the incorporation of metal species in the frame wall positions [95]. Acidic and basic properties as well as their strength can also be estimated using ammonia (NH_3), pyridine (C_5H_5N), carbon dioxide (CO_2) etc as probe molecules and their quantitative estimation by FTIR [96]. One drawback of IR is that almost all compounds absorb IR radiation so that the spectra of reaction mixtures can be very complex, hampering straightforward interpretation and assignments. However, data manipulation and processing techniques like deconvolution, spectral subtraction and chemometrics are helpful in extracting the desired information [97].

1.6.6. Diffuse Reflectance UV-Visible Spectroscopy (DR UV-Vis)

Diffuse reflectance spectroscopy (DRS) is a technique based on the reflection of light in the ultraviolet (UV), visible (VIS) and near-infrared (NIR) region by a powdered sample. In a DRS spectrum, the ratio of the light scattered from an 'infinitely thick' closely packed catalyst layer and the scattered light from an infinitely

thick layer of an ideal non-absorbing (white) reference sample is measured as a function of the wavelength, λ. The scattered radiation, emanating from the sample, is collected in an integration sphere and detected. The most popular continuum theory describing diffuse reflectance effect is the Schuster-Kubelka-Munk (SKM) theory [98]. If the sample is infinitely thick, the diffuse reflection of the sample (R_∞) is related to an apparent absorption (K) and apparent scattering coefficient (S) by the SKM equation: $F(R_\infty) = (1- R_\infty)^2/2R_\infty = K/S$. At low concentrations of supported transition metal ions (TMI), this equation is a good representation of the absorption spectrum and allows a quantitative determination of the transition metal ions. UV-Vis spectroscopy generally deals with the study of electronic transitions between orbital or bands of atoms, ions or molecules. One of the advantages of DRS is that the obtained information is directly chemical in nature since outer shell electrons of the transition metal ions are probed. This further provides information about the oxidation state and coordination environment of transition metal ions in the solid matrices. Thus DRS is a sensitive technique to examine the type of the metal sites, *viz.,* framework or extra-framework, in which metal ion or cluster exist [99]. For most of the isomorphously substituted metal-containing molecular sieves, transitions in the UV region (200-400 nm) are of prime interest. The disadvantage of DRS is that the signals are usually broad and overlap with each other, leading to a biased spectral analysis. In addition, the origin of the specific electronic transition is sometimes difficult to isolate due to its dependence on the local coordination environment, the polymerization degree and the specific oxidation state.

1.6.7. X-Ray Photoelectron Spectroscopy (XPS)

XPS (also referred by the acronym ESCA, Electron Spectroscopy for Chemical Analysis) is a non-destructive surface analysis technique, based upon one of the fundamental interactions of photons with matter viz. the photoelectric effect [100]. XPS provides information on the elemental composition, the oxidation state of the elements and in favorable cases on the dispersion of one phase over another. In this technique, sample surface is irradiated with X-rays and the emitted photoelectrons are measured. When an atom absorbs a photon of energy hν, a core or valence electron with binding energy E_b is ejected with kinetic energy E_k: $E_k = h\nu - E_b$, where h is Planck's constant, ν is the frequency of the exciting radiation, E_b is the binding energy of the photoelectron relative to the Fermi level of the sample and is the work function of the spectrometer. The photoelectrons ejected from an atom in the solid have different kinetic energies, according to the electronic level and the type of atom they come from. As the electronic structure of an atom is a unique fingerprint of this atom, photoelectron spectra allow an excellent elemental analysis of the target sample. XPS entails emission from both core and valence electrons of the solid, the stimulating X-ray sources being Al K_α (1486.6 eV) or Mg K_α (1253.6 eV). Their photon energy is high enough to reach at least one core level of any element and also their natural line width is small enough to allow the recording of well-resolved photoelectron spectra. XPS spectrum is usually a plot of the intensity of photoelectrons versus binding energy. Since the electrons whose energies are analyzed in XPS arise from a depth of not greater than about 5 nm, this technique is highly surface specific. A set of binding energies is characteristic for an element and hence XPS can be used to analyze the

composition of samples, considering the area of the peak and cross section for photoemission [101]. An experimental problem in XPS is that electrically insulating samples may charge during measurements, as photoelectrons leave the sample. Due to the positive charge on the sample, all XPS peaks in the spectrum shift by the same amount to higher binding energies. Calibration for this effect can be done by using C_{1s} binding energy of 284.9 eV from carbon contamination, which is present on most of the catalysts. Though XPS provides information about the oxidation state and the chemical environment of a given atom due to shift in the binding energies, the structural information is, however, limited in case of supported vanadium oxides and chromium oxides [102].

1.7. CATALYTIC APPLICATIONS AND PROSPECTS

In recent years, environmental and economic considerations have raised strong interest to redesign commercially important process so that the use of harmful substances and the generation of toxic wastes can be avoided. Zeolite plays a key role in the development of environmentally benign process in the production of fine chemicals. However, zeolites posses severe limitations when large reactant molecules are involved, due to the diffusional restrictions imparted from the small pore channels of microporous solids [103]. Hence, because of the large pore size than the zeolite based porous materials, mesoporous materials stood for the extension of catalytic applications of zeolites for the conversion of bulky molecules. Through the development of hybrid organic-inorganic mesoporous solids, much progress has been made in the last few years towards the applications of mesoporous solids in various

areas of heterogeneous catalysis. The concept of 'heterogenization' of homogenous catalysts over organic-inorganic hybrid mesoporous materials possessing reactive functional sites provide the prospective for extending the benefits of heterogeneous catalysis to homogeneous systems. These benefits include easier separation of catalyst and reaction products leading to shorter work up times, improved process efficiency and better reuse of the supported catalysts. However, the prime requirement of the heterogenization approach is to maintain the stability of the heterogenized complex, such that it does not decompose or leach out from the solid support to the liquid phase during the course of reaction, and at the same time retains high activity and selectivity. Reactions that have been studied using functionalised mesoporous solids include acid-base catalysis [104,105], oxidations [106], reductions [107], enantioselective catalysis [108] and other catalytic for fine chemicals [109]. It has been noted that the confinement of the catalyst or active sites in the mesoporous channels improved the overall activity of the catalysts compared to attachment over amorphous or non-porous silica supports. These improved results apparently stemed out due to the confined environment of the mesopore channels. In some cases, the performance of the mesoporous catalyst was found to be directly depend on the pore size of the mesopore host, since depending on the pore size the accessibility of the active sites in the mesopores gets varied [110]. For instance, in the hydrogenation of olefins (styrene, trans-and cis-stilbene, α-methyl styrene and limonene), the hydrido chloro carbonyl tris-(triphenylphosphine) ruthenium complex ($RuHCl(CO)(PPh_3)_3$ immobilized over aminopropyl functionalised mesoporous SBA-15 shows superior catalytic activity than the MCM-41 sample, even though both mesoporous supports shows higher conversion

and turnover frequency than the unsupported ruthenium complex. The superior catalytic activity of SBA-15 than MCM-41 is attributed to the easier access of substrate molecules to the active sites in SBA-15 due to its larger pore size than the MCM-41 host matrix [111]. In this section, the catalytic applications and prospects of metal-containing mesoporous materials and organo-modified mesoporous materials for various oxidation and epoxidation reactions are briefly reviewed.

1.7.1 Oxidation Reactions

The first examples of liquid phase catalytic oxygen transfer dates back to 1936. The so-called Milas reagents were formed by reaction of transition metal oxides with a solution of H_2O_2 in tert-butanol resulting in soluble inorganic peracids [112]. These catalysts were used for the vicinal dihydroxylation of olefins but with certain metal oxides like MoO_3 or WO_3, selective epoxidation was observed. From these basics, a great deal of effort has been put into the development of transition metal based catalysts, as homogeneous and heterogeneous, for various selective oxidation reactions [113]. Based on the key intermediate involved in the oxygen transfer step, the metal catalyzed oxidations can be divided mainly into two categories [114]. The first one involves a peroxometal species, while the second one involves an oxometal pathway. In general, titanium, vanadium and molybdenum catalyzed reactions are believed to occur via peroxometal pathway [115], while chromium [116] and ruthenium [117] catalyzed reactions are supposed to proceed through oxometal species [118]. Metallosilicate molecular sieves with MFI topologies (*e.g.* TS-1, VS-1) have been extensively investigated as heterogeneous catalysts for various selective oxidation and

epoxidation reactions [119]. However, as mentioned earlier, the catalytic properties of these molecular sieves can be utilized only for small molecules, due to the small pore size of these materials. In this regard, the advent of metal-containing mesoporous solids that can accomodate bulky molecules inside the pore channels widened the range of catalysts available for selective oxidation reactions using peroxides and air as oxidants, few of which are summarized in Table 1.2. Further, the advent of various organic-inorganic hybrid mesoporous materials having reactive functional groups helps to immobilize various metal and metal complexes inside the pore channels of the mesoporous materials. Compared to the metal-substituted mesoporous materials, these methods provides better active site isolations and also helps to increase the stability of the metal-containing mesoporous materials, if the bonding between the ligand and metal is robust.

Recently, there is much interest in substituting process that use pollutant oxidants with more environmentally acceptance ones. Besides the prime properties like price and ease of handling, the choice of oxidants depends mainly upon two factors *viz.,* the nature of the corresponding by-product and the active-oxygen content. The former property is important in terms of environmental considerations, while the latter factor influences the overall productivity of the process. In this respect, molecular oxygen is an attractive choice. However, the free radical nature of the reaction restricts its applicability to a rather small number of molecules. Hence, for the catalytic epoxidation and oxidation reactions of a wide variety of organic molecules, organic peroxides as well as hydrogen peroxide was used as single oxygen donors. Even though, organic peroxides are more active oxidants than hydrogen peroxide, they

are more expensive and the active oxygen content is rather low. Moreover, usage of organic peroxides generates stoichiometric amount of corresponding alcohols, which in most cases complicates the separation process. Hence the preferred oxidant in most of the oxidation or epoxidation process is hydrogen peroxide.

Table 1.2. Oxidation reactions over surface modified mesoporous silica

No.	Catalyst	Reaction	References
1	Ti-MCM-41	Epoxidation of styrene, 1-octene, cyclododecane	120
2	Ti-HMS	Epoxidation of cyclooctene, styrene	121
3	Cr-MCM-41	Oxidation of 1-naphthol, cyclohexane	122
4	Cr-MCM-48	Oxidation of ethylbenzene	123
5	Fe-MCM-41	Epoxidation of styrene	124
6	Co-MCM-41	Oxidation of styrene, benzene, 1-hexene	125
7	Sn-MCM-41	Oxidation of 1-naphthol, Baeyer-Villiger reaction	126

Although hydrogen peroxide (H_2O_2) provides distinguishable advantageous feature than the organic peroxides, two main problems are generally encountered when H_2O_2 was used as an oxidant in presence of redox molecular sieves and both these problems are related to the presence of water formed during the reaction. The first and most important problem is related to the irreversible hydrolysis of the siloxy-metal (Si-O-M) units in the active sites. The second problem frequently observed is that, water obstructs the active sites of the catalyst and thereby sterically prevents the alkene, in epoxidation reaction, or hydrocarbons, in oxidation reactions, to react with the active site. This usually results in a decreased activity of the catalyst while the former problem severely limits the reusability of the catalysts [127]. Since the

commercially available oxidant sources of hydrogen peroxide and organic peroxides, like the *tert*-butyl hydroperoxide, contain water to some extent, use of oxidants like urea-hydrogen peroxide (UHP) or hydrophobic catalyst surface are better alternatives to overcome such difficulties [128]. However, in heterogeneous systems with clean oxidants like H_2O_2, it is an environmentally friendly alternative to traditional oxidation reactions and hence attention had also been devoted to the synthesis of stable metal-containing mesoporous materials by the judicious decoration of the internal pore size of the mesoporous materials with various organic groups [129]. Hence, the development of environmentally friendly, safer and effective heterogeneous redox catalysts seems to be a challenging task to the research community.

1.8. SCOPE AND OBJECTIVES OF THE THESIS

The main aim of this thesis was to heterogenize transition metals over solid mesoporous supports for the oxidation reaction under different set of conditions. Recently, the area of catalysis for the transformation of bulkier molecules over metal containing and organo-modified metal containing mesoporous materials assumes significant importance for fine chemical synthesis and petroleum [130]. The incorporation of various heteroatoms in the framework and pore channels of different mesoporous materials had been systematically studied, characterized and used as catalysts in various oxidation reactions. Various intriguing physical properties like high surface area, ordered pore channels and high-density silanol sites of the mesoporous molecular sieves were also exploited for the heterogenization of catalytically reactive species by post synthesis method. In-depth characterizations of

all catalyst systems are highlighted to understand the mode of interaction of the active sites with the mesoporous silicate network and thereby to evaluate the structure-catalytic activity relations and stability of the mesoporous solids.

Cobalt and zirconium containing mesoporous materials were active in a number of liquid phase oxidation reaction especially the side chain oxidation using H_2O_2 and TBHP as oxidants. However, the catalytic performance depends on the cobalt species viz. incorporated, grafted and immobilized. Environmental concern gives further impetus for the development of stable and leaching free catalyst.

The specific problems chosen are:

(i) Synthesis of mesoporous silica materials viz. Si-MCM-41 and HMS.

(ii) Synthesis of cobalt-containing mesoporous materials MCM-41 by various preparation routes and application of these materials in the oxidation reaction of ethylbenzene and diphenylmethane.

(iii) Synthesis of cobalt-containing mesoporous materials HMS by various preparation routes and application of these materials in the oxidation reaction of ethylbenzene and diphenylmethane.

(iv) Synthesis of zirconium-containing mesoporous materials MCM-41 and HMS by various preparation routes and application of these materials in the oxidation reaction of aniline and styrene.

(v) Synthesis of zirconium-containing mesoporous materials HMS by various preparation routes and application of these materials in the oxidation reaction of aniline and styrene.

(vi) Detailed characterization of cobalt and zirconium containing MCM-41 and HMS.

1.9. OUTLINE OF THE THESIS

The thesis is presented in SIX chapters, a brief summary of which is given below.

Chapter 1 presents brief history of catalyst and the phenomenon of catalysis. The thermodynamic aspects of the catalyst were discussed in short with the energy profile diagram. The information about development and applications of various porous materials has been stated. The general introduction about various physicochemical aspects of mesoporous had been mentioned. The different characteristic properties of these materials, synthesis parameters, formation mechanisms, different approaches for surface-functionalization, characterization techniques and application as supports for different catalytically active transformations are discussed in brief. The scope and objectives of the present work have been outlined at the end of this chapter.

Chapter 2 deals with the synthesis of cobalt-containing mesoporous MCM-41 and HMS by different synthesis methods (direct substitution, grafting and immobilization). The materials were characterized by XRD, N_2 sorption technique, FT-IR, UV-Vis, AAS, TEM and SEM. The main emphasis was given on determining the local environment of metal species.

Chapter 3 deals with the catalytic activity of the cobalt containing MCM-41 and HMS for the oxidation of ethylbenzene and diphenylmethane using different oxidant [30 wt % hydrogen peroxide (H_2O_2) and 70 wt % ter. butyl hydroperoxide (TBHP)]

under different reaction conditions and compared with zirconium containing MCM-41 and studied in detail.

Chapter 4 deals with the synthesis of zirconium-containing mesoporous MCM-41 and HMS by different synthesis methods (direct substitution, grafting and immobilization). The materials were characterized by XRD, N_2 sorption technique, FT-IR, UV-Vis, AAS, TEM and SEM. The characterization was mainly focused to trace out coordination and oxidation state of the zirconium species.

Chapter 5 deals with the potential use of zirconium containing MCM-41 and HMS for the oxidation of aniline and styrene with different reaction parameters. The main focus was to use these zirconium containing MCM-41 and HMS for the selective oxidation reactions.

Chapter 6 summarizes the results obtained and the basic findings of the present study.

1.10. References

[1] J. J. Berzelius, P. A. Reseanteckningar, Norstedt & Soner, Stockholm, 1903.

[2] www.answers.com/topic/catalysis

[3] S. Green, Industrial Catalysis, Macmillan Company, New York, 1928.

[4] (a) J. R. Partington, A history of chemistry, Vol. 4, Macmillan, London, 1964. (b) J. Mellor, J. Phys. Chem., 7 (1903) 557.

[5] G. M. Kirchhoff, J. Schweiggers, 4 (1812) 108.

[6] G. M. Schwab, J. R. Anderson, M. Boudart (Eds.), Catalysis Science and Technology, Vol. 2, Springer, New York, 1981.

[7] B. H. Davis, G. Ertl, H. Knözinger and J. Weitkamp (Eds.), Handbook of Heterogeneous Catalysis, Vol. 1, VCH, Weinheim, 1997.

[8] J. R. Partington, A short history of chemistry, Macmillan, London, 1939.G. Lemoine, Ann. Chim. Phys., 12 (1877) 145.

[9] K. S. W. Sing, D. H. Everett, R. A. W. Haul, L. Moscou, R. A. Pierotti, J. Rouquerol, T. Siemieniewska, Pure Appl. Chem. 57 (1985) 603.

[10] F. Schuth, K. Sing, J. Weitkamp, Handbook of Porous Solids, Vol. I–V, Wiley-VCH, Weinheim, 2002.

[11] M. E. Davis, C. Saldarriaga, C. Montes, J. Garces, C. Crowder, Nature 331 (1988) 698.

[12] B. J. Schoeman, J. Sterte, J. E. Otterstedt, J. Chem. Soc. Chem. Commun. (1993) 994.

[13] (a) A. H. Janssen, A. J. Koster, K. P. de Jong, Angew. Chem. Int. Ed. 40 (2001)

1102. (b) I. Schmidt, A. Boisen, E. Gustavsson, K. Stahl, S. Pehrson, S. Dahl, A. Carlsson, C. J. H. Jacobsen, Chem. Mater. 13 (2001) 4416.

[14] (a) V. Chiola, J. E. Ritsko, C. D. Vanderpool, US Patent No. 3 556, 725, 1971. (b) F. Di Renzo, H. Cambon, R. Dutartre, Micropor. Mater. 10 (1997) 283.

[15] J. S. Beck, C. T. W. Chu, I. D. Johnson, C. T. Kresge, M. E. Leonowicz, W. J. Roth, J. W. Vartuli, US Patent 91/11390, 1991.

[16] (a) C. T. Kresge, M. E. Leonowicz, W. J. Roth, J. C. Vartuli, J. S. Beck, Nature 359 (1992) 710. (b) J. S. Beck, J. C. Vartuli, W. J. Roth, M. E. Leonowicz, C. T. Kresge, K. D. Schmitt, C. Chu, D. H. Olson, E. W. Sheppard, S. B. McCullen, J. B. Higgins, J. L. Schenkler, J. Am. Chem. Soc. 114 (1992) 10834.

[17] T. Yanagisawa, T. Shimizu, K. Kuroda, C. Kato, Bull. Chem. Soc. Jpn. 63 (1990) 988.

[18] (a) S. Inagaki, Y. Fukushima, K. Kuroda, J. Chem. Soc. Chem. Commun. (1993) 680. (b) S. Inagaki, A. Koiwai, N. Suzuki, Y. Fukushima, K. Kuroda, Bull. Chem. Soc. Jpn. 69 (1996) 1449.

[19] (a) A. Corma, Chem. Rev. 97 (1997) 2373. (b) U. Ciesla, F. Schuth, Micropor. Mesopor. Mater. 27 (1999) 131. (c) M. Linden, S. Schacht, F. Schuth, A. Steel, K. Unger, J. Porous. Mater. 5 (1998) 177. (d) A. Tuel, Micropor. Mesopor. Mater. 27 (1999) 151. (e) P. Selvam, S.K. Bhatia, C.G. Sonwane, Ind. Eng. Chem. Res. 40 (2001) 3237.

[20] (a) Y. Liu, T. J. Pinnavaia, J. Mater. Chem. 12 (2002) 3179. (b) J.M. Thomas, Angew. Chem. Int. Ed. 38 (1999) 3588. (c) R. Anwander, Chem. Mater. 13

(2001) 4419. (d) J.Y. Ying, C. P. Mehnert, M. S. Wong, Angew. Chem. Int. Ed. 38 (1999) 56. (e) X. He, D. Antonelli, Angew. Chem. Int. Ed. 41 (2002) 214.

[21] (a) A. P. Wight, M. E. Davis, Chem. Rev. 102 (2002) 3589. (b) D. E. De Vos, M. Dams, B. F. Sels, P. A. Jacobs, Chem. Rev. 102 (2002) 3615. (c) G. J. de A. A. Soler-Illia, C. Sanchez, B. Leveau, J. Patarin, Chem. Rev. 102 (2002) 4093. (d) D. Trong On, D. Desplantier-Giscard, C. Danumah, S. Kaliaguine, Appl. Catal. A: Gen. 253 (2003) 545. (e) A. Wingen, F. Kleitz, F. Schuth, M. Baerns (Ed.), Basic Principles in Applied Catalysis, Springer, Berlin, 2003, P. 281. (f) F. Schuth, Chem. Mater. 13 (2001) 3184.

[22] (a) F. Di Renzo, A. Galarneau, P. Trens, F. Fajula, in: F. Schuth, K. S. W. Sing, J. Weitkamp (Eds.), Handbook of Porous Solids, Wiley-VCH, Weinheim, 2002, 1311, (b) A. Monnier, F. Schuth, Q. Huo, D. Kumar, D. Margolese, R. S. Maxwell, G. Stucky, M. Krishnamurty, P. Petroff, A. Firouzi, M. Janicke, B. Chmelka, Science 261 (1993) 1299. (c) Q. Huo, D. Margolese, U. Ciesla, P. Feng, T. Gier, P. Sieger, R. Leon, P.M. Petroff, U. Ciesla, F. Schuth, G. Stucky, Nature 368 (1994) 317.

[23] (a) D. M. Antonelli, J. Y. Ying, Angew. Chem. Int. Ed. 34 (1995) 2014. (b) U. Ciesla, S. Schacht, G. D. Stucky, K. Unger, F. Schuth, Angew. Chem. Int. Ed. Engl. 35 (1996) 541.

[24] C. T. Kresge, M. E. Leonowicz, W. J. Roth, J. C. Vartuli (Mobil Oil Corp.), US-A 5098 684, 1992.

[25] J. S. Beck, J. C. Vartuli, G. J. Kennedy, C. T. Kresge, W. J. Roth, S. E.

Schramm, Chem. Mater. 6 (1994) 1816.

[26] C. F. Cheng, H. He, W. Zhou, J. Klinowski, Chem. Phys. Lett. 244 (1995) 117.

[27] A. Monnier, F. Schuth, Q. Huo, D. Kumar, D. I. Margolese, R. S. Maxwell, G. D. Stucky, M. Krishnamurthy, P. Petroff, A. Firouzi, M. Janicke, B. F. Chmelka, Science 261 (1993) 1299.

[28] G. D. Stucky, A. Monnier, F. Schuth, Q. Huo, D. I. Margolese, D. Kumar, M. Krishnamurthy, P. Petroff, A. Firouzi, M. Janicke, B. F. Chmelka, Mol. Cryst. Liq. Cryst. 240 (1994) 187.

[29] (a) A. Firouzi, D. Kumar, L. M. Bull, T. Besier, P. Sieger, Q. Huo, S. A. Walker, J. A. Zasadzinski, C. Glinka, J. Nicolas, D. I. Margolese, G. D. Stucky, B. F. Chmelka, Science 267 (1995) 1138. (b) A. Firouzi, F. Atef, A. G. Oertli, G. D. Stucky, B. F. Chmelka, J. Am. Chem. Soc. 119 (1997) 3596.

[30] (a) Q. Huo, D. I. Margolese, U. Ciesla, P. Feng, P. Sieger, R. Leon, P. Petroff, F. Schuth, G. D. Stucky, Nature 368 (1994) 317. (b) Q. Huo, D. I. Margolese, U. Ciesla, D. G. Demuth, P. Feng, T. E. Gier, P. Sieger, A. Firouzi, B. F. Chmelka, F. Schuth, G. D. Stucky, Chem. Mater. 6 (1994) 1176.

[31] S. A. Bagshaw, E. Prouzet, T. J. Pinnavaia, Science 269 (1995) 1242.

[32] (a) P. T. Tanev, T. J. Pinnavaia, Chem. Mater. 8 (1996) 2068. (b) P. T. Tanev, T. J. Pinnavaia, Science 271 (1996) 1267. (c) P. T. Tanev, T. J. Pinnavaia, Science 267 (1995) 865. (d) S. S. Kim, W. Zhang, T. J. Pinnavaia, Science 282 (1998) 1302. (e) D. M. Antonelli, J. Y. Ying, Angew. Chem. Int. Ed. 35 (1996) 426. (f) A. Davidson, Curr. Opinion in Colloid & Inter. Sci. 7 (2002) 92.

[33] D. M. Antonelli, J. Y. Ying, Angew. Chem. Int. Ed. 35 (1996) 426.

[34] (a) J. Y. Ying, C. P. Mehnert, M. S. Wong, Angew. Chem. Int. Ed. 38 (1999) 56. (b) A. Sayari, S. Hamoudi, Chem. Mater. 13 (2001) 3151.

[35] A. P. Wight, M. E. Davis, Chem. Rev. 102 (2002) 3589.

[36] (a) D. E. De Vos, M. Dams, B. F. Sels, P. A. Jacobs, Chem. Rev. 102 (2002) 3605. (b) X. Feng, G. E. Fryxell, l. Q. Wang, A. Y. Kim, J. Liu, K. M. Kemner, Science 276 (1997) 923. (c) D. Brunel, N. Bellocq, P. Sutra, A. Cauvel, M. Lasperas, P. Moreau, F. D. Renzo, A. Galarneau, F. Fajula, Coord. Chem. Rev. 178 (1998) 1085. (d) A. Stein, B. J. Melde, R. C. Schroden, Adv. Mater. 12 (2000) 1403.

[37] (a) T. Yokoi, H. Yoshitake, T. Tatsumi, J. Mater. Chem. 14 (2004) 951. (b) H-P. Lin, L-Y. Yang, C-Y. Mou, S-B. Liu, H-K. Lee, New J. Chem. 24 (2000) 253. (c) H. Q. Yang, G. Y. Zhang, X. L. Hong, Y. Y. Zhu, Microporous Mesoporous Mater. 68 (2004) 119.

[38] P. M. Price, J. H. Clark, D. J. Macquarrie, J. Chem. Soc., Dalton Trans. 2000, 101.

[39] X. S. Zhao, G. Q. Lu, J. Phys. Chem. B 102 (1998) 1556.

[40] A. Stein, B. J. Melde, R. C. Schroden, Adv. Mater. 12 (2000) 1403.

[41] J. Liu, X. Feng, G. E. Fryxell, L. Q. Wang, A. Y. Kim, M. Gong, Adv. Mater. 10 (1998) 161.

[42] K. K. Unger, Porous Silica- Its Properties and Use as Support in Column Liquid Chromatography, Vol. 16, Elsevier, Amsterdam, 1979.

[43] L. Mercier, T. J. Pinnavaia, Environ. Sci. Tech. 32 (1998) 2749.

[44] J. Liu, G. E. Fryxell, S. Mattigod, T. S. Zemanian, Y. Shin, L. Q. Wang, in Proc. Nanoporous Materials II, Banff, Canada, 2000

[45] T. Kimura, S. Saeki, Y. Sugahara, K. Kuroda, Langmuir 15 (1999) 2794.

[46] (a) X. S. Zhao, G. Q. Lu, J. Phys. Chem. B 102 (1998) 1556. (b) R. Anwander, C. Palm, J. Stelzer, O. Groeger, E. Engelhardt, Stud. Surf. Sci.Catal. 117 (1998) 135. (c) R. Anwander, I. Nagl, M. Widenmeyer, G. Engelhardt, O. Groeger, C. Palm, T. Roser, J. Phys. Chem. B 104 (2000) 3532. (d) V. Antochshuk, M. Jaroniec, J. Phys. Chem. B 103 (1999) 6252. (e) C. P. Jaroniec, M. Kruk, M. Jaroniec, A. Sayari, J. Phys. Chem. B 102 (1998) 5503.

[47] (a) R. Anwander, C. Palm, J. Stelzer, O. Groeger, E. Engelhardt, Stud. Surf. Sci.Catal. 117 (1998) 135. (b) R. Anwander, I. Nagl, M. Widenmeyer, G. Engelhardt, O. Groeger, C. Palm, T. Roser, J. Phys. Chem. B 104 (2000) 3532.

[48] T. Asefa, M. Kruk, M. J. MacLachlan, N. Coombs, H. Grondey, M. Jaroniec, G. A. Ozin, J. Am. Chem. Soc. 123 (2001) 8520.

[49] M. H. Lim, C. F. Blanford, A. Stein, J. Am. Chem. Soc. 119 (1997) 4090.

[50] M. H. Lim, C. F. Blanford, A. Stein, Chem. Mater. 10 (1998) 467.

[51] W. M. Van Rhijn, D. E. De Vos, B. F. Sels, W. D. Bosaert, P. A. Jacobs, Chem. Commun. (1998) 317.

[52] (a) J. H. Clark, D. J. Macquarrie, Chem. Commun. (1998) 853. (b) D. Brunel, Micropor. Mesopor. Mater. 27 (1999) 329.

[53] P. Sutra, D. Brunel, Chem. Commun. (1996) 2485.

[54] M. H. Lim, A. Stein, Chem. Mater. 11 (1999) 3285.

[55] D. S. Shepherd, W. Zhou, T. Maschmeyer, J. M. Malters, C. L. Roper, S. Parsons, B. F. G. Johnson, M. J. Duer, Angew. Chem. Int. Ed. 37 (1998) 2719.

[56] F. De Juan, E. R. Hitzky, Adv. Mater. 12 (2000) 430.

[57] V. Antochshuk, M. Jaroniec, Chem. Commun. (1999) 2373.

[58] C. Sanchez, F. Ribot, New J. Chem. 18 (1994) 1007.

[59] (a) S. L. Burkett, S. D. Sims, S. Mann, Chem. Commun. (1996) 1367. (b) D. J. Macquarrie, Chem. Commun. (1996) 1961. (c) Q. Huo, D. I. Margolese, G. D. Stucky, Chem. Mater. 8 (1996) 1147.

[60] A. Stein, B. J. Melde, R. C. Schroden, Adv. Mater. 12 (2000) 1403.

[61] (a) D. S. Shepherd, W. Zhou, T. Maschmeyer, J. M. Malters, C. L. Roper, S. Parsons, B. F. G. Johnson, M. J. Duer, Angew. Chem. Int. Ed. 37 (1998) 2719. (b) S. R. Hall, C. E. Fowler, B. Lebeau, S. Mann, Chem. Commun. (1999) 201. (c) F. Babonneau, L. Leite, S. Fontlupt, J. Mater. Chem. 9 (1999) 175. (d) V. Goletto, V. Dagry, F. Babonneau, Mater. Res. Soc. Symp. Proc. 576 (1999) 229. (e) L. Mercier, T. J. Pinnavaia, Chem. Mater. 12 (2000) 188. (f) R. Richer, L. Mercier, Chem. Commun. (1998) 1775. (g) J. Brown, R. Riche, L. Mercier, Microporous Mesoporous Mater. 37 (2000) 41.

[62] (a) A. Corma, Chem. Rev. 97 (1997) 2373. (b) A. Sayari, Chem. Mater. 8 (1996) 1840.

[63] J. Y. Ying, C. P. Mehnert, M. S. Wong, Angew. Chem. Int. Ed. 38 (1999) 56.

[64] R. A. Sheldon, M. Wallau, I. W. C. E. Arends, U. Schuchardt, Acc. Chem. Res.

31 (1998) 485.

[65] (a) M. Janicke, D. Kumar, G. D. Stucky, B. F. Chmelka, Stud. Surf. Sci. Catal. 84 (1994) 243. (b) M. Hartmann, C. Bischof, Stud. Surf. Sci. Catal. 117 (1998), 249. (c) Z. Luan, H. He, C. F. Cheng, W. Zhou, J. Klinowski, J. Phys. Chem. B 99 (1995) 1018.

[66] D. R. Rolison, Science, 299 (2003) 1698.

[67] P. T. Tanev, M. Chibwe, T. J. Pinnavaia, Nature 368 (1994) 321.

[68] D. Wei, W. T. Chueh, G. L. Haller, Catal. Today 51 (1999) 501.

[69] (a) R. B. Borade, A. Clearfield, Catal. Lett. 31 (1995) 267. (b) Q. Kan, V. Fornes, F. Rey, A. Corma, J. Mater. Chem. 10 (2000) 993.

[70] (a) T. Ishikawa, M. Matsuda, A. Yasukawa, J. Chem. Soc., Faraday Trans. 92 (1996) 1985. (b) A. Jentys, N. H. Pham, H. J. Vinek, J. Chem. Soc., Faraday Trans. 92 (1996) 3287.

[71] (a) A. Corma, J. L. Jorda, M. T. Navarro, F. Rey, Chem. Commun. (1998) 1899. (b) N. Igarashi, S. Kidani, R. Ahemaito, K. Hashimoto, T. Tatsumi, Micropor. Mesopor. Mater. 81 (2005) 97.

[72] A. Bhaumik, T. Tatsumi, J. Catal. 189 (2000) 31.

[73] (a) A. Bhaumik, M. P. Kapoor, S. Inagaki, Chem. Commun. (2003) 470. (b) M. P. Kapoor, A. K. Sinha, S. Seelan, S. Inagaki, S. Tsubota, H. Yoshida, M. Haruta, Chem. Commun. (2002) 2902. (c) M. A. Wahab, C-S. Ha, J. Mater. Chem. 15 (2005) 508. (d) Q. Yang, Y. Li, L. Zhang, J. Yang, J. Liu, C. Li, J. Phys. Chem. B 108 (2004) 7934.

[74] (a) A. Bhaumik, M. P. Kapoor, S. Inagaki, Chem. Commun. (2003) 470.

[75] (a) Q. Yang, Y. Li, L. Zhang, J. Yang, J. Liu, C. Li, J. Phys. Chem. B 108 (2004) 7934. (b) Y. Xia, W. Wang, R. Mokaya, J. Am. Chem. Soc. 127 (2005) 790. (c) Q. Yang, J. Yang, Z. Feng, Y. Li, J. Mater. Chem. 15 (2005) 4268.

[76] J. Patarin, Angew. Chem. Int. Ed. 43 (2004) 1.

[77] (a) S. Hitz, R. Prins, J. Catal. 168 (1997) 194. (b) P. T. Tanev, T. J. Pinnavaia, Chem. Mater. 8 (1996) 2068.

[78] H. Lee, S. I. Zones, M. E. Davis, Nature 425 (2003) 385.

[79] (a) N. Husing, Angew. Chem. Int. Ed. 43 (2004) 3216. (b) C-H. Lee, T-S. Lin, CY. Mou, J. Phys. Chem. B 107 (2003) 2543. (c) C. D. Nunes, M. Pillinger, A. A. Valente. J. Rocha, A. D. Lopes, I. S. Goncalves, Eur. J. Inorg. Chem. (2003) 3870. (d) L. L. Welbes, A. S. Borovik, Acc. Chem. Res. 38 (2005) 765. (e) A. Taguchi, F. Schuth, Microporous Mesoporous Mater. 77 (2004) 1. (f) C. T. Fischel, R. J. Davis, J. M. Garcer, J. Catal. 163 (1996) 141. (g) R. Ryoo, C. H. Ko, J. M. Kim, R. Howe, Catal. Lett. 37 (1996) 29.

[80] (a) J. Jamis, J. R. Anderson, R. S. Dickson, E. M. Campi, W. R. Jackson, J. Organomet. Chem. 627 (2001) 37. (b) K. Mukhopadhyay, B. R. Sarkar, R. V. Chaudhari, J. Am. Chem. Soc. 124 (2002) 9692. (c) C. Baleizao, B. Gigante, M. J. Sabatier, H. Garcia, A. Corma, Appl. Catal. A. Gen. 288 (2002) 279. (d) S. Xiang, Y. Zhang, Q. Xin, C. Li, Angew. Chem. Int. Ed. 41 (2002) 821. (e) A. Poppl, P. Baglioni, L. Kevan, J. Phys. Chem. 99 (1995) 14156. (f) W. Bohlmann, K. Schandert, A. Poppl, H. C. Semmelhack, Zeolites 19 (1997) 297.

[81] D. J. Cole Hamilton, Science 299 (2003) 1702.

[82] (a) D. E. De Vos, M. Dams, B. F. Sels, P. A. Jacobs, Chem. Rev. 102 (2002) 3605. (b) W. F. Maier, J. A. Marten, S. Klein, J. Heilmann, R. Parton, K. Vercruysse, P. A. Jacobs, Angew. Chem. Int. Ed. 35 (1996) 180. (b) N. A. Herron, Inorg. Chem. 25 (1986) 4714.

[83] C. A. McNamara, M. J. Dixon, M. Bradley, Chem. Rev. 2002, 102, 3275.

[84] (a) J. W. Niemantsverdriet, Spectroscopic Methods in Heterogeneous Catalysis, VCH, Weinheim (1993) 82. (b) S. Biz, M. Occelli, Catal. Rev-Sci. Eng. 40 (1998) 329. (c) G. Bergeret in: Handbook of Heterogeneous Catalysis, Vol. 2, Eds, G. Ertl, H. Knozinger, J. Weitkamp, Wiley-VCH, Weinheim (1997) 464.

[85] W. H. Bragg, W. L. Bragg, The Crystalline State, Vol. 1, McMillan, New York, 1949.

[86] W. H. Bragg, W. L. Bragg, The Crystalline State, Vol. 1, McMillan, New York, 1949.

[87] S. Brunauer, P. H. Emmett, E. Teller, J. Am. Chem. Soc. 60 (1938) 309.

[88] E. P. Barrett, L. G. Joyner, P. P. Halenda, *J. Am. Chem. Soc*. **1951**, *73*, 373.

[89] J. I. Goldstein, H. Yakowitz (Eds.), Practical Scanning Electron Microscopy, Plenum Press, New York, 1975.

[90] G. Lawes, Scanning Electron Microscopy and X-Ray Microanalysis, John Wiley and Sons Ltd., Chichester, 1987.

[91] J. R. Fryer, Chemical Applications of Transmission Electron Microscopy, Academic Press, San Diego, 1979.

[92] J. M. Thomas, O. Terasaki, P. L. Gai, W. Zhou, J. Gonzalez-Calbet, Acc. Chem. Res. 34 (2001) 583.

[93] R. P. Eischens, W. A. Pliskin, Adv. Catal. 10 (1958) 1.

[94] (a) C. C. Freyhardt, M. Tsapatsis, Jr. Balkus, M. E. Balkus, M. E. Davis, Nature 381 (1996) 295. (b) P. A. Jacobs, W. Y. Martier, Zeolites 2 (1982) 226.

[95] (a) B. Notari, Stud. Surf. Sci. Catal. 37 (1987) 413. (b) G. N. Vayssilov, Catal.Rev. (1997) 209.

[96] J. Ryczkowski, Catal. Today 68 (2001) 263.

[97] J. W. Niemantsverdriet, Spectroscopic Methods in Heterogeneous Catalysis, VCH, Weinheim, 1993.

[98] (a) B. M. Weckhuysen, R. A. Schoonheydt, Catal. Today 49 (1999) 441. (b) R. A. Schoonheydt, Diffuse Reflectance Spectroscopy in Characterization of Heterogeneous Catalysts, F. Delannay (Ed.) Marcel Dekker, New York, 1984.

[99] (a) B. M. Weckhuysen, I. P. Vannijvel, R. A. Schoonheydt, Zeolites 15 (1995) 482. (b) X. T. Gao, I. E. Wachs, J. Phys. Chem. B 104 (2000) 1261. (c) X. T. Gao, I. E. Wachs, J. Catal. 188 (1999) 325.

[100] (a) T. A. Carlson, X-Ray Photoelectron Spectroscopy, Dowden, Hutchinson & Ross: Stroudsburg, PA, 1978. (b) D. Briggs, M. P. Seah (Eds.), Practical Surface Analyses, Vol. 1: Auger and X-Ray Photoelectron Spectroscopy (2nd Ed.), New York, 1990.

[101] J. W. Niemantsverdriet, Spectroscopic Methods in Heterogeneous Catalysis, VCH, Weinheim, 1993.

[102] (a) B. M. Weckhuysen, D. M. Keller, Catal. Today 78 (2003) 25. (b) B. M. Weckhuysen, I. E. Wachs, R. A. Schoonheydt, Chem. Rev. 96 (1996) 3327.

[103] (a) A. Sayari, Chem. Mater. 8 (1996) 1840. (b) J. Y. Ying, C. P. Mehnert, M. S.Wong, Angew. Chem. Int. Ed. 38 (1999) 56.

[104] (a) W. M. Van Rhijn, D. E. De Vos, W. Bossaert, J. Bullen, B. Wouters, P. Grobet, P. A. Jacobs, Stud. Surf. Sci. Catal. 117 (1998) 183. (b) W. D. Bossaert, D. E. DeVos, W. M. Van Rhijn, J. Bullen, P. J. Grobet, P. A. Jacobs, J. Catal. 182 (1999) 156.

[105] (a) D. J. Macquarrie, Green Chem. (1999) 195. (b) A. Cauvel, G. Renard, D. Brunel, J. Org. Chem. 62 (1997) 749. (c) D. J. Macquarrie, D. B. Jackson, Chem. Commun. 1997) 1781. (d) R. A. Sheldon, R. S. Downing, Appl. Catal. A. Gen. 189 (1999) 163.

[106] (a) T. Maschmeyer, R. D. Oldroyd, G. Sankar, J. M. Thomas, I. J. Shannon, J. A. Klepetko, A. F. Masters, J. K. Beattie, C. R. A. Catlow, Angew. Chem. Int. Ed. 36 (1997) 1639. (b) C. J. Liu, S. G. Li, W. Q. Pang, C. M. Che, Chem. Commun. (1997) 65.

[107] (a) R. Anwander, C. P. Gerstberger, O. Groeger, G. Engelhardt, Chem. Commun. (1998) 1811. (b) S-G. Shyu, S-W. Cheng, D-L. Tzou, Chem. Commun. (1999) 2337.

[108] (a) N. Bellocq, S. Abramson, M. Laspyras, D. Brunel, P. Moreau, Tet. Assym. 10 (1999) 3229. (b) S. J. Bae, S-W. Kim, T. Hyeon, B. M. Kim, Chem. Commun. (2000) 31.

[109] (a) X. Lin, G. K. Chuah, S. Janicke, J. Mol. Catal. A. Chem. 150 (1999) 287. (b) G. Gerstberger, C. Palm, R. Anwander, Chem. Eur. J. 5 (1999) 997.

[110] T. Asefa, M. Kruk, M. J. MacLachlan, N. Coombs, H. Grondey, M. Jaroniec, G.A. Ozin, J. Am. Chem. Soc. 123 (2001) 8520.

[111] T. Joseph, S. S. Deshpande, S. B. Halligudi, A. Vinu, S. Ernst, M. Hartman, J. Mol. Catal. A. Chem. 206 (2003) 13.

[112] (a) N. A. Milas, S. Sussman, J. Am. Chem. Soc. 58 (1936) 1302. (b) N. A. Milas, S. Sussman, J. Am. Chem. Soc. 59 (1937) 2345. (c) N. A. Milas, J. Am. Chem. Soc. 59 (1937) 2342.

[113] K. A. Jorgensen, Chem. Rev. 89 (1989) 431.

[114] (a) R. A. Sheldon, J. Dakka, Catal. Today 19 (1994) 215. (b) H. E. B. Lempers, R. Garcia, R. A. Sheldon, J. Org. Chem. 63 (1998) 1408.

[115] (a) H. Mimoun, M. Mignard, P. Brechot, L. Saussine, J. Am. Chem. Soc. 108 (1986) 3711. (b) H. Mimoun, Catal. Today 1 (1987) 281. (c) E. S. Gould, R. R. Hiatt, K. C. Irwin, J. Am. Chem. Soc. 90 (1968) 4573. (d) A. Waldemar, A. Corma, I. Reddy, M. Renz, J. Org. Chem. 62 (1997) 3631.

[116] J. Muzart, Chem. Rev. 92 (1992) 113.

[117] C-M. Che, Pure Appl. Chem. 2 (1995) 225.

[118] M. H. Lim, C. F. Blanford, A. Stein, J. Am. Chem. Soc. 119 (1997) 4090.

[119] (a) G. Bellussi, M. S. Rigutto, Stud. Surf. Sci. Catal. 85 (1994) 177. (b) W. M. Meier, D. H. Olson, Ch. Baerlocher, Zeolites 17 (1996) 1. (c) P. R. H. Prasad Rao, A. A. Belhekar, S. G. Hegde, A. V. Ramaswamy, P. Ratnasamy, J. Catal.

141 (1993) 595. (d) T. Selvam, A. P. Singh, J. Chem. Soc., Chem. Commun. (1995) 883.

[120] (a) V. Hulea, E. Dumitriu, Appl. Catal. A. Gen. 277 (2004) 99. (b) A. Corma, P. Esteve, A. Martinez, J. Catal. 161 (1996) 11. (c) K. A. Koyano, T. Tatsumi, Microporous Mater. 10 (1997) 259.

[121] (a) J. M. R. Gallo, I. S. Paulino, U. Schuchardt, Appl. Catal. A. Gen. 266 (2004) 223. (b) W. Zhang, M. Froba, J. Wang, P. T. Tanev, J. Wong, T. J. Pinnavaia, J. Am. Chem. Soc. 118 (1996) 9164.

[122] (a) N. Ulagappan, C. N. R. Rao, Chem. Commun. (1996) 1047. (b) A. Sakthivel, P. Selvam, J. Catal. 211 (2002) 134. (c) A. Sakthivel, S. E. Dapurkar, P. Selvam, Catal. Lett. 77 (2001) 155.

[123] (a) R. J. Mahalaingam, S. K. Badamali, P. Selvam, Chem. Lett. (1999) 1121. (b) S. E. Dapurkar, A. Sakthivel, P. Selvam, New J. Chem. 27 (2003) 1184.

[124] Y. Wang, Q. Zhang, T. Shishido, K. Takehira, J. Catal. 209 (2002) 186.

[125] (a) V. Parvulescu, B. L. Su, Catal. Today 69 (2001) 315. (b) R. Neumann, A. M. Khenkin, Chem. Commun. (1996) 2643. (c) Q. Tang, Q. Zhang, H. Wu, Y. Wang, J. Catal. 230 (2005) 393.

[126] (a) K. Chaudhari, T. K. Das, P. R. Rajmohanan, L. Lazar, S. Sivasanker, A. J. Chandwadkar, J. Catal. 183 (1999) 281. (b) A. Corma, M. T. Navarro, L. Nemeth, M. Renz. Chem. Commun. (2001) 2190.

[127] (a) M. L. W. Vorstenbosch, Ph.D Thesis, Schuit Institute of Catalysis, Eindhoven University of Technology, The Netherlands, 2002. (b) S. Shylesh, A.

P. Singh, J. Catal. 228 (2004) 333.

[128] S. C. Laha, R. Kumar, J. Catal. 204 (2001) 64.

[129] (a) A. Corma, J. L. Jorda, M. T. Navarro, F. Rey, Chem. Commun. (1998) 1899. (b) N. Igarashi, S. Kidani, R. Ahemaito, K. Hashimoto, T. Tatsumi, Microporous Mesoporous Mater. 81 (2005) 97. (c) A. Bhaumik, T. Tatsumi, J. Catal. 189 (2000) 31. (d) A. Bhaumik, M. P. Kapoor, S. Inagaki, Chem. Commun. (2003) 470. (e) M. P. Kapoor, A. K. Sinha, S. Seelan, S. Inagaki, S. Tsubota, H. Yoshida, M. Haruta, Chem. Commun. (2002) 2902. (f) M. A. Wahab, C-S. Ha, J. Mater. Chem. 15 (2005) 508. (g) Q. Yang, Y. Li, L. Zhang, J. Yang, J. Liu, C. Li, J. Phys. Chem. B 108 (2004) 7934.

[130] (a) A. Sayari, Chem. Mater. 8 (1996) 1840. (b) A. Taguchi, F. Schuth, Micropor. Mesopor. Mater. 77 (2004) 1.

2.1. Introduction

In 1992, scientist at Mobil Oil Corporation discovered new family of mesoporous materials, M41S family (MCM-41, MCM-48, MCM-50) [1,2]. MCM-41 posses hexagonal arrangement of mono dimensional pores with pore diameter of 20-100 Å. It has large surface area (more than 1000 m^2g^{-1}), which is attractive for the designing new selective heterogeneous catalyst in production of fine chemicals on large scale [1-3]. Moreover, the large pore volume is noticeable that facilitate its application for the bulkier molecules. One of the striking features of this material is that the wide range of pore diameters can be obtained very easily by changing the alkyl chain length of the template molecule. Moreover, it has higher surface areas as well as high hydrocarbon sorption capacity [2]. It is believed that MCM-41 materials are formed by LCT (Liquid Crystalline Templating) mechanism where the ionic interaction of surfactant and silica takes place. Later, some innovative mesoporous materials like SBA-15 [4], KIT-6 [5] and HMS [6] were reported.

For the first time Pinnavaia and co-workers used the neutral surfactant (amine surfactant) for the synthesis of mesoporous materials. In the formation of these materials neutral templating mechanism (S^oI^o) is operative which is based on hydrogen bonding and self-assembly between neutral primary amine surfactant (S^o) and neutral inorganic precursor (I^o) [6,7]. This neutral S^oI^o templating route afforded a distinguishable subset of hexagonal molecular sieves, designated as HMS [6]. Unlike MCM-41, HMS materials lack higher order Bragg reflections in the XRD patterns while the electron diffraction patterns showed that they possessed hexagonal symmetry similar to MCM-41. Tanev et al reported the synthesis of titanium

containing hexagonal mesoporous silica (Ti-HMS) by using neutral amine surfactant for the first time and shown its high catalytic activity than the Ti-MCM-41 catalysts for bulky substrates [6,8]. Mesoporous materials have the potential to use as catalyst and support materials for catalytically active metal and metal oxides.

Compared to conventional microporous zeolite, mesoporous materials possess many advantages such as high surface area, large pore size, narrow pore size distribution, and an ordered structure. However, the amorphous framework and the lack of active centers in the pure silica mesoporous material restricted their direct application. As a result, more research work concerning mesoporous material has been focused on enhancing their activity through chemical modification. Synthetic routes exploit various advantageous properties of mesoporous silica by the isomorphous substitution, impregnation, grafting and encapsulation of metal and metal complexes. Metal containing mesoporous materials had been studied as model catalyst for shape selective reactions of larger molecules, as a catalytic membrane, and for other important reactions such as reforming, oxidation and polymerization [9-12]. Because of the flexible structure of the amorphous silica wall, different kinds of heteroatom have been incorporated into the silica matrix with little structural deterioration. After the invention of mesoporous molecular sieves, efforts have been made in the area of incorporation of metal by different methods. Further investigation of different types of metal species and their effect in overall performance of the catalyst in the reaction of bulky molecules have been studied. The incorporation of cations like Al and Ti in the SiO_2 matrix results in a substantial increase of surface acidity as in the case of zeolites and such solids can be employed as acid catalyst whereas incorporation of cations like

Mn, Ni and Co lead to material with sites suitable for redox catalytic operations [13-17]. The silicate framework of MCM-41 is modified by isomorphous substitution of Al, Ti, Cr, Fe, Co and Sn [2,18-24]. Until now, elements like Ti, V, Al, B, Ga, and Fe were successfully incorporated in the framework of HMS [8,25,26].

This chapter describes in detail the synthesis (by different methods) and characterization of cobalt containing mesoporous silica materials. The chapter is divided into two sections, the first section deals with cobalt containing MCM-41 and second section deals with cobalt containing HMS.

2.2. Synthesis and Characterization of Cobalt containing MCM-41

2.2.1 Experimental

Chemicals used were fumed silica (99 % SiO_2, Aldrich), cetyl trimethyl ammonium bromide (CTMABr, Aldrich), sodium hydroxide (NaOH, Merck), trimethoxy propyl amine silane [97 %, $(CH_3CH_2O)_3Si(CH_2)_3NH_2$] and cobalt acetylacetone [$Co(acac)_2$, 99 %, Across]. All the chemicals were used without further purification.

2.2.1.1 Synthesis

2.2.1.1.1. Synthesis of Mesoporous MCM-41

Fumed silica and cetyltrimethylammonium bromide were used as silica source and surfactant, respectively. In a typical synthesis, CTMABr was dissolved in Sodium hydroxide (NaOH) solution. To this, fumed silica was added slowly and stirred for 6 h. The molar gel composition was as follows

$$1SiO_2: 0.19CTMABr: 0.4\ NaOH: 78H_2O$$

Finally, pH of the gel was maintained at 10.9 using dil. HCl. The gel was transferred to glass bottle (autoclavable) and kept in oil bath maintained at 100 ^oC for 48 h. Mixture was filtered, washed several times with distilled water under vacuum and dried at 100 ^oC. The as synthesized material was calcined at 525 ^oC for 12 h.

2.2.1.1.2. Synthesis of cobalt substituted MCM-41 (Co-MCM-41)

Co-MCM-41 was synthesized by direct hydrothermal method with different Si/Co ratio. Fumed silica was added slowly to the mixture, containing NaOH and

CTMABr, with constant stirring. After 1 h, calculated amount of cobalt acetylacetone for the respective Si/Co ratio was added and stirring was continued for another 5 h. The molar gel composition was

$$1\ SiO_2: x\ Co(acac)_2: 0.19\ CTMABr: 0.4\ NaOH: 120\ H_2O$$

Where 'x' is the calculated amount of cobalt acetylacetone for different Si/Co ratios. The pH of the gel was maintained at 10.5. The gel was transferred to autoclavable bottle kept in oil bath maintained at 100 ^oC for 3 days. Finally it was filtered, washed several times with distilled water and dried in air at 100 ^oC for 12 h. As synthesized material was calcined as described earlier. The materials were designated as Co-MCM-41 (100) and Co-MCM-41 (50) for Si/Co ratio of 100 and 50, respectively.

2.2.1.1.3. Synthesis of cobalt-grafted MCM-41 (Co/MCM-41)

Cobalt acetylacetone (0.094 and 0.182 g for 1 and 2 wt. % loading respectively) was dissolved in anhydrous toluene. To this, 2 g MCM-41 was added and refluxed at 100 ^oC for 12 h with constant stirring. Solvent was removed at its boiling temperatures using rotavapor. The sample was dried and calcined at 450 ^oC to remove the organic matter. Samples were designated as Co/MCM-41 (100) and Co/MCM-41 (50) for 1 and 2 wt % cobalt loading, respectively.

2.2.1.1.4. Synthesis of cobalt immobilized on MCM-41 (Co-/MCM-41)

Equal moles of trimethoxy propyl amine silane and cobalt acetylacetone (0.175 g of Cobalt acetylacetone and 0.126 g of trimethoxy propyl amine silane) were mixed in 100 ml toluene and stirred at room temperature for 6 h. After half an hour, 2 g MCM-41 was added to the solution. The resulting solution was kept in oil bath

maintained at 100 ^{0}C for 10 h with constant stirring. It was filtered, washed with acetone and dried at 70 ^{0}C for 6 h. Sample was designated as Co-/MCM-41.

2.2.1.2. Characterization

Powder X-ray diffraction pattern of the samples were recorded on a Rigaku D max III VC Ni filtered Cu Kα radiation, λ = 1.54 Å between 1 and 10 (2θ angle) with a scanning rate of 1^o/min. The specific surface area, total pore volume and average pore diameter were measured by the N_2 adsorption desorption method using NOVA 1200 (Quanta Chrome) instrument. The samples were activated at 300 ^{o}C for 3 h under vacuum and then adsorption desorption was conducted by passing nitrogen over the samples which was kept under liquid nitrogen. Pore size distribution was obtained by applying BJH pore analysis method to the desorption branch of nitrogen adsorption isotherm. SEM micrograph of the cobalt containing samples were obtained on JEOL-JSM 520 scanning microscope while the TEM images were performed on a JEOL-TEM 1200 EX instrument with 100 kV accelerating voltage to probe the mesoporosity of the material. Cobalt content in the samples was determined by atomic absorbance analysis using Perkin Elmer 11013 spectrometer after dissolution of the samples in HCl-HF solution. Diffuse reflectance UV-Vis spectra of the powder samples were recorded in the range 200-800 nm on Shimadzu UV 2101 PC spectrometer equipped with a diffuse reflectance attachment, using $BaSO_4$ as the reference. XPS measurements were performed on a VG Microtech ESCA 3000 instrument using non-monochromatized Mg Kα radiation at a pass energy of 50 eV and an electron take off

angle of 60 ^{o}. The correction of binding energy (B.E.) was performed by using the C_{1s} peak of carbon at 285 eV as reference.

2.2.2. Results and discussion

2.2.2.1. Powder X-ray diffraction

The low angle XRD patterns of the calcined MCM-41, Co-MCM-41, Co/MCM-41 and Co-/MCM-41 were shown in Fig. 2.1A. MCM-41 mesoporous material exhibits four *hkl* diffraction peaks consistent with the highly ordered structure of a hexagonal pore arrays. The first diffraction peak in MCM-41 related to the (100) plane exhibits the highest intensity among all the calcined samples. In addition to main reflection peak at low angle (2θ), the less intense secondary reflections due to plane (100), (200) and (210) are well distinguished which indicate the higher long range ordering of the mesoporous channels [1,2]. In cobalt incorporated MCM-41 (Si/Co = 100 and 50), four reflection peaks, characteristic of the hexagonal mesoporous structure, are clearly seen although the intensity is less when compared with pure MCM-41.

It has been found that with the increase in cobalt content, intensity of the main peak (100) decreases. This indicates fall in long range ordering of the mesoporous channels after incorporating the cobalt ion. Lattice parameter value (a_0) was observed 40.8 Å for pure MCM-41. In Co-MCM-41 (100), a_0 value is 44.1 Å, which is more than the corresponding value for pure MCM-41. This shows the incorporation of

cobalt in the framework. However, the decrease in the a_0 value has been observed for the sample Co-MCM-41 (50) but it is more than pure MCM-41 (Table 1).

This is due to some cobalt ions settled on the mesoporous silica wall and slightly decreases the a_0 value when it is compared with Co-MCM-41 (100). Hence we conclude that only certain amount of cobalt is accommodated in the framework beyond which it prefers to settle on the silica framework.

Table 2.1. Physical properties of cobalt containing MCM-41

Entry	Catalyst	Si/Co [a] (molar ratio)	2θ angle (deg.)	a_0 [b] (Å)	S_{BET} [c] (m^2g^{-1})	D_p [d] (Å)
1	MCM-41	-	2.50	40.80	1010	31.00
2	Co-MCM-41 (100)	107	2.31	44.11	1073	32.67
3	Co-MCM-41 (50)	47	2.37	43.00	1035	31.80
4	Co/ MCM-41 (100)	121	2.56	39.82	832	29.91
5	Co/ MCM-41 (50)	56	2.65	38.46	810	28.40
6	Co-/ MCM-41	62	2.90	35.15	700	-

[a] Cobalt content estimated by AAS analysis.

[b] Unit cell parameter values calculated using $a_0 = 2d_{100}/\sqrt{3}$.

[c] S_{BET} is the surface area calculated by BET method.

[d] D_p is the average pore diameter.

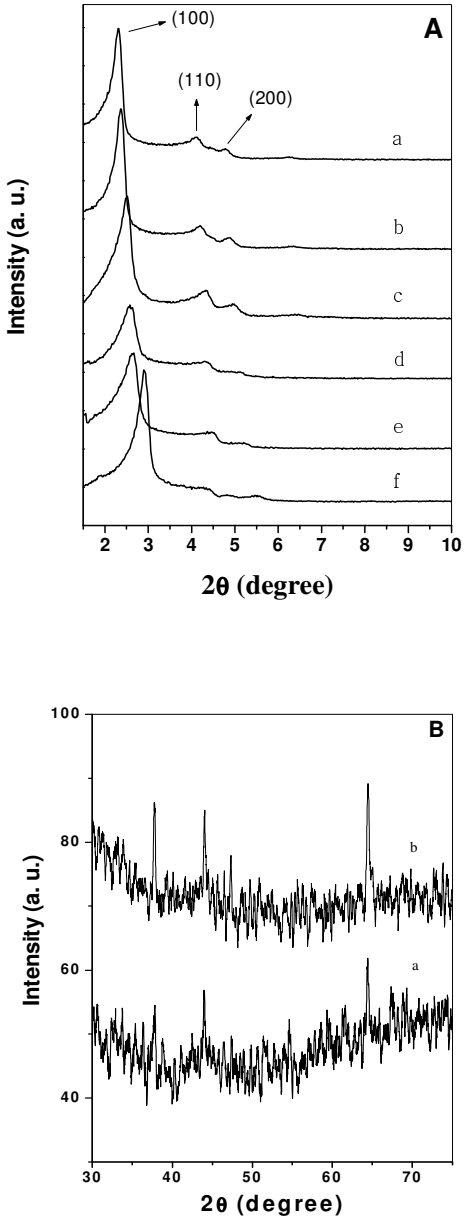

Fig. 2.1. XRD patterns of [A] (a) Co-MCM-41 (100), (b) Co-MCM-41 (50), (c) pure MCM-41, (d) Co/MCM-41 (100), (e) Co/MCM-41 (50) and (f) Co-/MCM-41; [B] Higher angle XRD pattern for samples (a) Co-MCM-41 (100) and (b) Co-MCM-41 (50).

In cobalt grafted MCM-41 samples, a_0 value decreases with the increasing amount of cobalt loading due to placement of the cobalt on the framework of MCM-41 thereby blocking the mesoporous channels. In cobalt immobilized MCM-41 samples, only (100) reflection peak is present. Absence of higher order reflection peaks indicates less ordering and homogeneity is lost after immobilization and hexagonal structure gets distorted. Moreover decrease in a_0 value is remarkable because of the presence of 3-amino propyl trimethoxy silane and cobalt. The higher angle XRD shows the presence of characteristic peaks of Co_3O_4 in cobalt incorporated MCM-41 (Fig. 2.1B). However the intensity is too low indicating the low amount of formation of microcrystal of cobalt oxide on the wall of MCM-41. It is very interesting to know that even for small amount of cobalt in Co-MCM-41 (100), peaks appeared in higher angle XRD. This may be due to synthesis procedure carried out in basic medium. Cobalt has property to form cluster like compound in highly basic condition. No such higher angle reflection peak was found in grafted cobalt samples.

2.2.2.2. N_2 adsorption desorption isotherms

Nitrogen adsorption-desorption isotherms and the corresponding BJH pore size distribution were shown in Fig. 2.2 and 2.3 [27,28]. All the isotherms exhibit type IV isotherms (IUPAC classification), characteristic of mesoporous material, with a sharp inflection at a relative pressure (P/P_o) in the range 0.3-0.5 due to condensation of N_2 in the pore channels [1,2]. In pore size distribution curve (Fig. 2.3), narrow and sharp peak is observed in the diameter range 20-25 Å showing uniform pore size. The isotherms of the cobalt incorporated samples (Co-MCM-41) show small hysterisis

loop in the lower pressure regions. We noted that the surface areas of Co-MCM-41 samples (1073 m^2g^{-1}) are comparatively more than pure MCM-41 (1010 m^2g^{-1}) and it is decreasing with the increase in metal content. The more surface area for Co-MCM-41 is an indication of well dispersion of cobalt atoms. In grafted Co/MCM-41 (with cobalt loading 1 and 2 wt %) and immobilized Co-/MCM-41samples surface area, pore volume and pore diameter was found decreased (Table 2.1). It is expected since in grafting and immobilization cobalt resides on the wall of mesoporous silica. It is found that for immobilized cobalt samples decrease in the surface area, pore volume and average pore diameter is more because of covalent bonding of the spacer on the wall of silica wall. This is in accordance with XRD result.

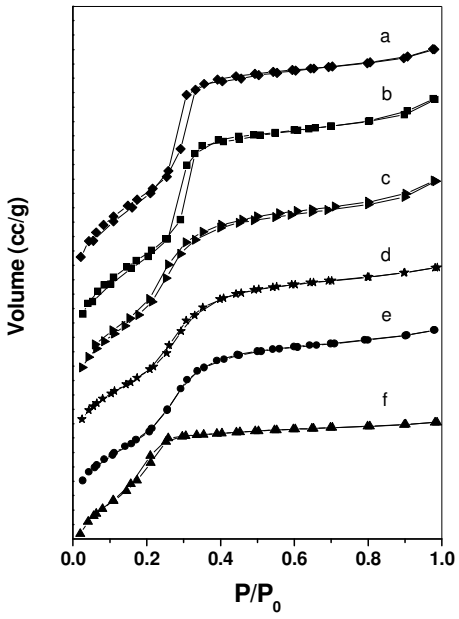

Fig. 2.2. N_2 adsorption desorption isotherms of (a) Co-MCM-41 (100), (b) Co-MCM-41 (50), (c) pure MCM-41, (d) Co/MCM-41 (100), (e) Co/MCM-41 (50) and (f) Co-/MCM-41.

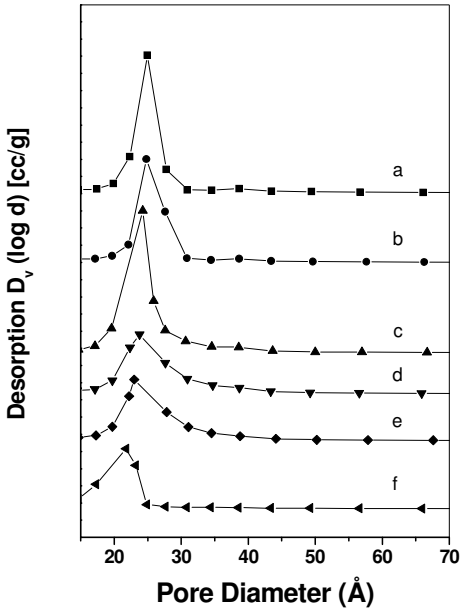

Fig. 2.3. Pore size distribution curves (calculated by BJH method) for the samples (a) Co-MCM-41 (100), (b) Co-MCM-41 (50), (c) pure MCM-41, (d) Co/MCM-41 (100), (e) Co/MCM-41 (50) and (f) Co-/MCM-41.

2.2.2.3. IR spectroscopy

Fig. 2.4A show the FT-IR spectra of the MCM-41 and cobalt containing MCM-41 in the range of 4000-400 cm^{-1}. Two bands around 1082 and 1228 cm^{-1} are associated to the internal and external asymmetric Si–O stretching modes. A strong band at 960 cm^{-1} is seen in the FT-IR spectra of MCM-41 and Co-MCM-41, attributed to stretching vibration of Si–O–Si and Si–O–Co bond. This band can be interpreted in terms of the overlapping of both Si–OH and Co–O–Si bond vibrations [29].

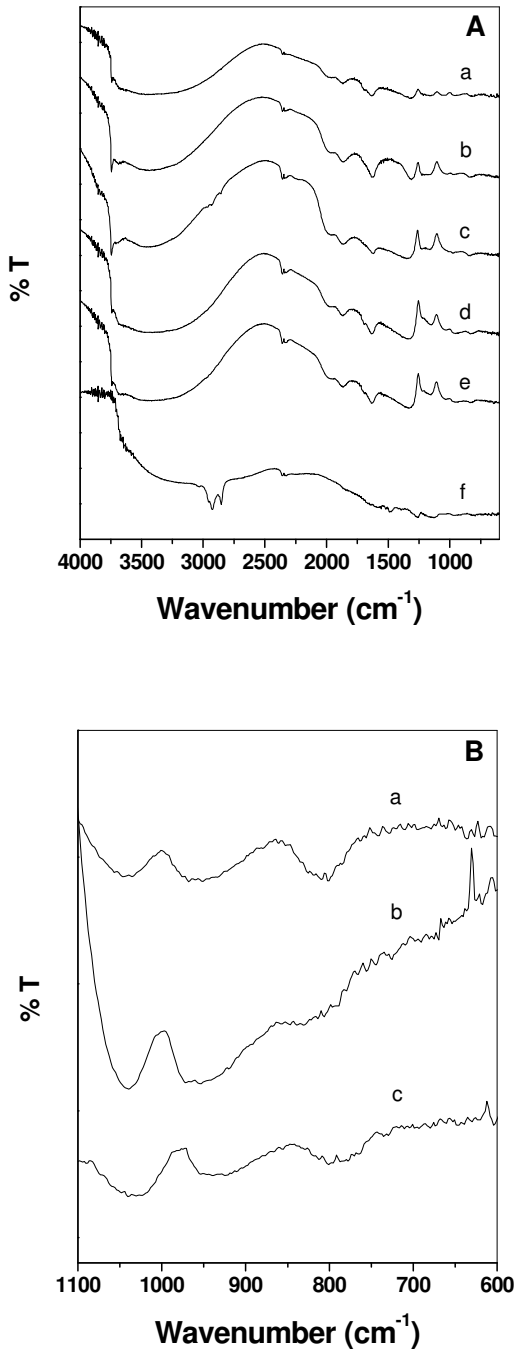

Fig. 2.4. FT-IR of [A] (a) Co-MCM-41 (100), (b) Co-MCM-41 (50), (c) pure MCM-41, (d) Co/MCM-41 (100), (e) Co/MCM-41 (50) and (f) Co-/MCM-41; [B] for samples (a), (b) and (c), it is shown in the range 1100-600 cm^{-1}.

In Fig. 2.4B, it is clearly seen that the intensity of the peak at 960 cm^{-1} is increasing with the cobalt content, which is taken as the proof for the incorporation of cobalt ions. A sharp absorption band at 3738 cm^{-1} ascribed to free Si–OH groups. In the Co-/MCM-41 sample, the broad NH_2 stretching band at 3250-3450 cm^{-1} and N–H deformation peak around 1540-560 cm^{-1} confirm the successful functionalisation of 3-amino propyl trimethoxy silane on the wall of MCM-41. It also displays the N–H bending mode (primary amine) at 1546 cm^{-1} and C–H stretching at 2944 cm^{-1}, which indicate the presence of $-Si(CH_2)_3NH_2$ on the wall surface [29].

2.2.2.4. Electron Microscopy

Fig. 2.5. Shows the SEM and TEM of MCM-41 and Co-MCM-41 (100). From the XRD results as discussed earlier, it is clear that that morphology is hexagonal since high reflection peaks are present (characteristic of hexagonal structure). However the SEM and TEM show the morphology, which seems like spherical with uniform particle size. Earlier Haskouri et al. [30] reported the transformation of hexagonal to spherical morphology for the Co-MCM-41 material in spite of high reflection peaks in the XRD. TEM images clearly indicate that most of the particles are agglomerated in Co-MCM-41.

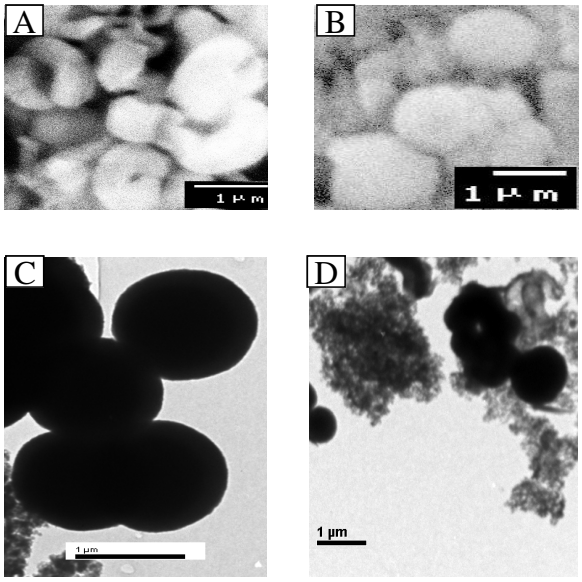

Fig. 2.5. SEM picture of (A) pure MCM-41, (B) Co-MCM-41 (100); TEM picture of (C) pure MCM-41, (D) Co-MCM-41 (100).

2.2.2.5. UV-Vis spectroscopy

Fig. 2.6A shows the DR UV-Vis spectra of the calcined cobalt incorporated samples. All samples exhibit triplet absorption bands viz 15472, 17015, and 19019 cm^{-1} in the visible region. The triplet is assigned to $^4A_2(F) \rightarrow {}^4T_1(P)$ transition of Co(II) in the tetrahedral environment in the framework [31-34]. We observed that the intensity of the triplet is increasing with the metal content. Moreover, the position of the peak at 17015 cm^{-1} is shifting towards the lower wavenumber which clearly shows the peak corresponding to framework tetrahedral Co(II) and extraframework tetrahedral Co(II) (which arises at 17300 and 16850 cm^{-1}) is overlapping [35]. After the triplet, shoulder appears in the energy range of 19500-22400 cm^{-1}.

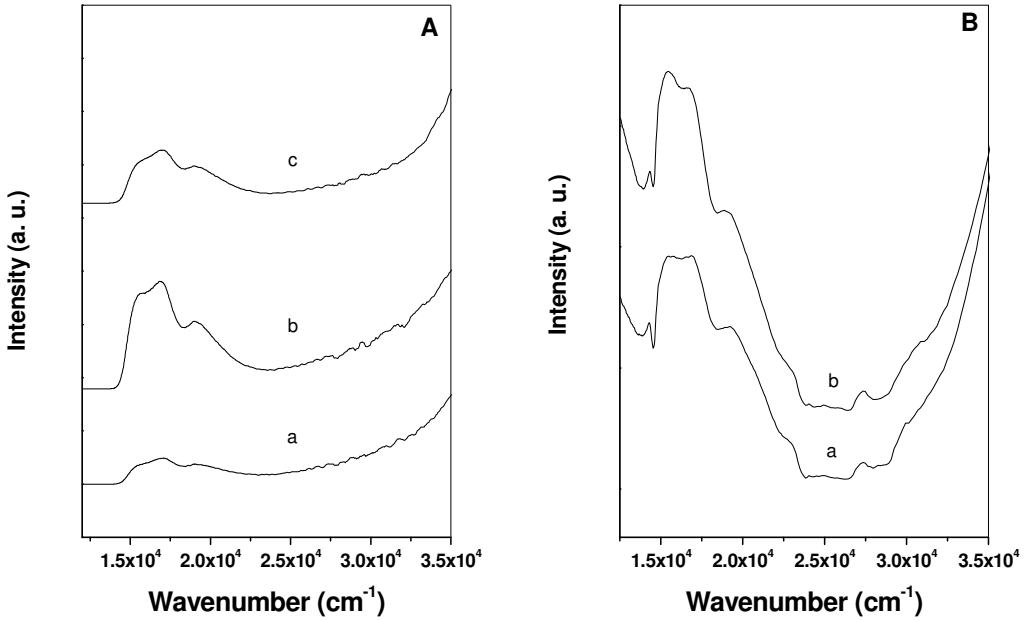

Fig. 2.6. UV-Vis spectra of [A] (a) Co-MCM-41 (100), (b) Co-MCM-41 (50), (c) Co-/MCM-41; [B] (a) Co/MCM-41 (100), (b) Co/MCM-41 (50).

However, the intensity of this shoulder is more prominent in Co-MCM-41 with Si/Co ratio of 50 than 100. This shoulder is due to octahedral Co(II) species and suggest that with increasing the cobalt content, octahedral species are increasing. Co/MCM-41 (grafted) samples with different cobalt loading show characteristic transition corresponding to extraframework cobalt (II) in tetrahedral and octahedral coordination [Fig. 2.6B]. All the as synthesized cobalt containing samples were pink colored and after calcination color turns to deep blue [blue color is the characteristic of tetrahedral Co(II)] indicate the cobalt ions incorporated in the framework of mesoporous silica are in the divalent state with tetrahedral coordination geometry [36,37]. The spectrum of Co-/MCM-41 sample is same as Co-MCM-41 exhibiting triplet absorption bands at 15472, 17015, and 19019 cm^{-1} in the visible region.

2.2.2.6 X-ray Photoelectron Spectroscopy

Fig. 2.7A illustrates the X-ray photoelectron spectra of Co-MCM-41 samples with Si/Co ratio 100 and 50.

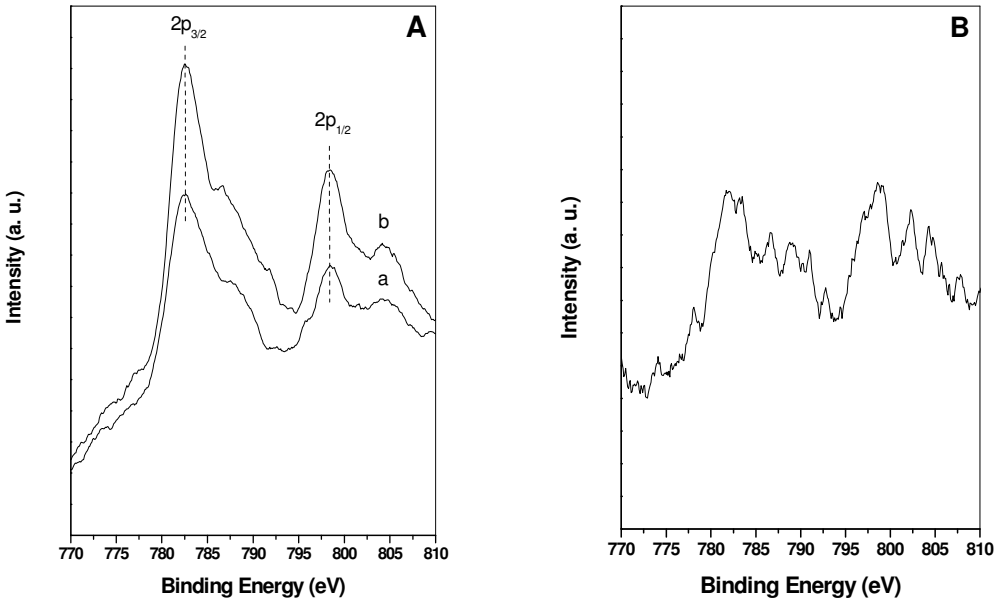

Fig. 2.7. XPS spectra of [A] (a) Co-MCM-41 (100) and (b) Co-MCM-41 (50); [B] Co/MCM-41 (50).

The Co2p transition splits into two peaks, $2p_{3/2}$ and $2p_{1/2}$. For the isolated cobalt binding energy value occurs at 782.2 and 797 eV for the $2p_{3/2}$ and $2p_{1/2}$, respectively. We observed that intensities of $2p_{3/2}$ and $2p_{1/2}$ peaks are increased with increasing the cobalt content. In these samples $2p_{3/2}$ peak was found at the energy value 782.4 eV suggesting the strong interaction of tetrahedral Co(II) with the silica wall [38]. It is important to note that the relative intensity of the shake up satellite slightly increases with respect to the increasing cobalt content and this feature is indicative of the presence of Co(II) species in the octahedral symmetry as found in CoO [39]. In cobalt-

grafted samples (Fig. 2.7B), Co/MCM-41 (50), the position of the $2p_{3/2}$ and $2p_{1/2}$ peaks was not been well identified. This shows the absence of bulk cobalt species on the framework.

2.3. Synthesis and Characterization of cobalt containing HMS

2.3.1 Experimental

The silica source used was tetraethyl orthosilicate (TEOS) [$Si(OC_2H_5)_4$, 98 %] obtained from Lancaster. Hexadecyl amine (HA) [$C_{16}H_{35}N$, 95%] and trimethoxy propyl amine silane [97 %, $(CH_3CH_2O)_3Si(CH_2)_3NH_2$] was obtained from Aldrich. Ethyl alcohol [C_2H_5OH, 99.9%] was purchased from Merck. Cobalt acetylacetone, [$Co(acac)_2$, 99 %], was supplied by Across. All reagents were used as received without further purification.

2.3.1.1. Synthesis

2.3.1.1.1. Synthesis of HMS

HMS was prepared by direct hydrothermal method. Tetraethyl orthosilicate (TEOS) and hexadecyl amine (HA) were used as inorganic precursor and structure directing agent, respectively. In a typical synthesis, first ethyl alcohol was added to water followed by addition of hexadecyl amine. It was stirred for half an hour at 30 ^oC. To this, TEOS was added very slowly. Stirring was continued for 3 h. The pH was

maintained at 7 with dil. HCl solution. The molar gel composition of the mixture was as follows,

1 TEOS: 0.35 HA: 10.75 EtOH: 139 H_2O

The gel was transferred to autoclavable bottle, kept in oil bath maintained at 100 ^oC for two days. Finally it was filtered, washed several times with distilled water and dried at 100 ^oC for 12 h. The as synthesized material was calcined at 525 ^oC for 12 h.

2.3.1.1.2. Synthesis of cobalt substituted HMS (Co-HMS)

Procedure for the synthesis of Co-HMS was same as for the synthesis of HMS. After the addition of TEOS to surfactant solution, ethanolic solution of cobalt acetylacetone was poured into gel in a dropwise manner. Stirring was continued for 3 h. P^H was maintained at 7. The molar gel composition of the mixture was as follows,

1 TEOS: x Co: 0.35 HA: 10.75 EtOH: 139 H_2O

Where 'x' is the calculated amount of cobalt acetate for different Si/Co ratios. The gel was transferred to autoclavable bottle kept in oil bath maintained at 95 to 100 ^oC for two days. Finally it was filtered, washed several times with distilled water and dried at 100 ^oC for 12 h. The as synthesized material was calcined at 525 ^oC for 12 h. It was designated as Co-HMS (100) and Co-HMS (50) for Si/Co ratio 100 and 50, respectively.

2.3.1.1.3. Synthesis of cobalt-grafted HMS (Co/HMS)

Cobalt acetylacetone (0.094 and 0.182 g for 1 and 2 wt. % loading, respectively) was dissolved in anhydrous toluene. To this 2 g HMS was added and refluxed at 100 ^oC for 12 h with constant stirring. Solvent was removed at its boiling temperatures using rotavapor. The sample was dried and calcined at 450 ^oC to remove

the organic matter. They were designated as Co/HMS (100) and Co/HMS (50) for 1 and 2 wt % cobalt loading, respectively.

2.3.1.1.4. Synthesis of cobalt immobilized on HMS (Co-/HMS*)*

Equal moles of trimethoxy propyl amine silane and cobalt acetylacetone (0.175 g of cobalt acetylacetone and 0.126 g of trimethoxy propyl amine silane) were mixed in 100 ml toluene at room temperature for 6 h. After half an hour 2 g HMS was added to the solution. The resulting solution was refluxed for 10 h with constant stirring. It was filtered, washed with acetone and dried at 70 ^{0}C for 6 h. Sample was designated as Co-/HMS.

2.3.1.2. Characterization

Powder X-ray diffraction pattern of the samples were recorded on a Rigaku D max III VC Ni filtered Cu Kα radiation, λ=1.5404 between 1 and 8 (2θ) with a scanning rate of 1^o/min. The specific surface area, total pore volume and average pore diameter measured by the N_2 adsorption desorption method using NOVA 1200 (Quanta Chrome) instrument. The samples were activated at 300 ^{o}C for 3 h under vacuum and then adsorption desorption was conducted by passing nitrogen over samples which was kept under liquid nitrogen. Pore size distribution was obtained by applying BJH pore analysis method to the desorption branch of nitrogen adsorption isotherm. SEM micrograph of the cobalt containing samples were obtained on JEOL-JSM 520 scanning microscope while the TEM images were performed on a JEOL-TEM 1200 EX instrument with 100 kV accelerating voltage to probe the mesoporosity of the material. Cobalt content in the samples was determined by atomic absorbance

analysis using Perkin Elmer 11013 spectrometer after dissolution of the samples in HCl-HF solution. Diffuse reflectance UV-Vis spectra of the powder samples were recorded in the range 200-800 nm on Shimadzu UV 2101 PC spectrometer equipped with a diffuse reflectance attachment, using BaSO4 as the reference. XPS measurements were performed on a VG Microtech ESCA 3000 instrument using non-monochromatized Mg Kα radiation at a pass energy of 50 eV and an electron take off angle of 60 ^{o}. The correction of binding energy (B.E.) was performed by using the C_{1s} peak of carbon at 285 eV as reference.

2.3.2. Results and discussion

2.3.2.1. Powder X-ray diffraction

Fig. 2.8 shows the X-ray diffraction (XRD) pattern of calcined cobalt substituted and grafted HMS samples with different amounts of cobalt. The XRD patterns are similar to the reports of Tanev et al. [3]. Unlike MCM-41 material, HMS shows only d_{100} reflection peak and the higher order Bragg's reflections are absent which suggests that the structure of the material is poorly ordered [40,41]. In Co-HMS samples, increasing cobalt amount results in a decrease in the intensity of d_{100} reflection peak and the peak gets broadened with a slight shift in 2θ angle towards lower value (Fig. 2.8A).

Moreover, compared to pure HMS sample, the cobalt containing samples shows an increase in the d-spacing values (Table 2.2) and thereby increases the unit cell values. In cobalt containing HMS, we observed that the a_0 values are greater than reported value [3,26,40,41].

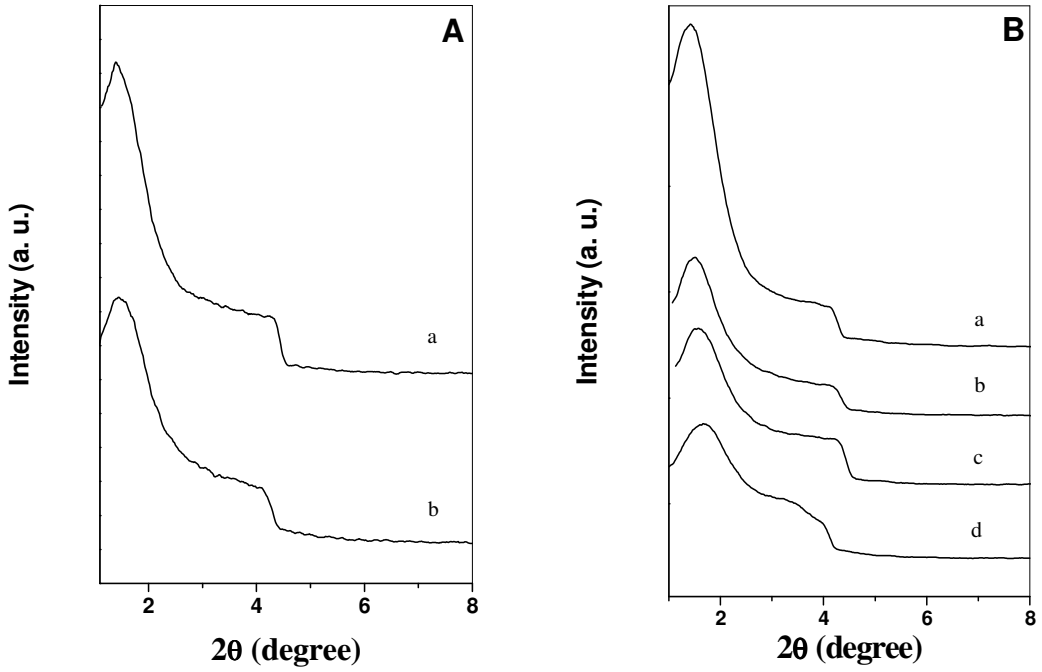

Fig. 2.8. Powder X-ray diffraction of calcined [A] (a) Co-HMS (100), (b) Co-HMS (50); [B] (a) HMS, (b) Co/HMS (100), (c) Co/HMS (50) and (d) Co-/HMS.

This phenomenon may be due to the high temperature hydrothermal synthesis performed in the present case, than the earlier reported room temperature synthesis. Indeed, Thomas et al claimed that with increase in synthesis temperature, pore- pore correlation distance systematically increased [40]. On the contrary, in case of Co/HMS sample, with an increase in amount of cobalt loading, the d_{100} reflection peak decreases with a corresponding shift to higher 2θ values due to accumulation of cobalt on surface of the wall (Fig. 2.8B).

Table. 2.2. Physical properties of cobalt containing HMS catalyst

Entry	Catalyst	Si/Co [a] (molar ratio)	2θ angle (deg.)	a_0 [b] (Å)	S_{BET} [c] / (m^2/g)	Pore volume V_p / (cc/g)
1	HMS	-	1.420	71.78	503	1.32
3	Co-HMS (100)	101	1.400	72.81	538	1.29
4	Co-HMS (50)	52	1.390	73.33	618	1.20
5	Co/HMS (100)	93	1.429	71.31	485	1.25
6	Co/HMS (50)	49	1.440	70.78	462	1.17
7	Co-/HMS	60	1.493	68.28	390	0.91

[a] Cobalt content estimated by AAS analysis.

[b] Unit cell parameter values calculated using $a_0 = 2d_{100}/\sqrt{3}$.

[c] S_{BET} is the surface area calculated by BET method.

2.3.2.2. Nitrogen adsorption desorption measurements

N_2 adsorption-desorption isotherms and pore size distribution curves, determined from the BJH method, of cobalt containing HMS materials are shown in Fig. 2.9 and 2.10 and the corresponding textural parameters are given in Table 2.2 [27,28]. Isotherms of all samples show isotherm of type IV, according to IUPAC classification, at higher relative pressures (P/P_o), which is typical of mesoporous materials with one dimensional cylindrical channels having bigger pore size [42]. Unlike MCM-41, the capillary condensation for the HMS samples was observed at higher relative pressure, indicating a pore enlargement and are consistent with the XRD results. Moreover, unlike the pore size distribution (PSD) curves obtained for M41S samples, the present HMS samples produce broad PSD curves.

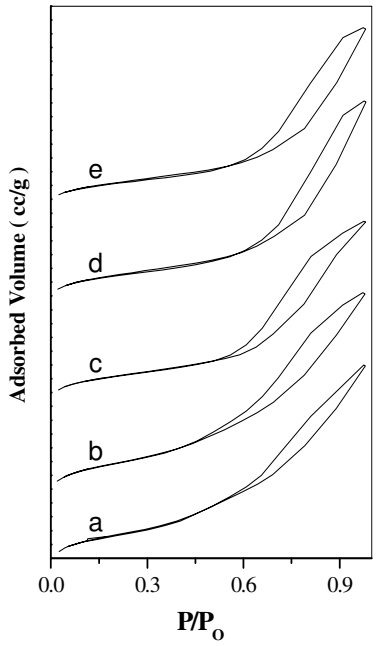

Fig. 2.9. N_2 adsorption desorption isotherms of (a) HMS, (b) Co/HMS (100), (c) Co/HMS (50), (d) Co-HMS (100), (e) Co-HMS (50).

These structural differences show a different pore array for the HMS materials, prepared by the amine templated inorganic materials. In addition we observed that the pore size of Co-HMS samples are higher than pure HMS samples. Such kind of result is noted for V-MCM-41 samples and is attributed to the substitution of vanadium in the frame wall positions [43]. Such a consideration in the present Co-HMS samples suggest that cobalt gets incorporated inside the framework and thereby enlarges its pore size. Surface area of pure HMS sample shows a high surface area of 503 m^2g^{-1} and after cobalt substitution surface area gets increased to 538 m^2g^{-1} for Co-HMS (100) and 618 m^2g^{-1} for Co-HMS (50). However, as expected, the surface area of the grafted catalysts gets decreased and amounts to 96.4 % and 92 % for Co/HMS (100) and Co/HMS (50) respectively. This decrease in surface area may be due to the partial

blockage of pores by forming cobalt oxide particles inside the pore channels by the post synthesis method. The decrease in surface area is more for the immobilized cobalt containing HMS samples. However, these modifications had not changed the overall structural features of the material, as observed from the XRD and sorption isotherms.

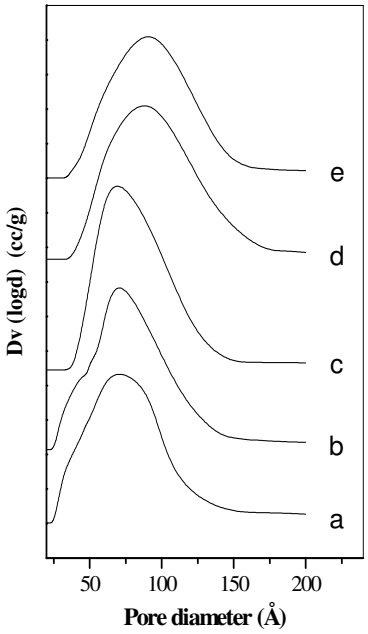

Fig. 2.10. BJH pore diameter of cobalt containing mesoporous material (a) HMS, (b) Co/HMS (1), (c) Co/HMS (2), (d) Co-HMS (100), (e) Co-HMS (50).

2.3.2.3. Electron Microscopy

Morphology and structural ordering of cobalt containing HMS samples were analyzed by electron microscopy studies and are shown in Fig. 2.11. SEM picture of Co-HMS samples shows discrete spherical particles of diameter ~ 0.5-2 μm. Contrary, cobalt grafted HMS samples show disordered spherical structures with the presence of agglomerated particles. Moreover, TEM images show the characteristic wormhole like morphology for both the cobalt-containing samples [40]. Similar to SEM results, TEM images of cobalt-grafted samples also show the presence of agglomerated particles. Thus, the electronic microscopic studies show that the morphology of the HMS sample differs with the way of introduction of metal species inside the HMS matrix viz. direct synthesis and post synthesis method.

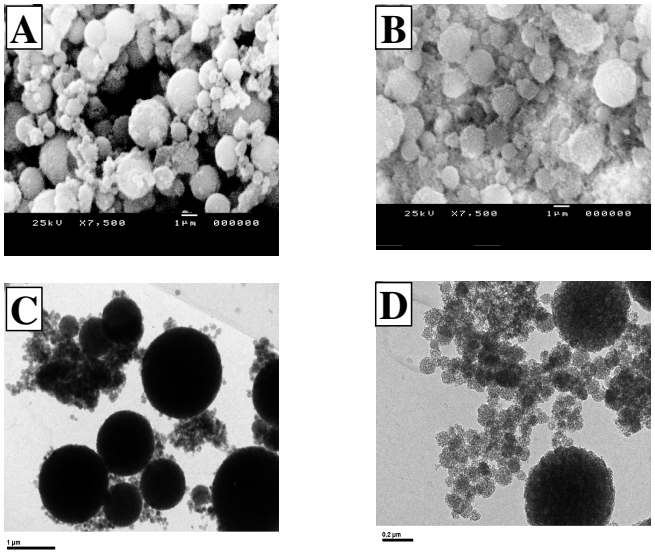

Fig. 2.11. SEM images of calcined cobalt containing mesoporous [A] Co-HMS (100), [B] Co/HMS (1); and TEM images of calcined cobalt containing mesoporous [C] Co-HMS (100), [D] Co/HMS (100).

2.3.2.4. Diffuse reflectance UV-Vis spectra

Diffuse reflectance UV–Vis spectroscopy is a powerful technique for gaining information about the coordination environment and oxidation states of metal species in various molecular sieves. Hence, to determine the coordination environment of cobalt inside the HMS samples, DR UV-Vis analyses was carried out in the range 12000- 35000 cm^{-1} and are given in Fig. 2.12.

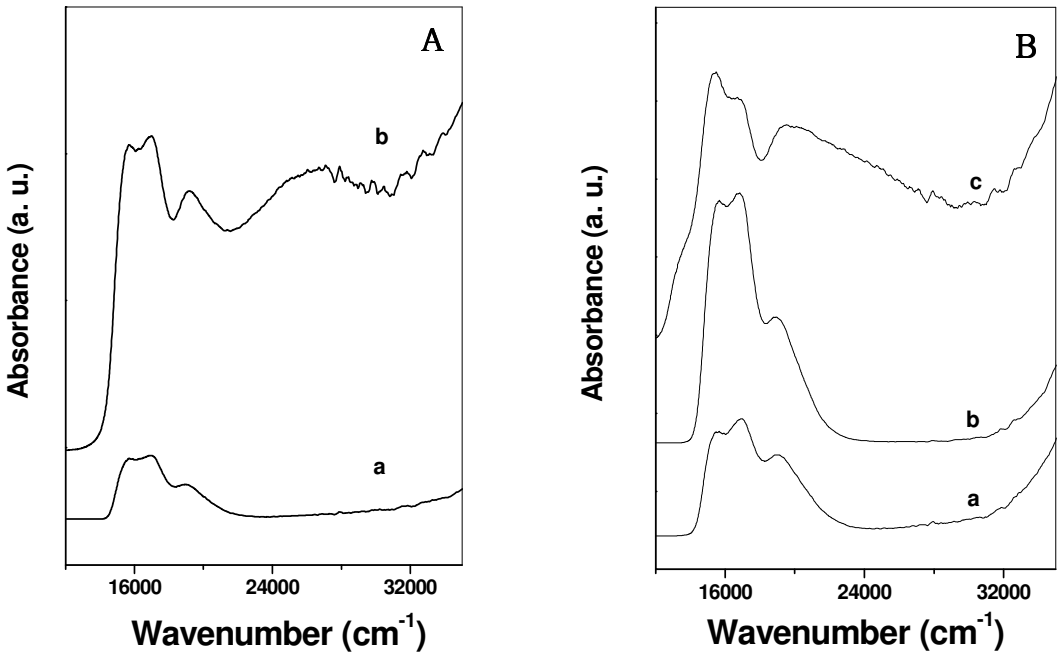

Fig. 2.12. Diffuse reflectance UV-Vis spectra of cobalt containing mesoporous materials [A] (a) Co-HMS (100), (b) Co-HMS (50), [B] (a) Co/HMS (100), (b) Co/HMS (50) and (c) Co-/HMS.

Irrespective of the synthesis method, UV-Vis analysis display an intense, three absorption maxima in the visible region. This triplet is assigned to the $^4A_2(F) \rightarrow {}^4T_1(P)$ transitions of high spin (d^7) Co^{2+} in tetrahedral position. This clearly indicates

that cobalt is in the tetrahedral coordination with the support surface and the blue colour of the samples further supports this assignment [31,33,34,44]. For Co-HMS (50), a broad peak was observed around 27000 cm^{-1} corresponding to the charge transfer bands of Co^{3+} in distorted tetrahedral position [34,45]. Moreover, it is apparent (from Fig. 2.12) that the intensities of the triplet bands gets increased and broadened with an increase in the cobalt content. Bands above the 35000 cm^{-1} are assigned to either charge transfer from O^{2-} to Co^{2+} or own absorption of molecular sieves [36,37].

2.3.2.5. X-ray photoelectron spectra

XPS helps in the identification of oxidation state by exact measurement of peak positions and separation as well as from certain spectral features. X-ray photoelectron spectra of cobalt incorporated and grafted samples are shown in Fig. 2.13. For the grafted samples, the Co $2p_{3/2}$ transition peak occurs at 781.7 eV while $2p_{1/2}$ at 797.9 eV. With increase in the metal content, intensity of the $2p_{3/2}$ and $2p_{1/2}$ peaks was increased with some broadening. The energy difference between $2p_{1/2}$ and $2p_{3/2}$ peaks is 15.6 eV. It is close to that of Co^{2+} (16 eV) rather than Co^{3+} compounds (15.0 eV) [38,39]. This clearly indicates the presence of cobalt in +2 oxidation state, which is in good agreement with the result from UV-Vis spectra. Interestingly, the Co-HMS samples were devoid from the characteristic 2p peak ($2p_{1/2}$ and $2p_{3/2}$), which may be due to the fewer amounts of surface cobalt species in case of hydrothermally synthesized Co-HMS samples. However, for the grafted Co/HMS the percentage of the cobalt species detected is very high because of the post synthesis grafting method.

Since XPS is a surface technique, the present results suggest that more cobalt species resides on the support surface in Co/HMS samples, while since the cobalt gets substituted inside the framework for Co-HMS samples, they are not detectable by the XPS. Hence the Co $2p_{1/2}$ and $2p_{3/2}$ peaks are very prominent for the Co/HMS than Co-HMS samples, even though both the catalysts contain similar cobalt content.

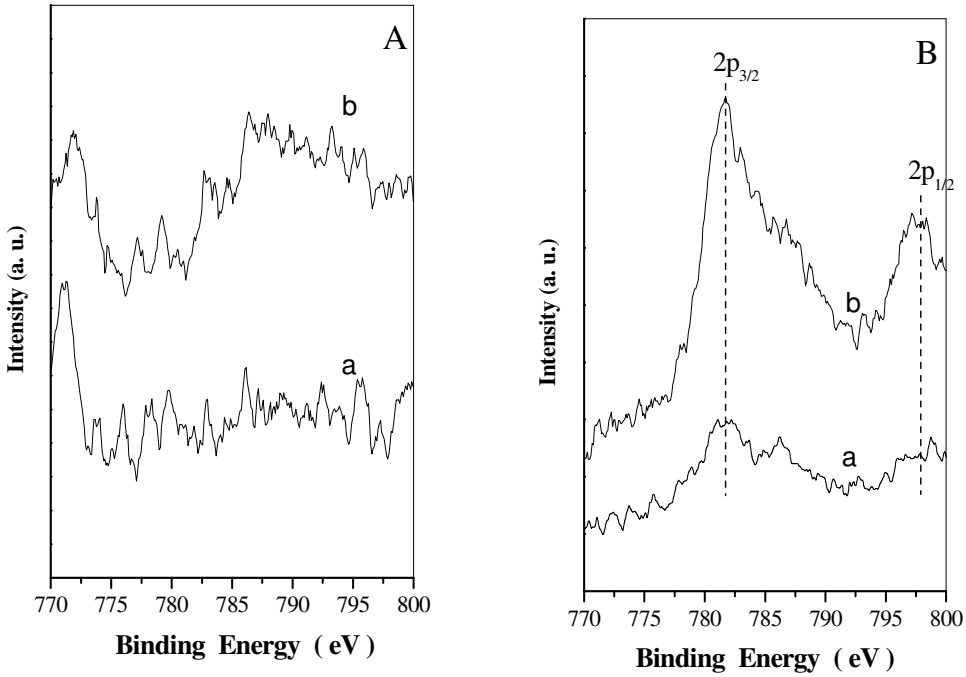

Fig. 2.13. XPS spectra of [A] (a) Co-HMS (100), (b) Co-HMS (50); [B] (a) Co/HMS (100), (b) Co/HMS (50).

2.4. References

[1] C. T. Kresge, M. E. Leonowicz, W. J. Roth, J. C. Vartuli, J. S. Beck, Nature 359 (1992) 710.

[2] J. S. Beck, J. C. Vartuli, W. J. Roth, M. E. Leonowicz, C. T. Kresge, K. D. Schmitt, C. Chu, D. H. Olson, E. W. Sheppard, S. B. McCullen, J. B. Higgins, J. L. Schenkler, J. Am. Chem. Soc. 114 (1992) 10834.

[3] P. Venuto, Stud. Surf. Sci. Catal. 105 (1997) 811.

[4] Q. Huo, R. Leon, P. M. Petroff and G. D. Stucky, Science 1995 (268) 1324.

[5] R. Ryoo, J. M. Kim, J. Y. Lee and C. H. Shin, Proceedings of the 11th International Zeolite Conference, Seoul, 1996.

[6] P. T. Tanev, M. Chibwe, T. J. Pinnavaia, Nature 368 (1994) 321.

[7] (a) S. A. Bagshaw, E. Prouzet, T. J. Pinnavaia, Science 269 (1995) 1242; (b) G. S. Attard, J. C. Gyde, C. G. Goltner, Nature 378 (1995) 366.

[8] S. Gontier, A. Tuel, Zeolites 15 (1995) 601.

[9] M. Guisnet, N. S. Gnep, S. Morin, J. Patarin, F. Loggia, V. Solinas, Mesoporous Molecular Sieves, 117 (1998) 591.

[10] S. Morin, P. Ayrault, S. ElMouahid, N. S. Gnep, M. Guisnet, Appl. Catal. A, 159 (1997) 317.

[11] C. Constantin, V. Parvulescu, A. Bujor, G. Popescu, B. L. Su, J. Mol. Catal. A 2004 (208) 245.

[12] V. Parvulescu, C. Constantin, G. Popescu, B. L. Su, J. Mol. Catal. A 208 (2004), 253.

[13] J.M. Campelo, D. Luna, R. Luque, J.M. Marinas, A.A. Romero, J.J. Calvino, M.P. Rodrýguez-Luque, J. Catal. 230 (2005) 327.

[14] D. Zhao, C. Nie, Y. Zhou, S. Xia, L. Huang, Q. Li, Catal. Today 68 (2001) 11.

[15] M.L. Occelli, S. Biz, A. Auroux, Appl. Catal. A 183 (1999) 231.

[16] R.M. Barrer, Hydrothermal Chemistry of Zeolites, Academic Press, New York, 1982.

[17] V.N. Romannikov, V.M. Mastikhin, S. Hocevar, B. Drzaj, Zeolites 3 (1983) 311.

[18] (a) V. Hulea, E. Dumitriu, Appl. Catal. A. Gen. 277 (2004) 99, (b) A. Corma, P. Esteve, A. Martinez, J. Catal. 161 (1996) 11, (c) K. A. Koyano, T. Tatsumi, Microporous Mater. 10 (1997) 259.

[19] (a) J. M. R. Gallo, I. S. Paulino, U. Schuchardt, Appl. Catal. A. Gen. 266 (2004) 223, (b) W. Zhang, M. Froba, J. Wang, P. T. Tanev, J. Wong, T. J. Pinnavaia, J. Am. Chem. Soc. 118 (1996) 9164.

[20] (a) N. Ulagappan, C. N. R. Rao, Chem. Commun. (1996) 1047, (b) A. Sakthivel, P. Selvam, J. Catal. 211 (2002) 134, (c) A. Sakthivel, S. E. Dapurkar, P. Selvam, Catal. Lett. 77 (2001) 155.

[21] (a) R. J. Mahalaingam, S. K. Badamali, P. Selvam, Chem. Lett. (1999) 1121, (b) S. E. Dapurkar, A. Sakthivel, P. Selvam, New J. Chem. 27 (2003) 1184.

[22] Y. Wang, Q. Zhang, T. Shishido, K. Takehira, J. Catal. 209 (2002) 186.

[23] (a) V. Parvulescu, B. L. Su, Catal. Today 69 (2001) 315, (b) R. Neumann, A. M. Khenkin, Chem. Commun. (1996) 2643, (c) Q. Tang, Q. Zhang, H. Wu, Y.

Wang, J. Catal. 230 (2005) 393.

[24] (a) K. Chaudhari, T. K. Das, P. R. Rajmohanan, L. Lazar, S. Sivasanker, A. J. Chandwadkar, J. Catal. 183 (1999) 281, (b) A. Corma, M. T. Navarro, L. Nemeth, M. Renz. Chem. Commun. (2001) 2190.

[25] J. S. Reddy, A. Sayari, Appl. Catal. A 148 (1996) 7, (b) J. S. Reddy, A. Sayari, J. Chem. Soc. Chem. Commun. (1995) 2231.

[26] A. Tuel, S. Gontier, Chem. Mater. 8 (1996) 114.

[27] E. P. Barrette, L. G. Joyner, P. P. Halenda, J. Am. Chem. Soc. 73 (1951) 373.

[28] S. Bruanaur, L. S. Deming, W. S. Deming, E. J. Teller, Am. Chem. Soc. 62 (1940) 1723.

[29] (a) X J. Chen, Q. Li, R. Xu, F. Xiao, Angew. Chem. Int. Ed. Engl. 34 (1995) 2694. (b) A. Jentys, N. H. Pham, H. Vinek, J. Chem. Soc., Faraday. Trans. 92 (1996) 3287. (c) C. Zhang, W. Zhou, S. Liu; J. Phys. Chem. B 109 (2005) 24319.

[30] J. El Haskouri, S. Cabrera, C.J. Gomez-Garcia, C. Guillem, J. Latorre, A. Beltran, D. Beltran, M.D. Marcos, P. Amoros, Chem. Mater. 16 (2004) 2805.

[31] A. Vinu, J. Dedecek, V. Murugesan, M. Hartmann, Chem. Mater. 14 (2002) 2433.

[32] C. Montes, M. E. Davis, B. Murray, M. Narayana, J. Phys. Chem. 94 (1990) 6425.

[33] F. A. Cotton, G. Wilkinson, Advanced Inorganic Chemistry, Wiley, New York, 1980.

[34] A. A. Verberckmoes, M. G. Uytterhoeven, R. A. Schoonheydt, Micropor. Mesopor. Mater. 22 (1998) 165.

[35] A. A. Verberckmoes, M. Uytterhoeven, R. Schoonheydt, Zeolites 19 (1997) 180.

[36] J. Dedecek, D. Kaucy, B. Wichterlova, Micropor. Mesopor. Mater. 483 (2000) 35.

[37] J. Dedecek, B. Wichterlova, J. Phys. Chem. B 103 (1999) 1462.

[38] L. Guszi, D. Bazin, Appl. Catal. A 188 (1999) 163.

[39] G. Fierro, M. A. Eberrhardt, M. Houlla, D. M. Herculles, W. K. Hall, J. Phys. Chem. 100 (1996) 8468.

[40] T. R. Pauly, T. J. Pinnavaia, Chem. Mater. 13 (2001) 987.

[41] P. T. Tanev, T. J. Pinnavaia, Chem. Mater. 8 (1996) 2068.

[42] J. H. De Boer, The Structure and Properties of Porous Materials (D. H. Everette and F. S. Stone Eds.), pp. 68, London, Butterworths (1958).

[43] S. Shylesh, A. P. Singh, J. Catal. 206 (2004) 230.

[44] D. L. Wood, J.P. Reimeka, J. Phys. Chem. 46 (1967) 3595.

[45] C. Montes, M. E. Davis, B. Murray, M. Narayana, J. Phys. Chem. 94 (1990) 6425.

3.1. INTRODUCTION

Metal containing mesoporous molecular sieves emerged as research field particularly in catalysis because of its intriguing properties like high surface area and large pore volume. Researchers employed these molecular sieves in various industrially important reactions e.g. acid-base, oxidation, reduction, hydrocarbon synthesis (from syn gases) etc. The commercial processes of selective side chain oxidation of alkyl aromatics are mainly based on homogeneous catalysis in solvents such as acetic acid and using oxygen as an oxidant [1-4]. The identification and implementations of effective catalytic systems for liquid phase oxidation, particularly in the manufacturing of fine chemicals is considered to be one of the major aims of chemical industries. The need for such a system is widely accepted, specifically to replace inorganic oxidants that are using stoichiometric amounts and other environmental issues. Heterogeneous catalysts had many inherent advantages such as ease of recovery and recycling of the catalyst as well as suitable for continuous processing. A number of different strategies for the heterogenisation of the redox active elements are being explored and include framework substituted molecular sieves.

The reaction temperature is more and demands the use of autoclave reactors, which is made using the special and costly material due to the corrosive medium. Furthermore, the formation of brominated byproducts (when used bromine as an activator) is an issue. Therefore there is a need for the development of new heterogeneous catalytic process for the synthesis of aromatic aldehydes and ketones. Vanadium and molybdenum based catalysts have been widely studied for the side

chain oxidation of alkyl aromatics [5-11]. Besides this iron based catalyst was studied for the selective oxidation of alkyl aromatics but the success is very limited [12,13].

Cobalt acts as a very good catalyst for Fischer-Tropsch reaction and had been further exploited for long chain hydrocarbon synthesis [14]. Besides this, its excellent performance in side chain oxidation of aromatics urged researchers to deal more about the redox properties. Selective oxidation of ethylbenzene and diphenylmethane are industrially important reactions. Acetophenone, one of the products from the oxidation of ethylbenzene finds uses as a specialty solvent, resin, flavoring agents, intermediates in the manufacture of pharmaceuticals and in organic synthesis. It can be synthesized from benzene and acetyl chloride, but it is prepared commercially by the air oxidation of ethylbenzene. Benzophenone and its variant are important chemicals. Benzophenone is commonly used as a photosensitizer in photochemistry. Its triplet is readily quenched by oxygen and can also react with a suitable hydrogen donor to form a ketyl radical [15].

The reports on oxidation of ethylbenzene over different catalysts are available. Ti, V and Sn containing silicalites with MFI structure were used by Mal et al [16]. Hermans et al. elucidated the mechanism of oxidation of ethylbenzene [17]. Mn containing MCM-41 was used by Pandurangan et al [18] for the oxidation of ethylbenzene. The oxidation of diphenylmethane over MnO_4^{-1} exchanged hydrotalcite and clay, alumina supported Cr and Mn were reported [19-21]. Earlier, attempts had been made to synthesize benzophenone using different strategies [22-30].

In this chapter, we reported in detail the liquid phase oxidation of ethylbenzene and diphenylmethane over cobalt containing mesoporous molecular sieves under different reaction parameters.

3.2. CATALYTIC OXIDATION OF ETHYLBENZENE OVER COBALT CONTAININING MCM-41 AND HMS

3.2.1. Reaction Procedure

Oxidation reactions of ethylbenzene (99 % purity, Lancaster) were performed in a round bottom flask fitted with a water condenser using *tert.* butyl hydroperoxide (TBHP, 70 wt %, Lancaster) as an oxidant. The reaction mixture of the ethylbenzene (1 g, 9.4 mmol) and TBHP (1.22 g, 9.4 mmol) was added to catalyst (5 wt % with respect to ethylbenzene) and heated at constant temperature 80 ^{o}C under magnetic stirring. At different time interval, the reaction mixture was withdrawn by syringe. The products were analyzed by gas chromatograph (Agilent, HP 6890) equipped with a flame ionization detector (FID) and a capillary column (5 µm cross linked methyl silicone gum x 0.2 mm x 50 m) and was further confirmed by GC-MS (Shimadzu 200A). Leaching of the metal during the course of reaction was verified by resubmission of the filtrate for further reaction at same reaction conditions.

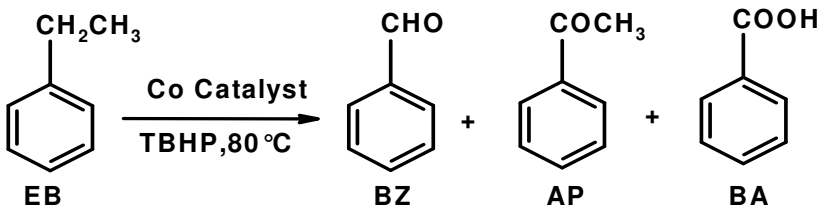

Scheme 3.1. Oxidation of Ethylbenzene

3.2.2. Oxidation of Ethylbenzene over Cobalt containing MCM-41

The oxidation of ethylbenzene was carried out in liquid phase results in the formation of three main important products viz. benzaldehyde (BZ), acetophenone (AP) and benzoic acid (BA) [Scheme 3.1]. BA is formed by over oxidation of BZ in the consecutive reaction steps. The EB oxidation was carried out using different oxidants such as hydrogen peroxide (H_2O_2) [30 wt %], *ter.* butyl hydrogen peroxide (TBHP) [70 wt %] and sodium hypochlorite (NaOCl) [4 wt %]. When NaOCl and H_2O_2 used as oxidant, the activity for the EB oxidation was negligible.

Remarkable activity was found when TBHP was used as an oxidant. In order to check the effect of substrate to oxidant ratio on the catalytic performance, the reactions were studied at ratio of EB:TBHP (1:1, 1:2 and 1:3). It was observed that catalytic activity is not affected by different ratio of EB: TBHP. This result is opposite as observed by Singh et al with Co-APO-11 where EB conversion and selectivity to AP were affected by different amount of TBHP [31].

We noted that all the cobalt-containing catalysts perform excellently in absence of solvent for the oxidation of EB. When different solvents were used, EB conversion was found lower than in the absence of solvent. This indicates that there is competition between the EB and solvent molecules for the active cobalt sites. With all the cobalt containing catalysts, conversion increases with reaction time. It was observed that EB conversion is found higher over incorporated cobalt catalyst than grafted and immobilized cobalt (Table 3.1).

Table 3.1. Performance of cobalt containing catalyst for ethylbenzene oxidation

Entry	Catalyst	EB Con. (wt %)	Selectivity (wt %)		
			BZ	AP	BA
1	MCM-41	-			
2	Co-MCM-41 (100)	36.1	18.2	71.0	9.5
3	Co-MCM-41 (50)	46.7	16.8	73.1	9.8
4	Co/ MCM-41 (100)	25.0	20.3	65.1	14.5
5	Co/ MCM-41 (50)	33.0	20.6	67.2	11.5
6	Co-/ MCM-41	26.8	9.1	85.0	5.9

Reaction Conditions: ethylbenzene 1 g; TBHP 1.22 g; catalyst 0.05 g, temperature 80 ^{o}C; reaction time 24 h (absence of solvent).
EB- ethylbenzene, BZ- benzaldehyde, AP- acetophenone, BA- benzoic acid.

Moreover, it is observed that with Co-MCM-41 samples, EB conversion increases with the increase in the amount of cobalt. For Co-MCM-41 (100) and Co-MCM-41 (50), the EB conversions in absence of solvent, after 24 h, were found 36.1 and 46.7 %, respectively (Fig 3.1A). The selectivity to AP was increased slightly after 24 h in absence of solvent [71 and 73 % for Co-MCM-41 (100) and Co-MCM-41 (50), respectively (Fig. 3.2B)]. Some extraframework octahedral cobalt species were found in Co-MCM-41 (50) as evident from UV-VIS spectra.

The catalytic results indicate that, the extra framework cobalt species also contribute to the EB conversion. Co/MCM-41 (100) and Co/MCM-41 (50) catalysts in the absence of solvent after 24 h gives 25 and 33 % EB conversion, respectively, which is lower than cobalt substituted MCM-41 catalyst. Even the selectivity to AP [65.1 and 67.2 % for Co/MCM-41 (100) and Co/MCM-41 (50) after 24 h,

respectively] is lower than observed with cobalt substituted MCM-41 catalyst (Table 3.1).

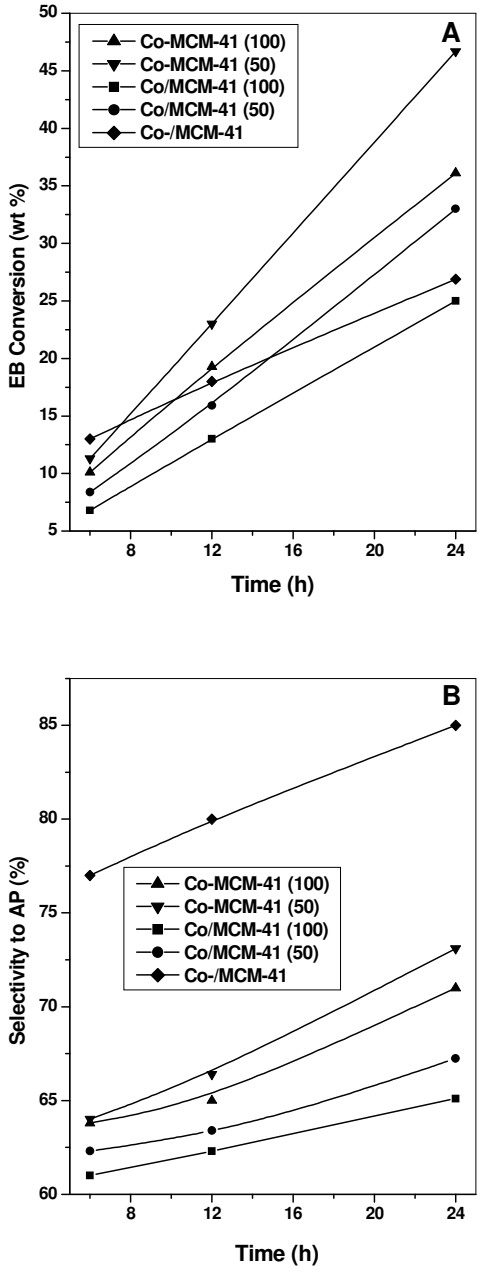

Fig. 3.1. Performance of various catalysts on (A) Ethylbenzene conversion Vs time and (B) Selectivity to acetophenone Vs time. Reaction Conditions: ethylbenzene 1 g, TBHP 1.22 g, catalyst 0.05 g, temperature 80 ^{o}C (in absence of solvent).

For Co-/MCM-41, though the EB conversion (26.8 %) is less, the highest selectivity to AP (85 %) was achieved among all the cobalt containing MCM-41 catalyst under study. When the cobalt species were immobilized on the solid support through the spacer, their points of attachment are removed from one another. Thus these active species are so far apart that the resulting solid can be seen as single site catalyst [32]. Another reason for the high selectivity to AP may be from the bond formed between cobalt and nitrogen (of the spacer), which makes the cobalt less hungry (because of donation of lone pair of electron from nitrogen to vacant d orbital). This may effect in reacting or coordinating cobalt with the ethylbenzene in selective manner.

Solvent effect is apparent when the reaction was studied in different solvents like ethanol, dichloromethane, acetone and acetonitrile. In different solvents, EB conversion after 24 h over Co-MCM-41 (100) is in the order of acetonitrile > dichloromethane > acetone > ethanol (Fig. 3.2A). Selectivity to AP in different solvents follows the order ethanol > acetonitrile > dichloromethane > acetone (Fig. 3.2B). When acetone was used as solvent, the reaction follows the pathway more selectively to BZ and BA. In acetone, AP is converting to BZ by over oxidation of methyl group of AP followed by release of CO_2 [33]. This shows rate of side reaction becomes faster with the progress of reaction. Thus it leads to increase in the selectivity to BZ and BA.

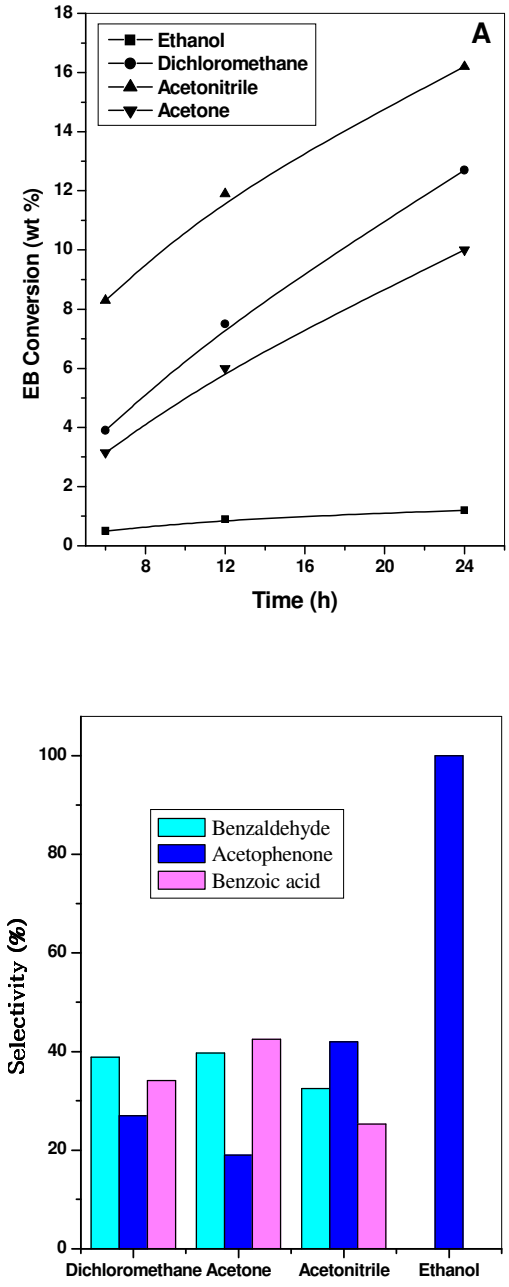

Fig. 3.2. Effect of various solvents on (A) Ethylbenzene conversion Vs time and (B) Selectivity (after 24 h) over Co-MCM-41 (100). Reaction Conditions: ethylbenzene 1 g, TBHP 1.22 g, catalyst 0.05 g, temperature 80 ^{o}C, solvent 5 g.

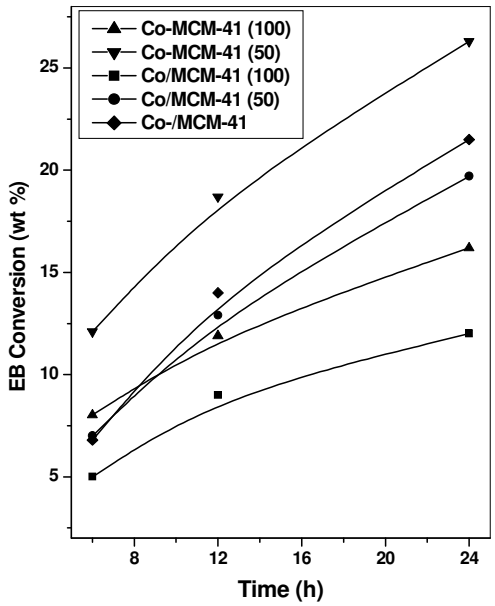

Fig. 3.3. Performance of the various catalysts in presence of acetonitrile with time. Reaction Conditions: ethylbenzene 1 g, TBHP 1.22 g, catalyst 0.05 g, temperature 80 ^{o}C, acetonitrile 5 g.

The catalytic activity of Co-MCM-41 (100), Co-MCM-41 (50), Co/MCM-41 (100), Co/MCM-41 (50) and Co-/MCM-41 were studied in acetonitrile medium. The rate of EB conversion after 24 h over different catalyst follows the order Co-MCM-41 (50) > Co-/MCM-41 > Co/MCM-41 (50) > Co-MCM-41 (100) > Co/MCM-41 (100) [Fig. 3.3]. Unlike, in the absence of solvent, the selectivity to AP decreased with the progress of reaction. This indicate that rate of side reaction becomes more prominent with the progress of the reaction leading to increase in the selectivity to BZ and BA.

In order to find the heterogeneity of the catalyst, leaching study was carried out using hot filtrate (catalyst was removed after 6 h) at similar reaction conditions. From Figs. 3.4 and 3.5, it is clear that catalysts are prone to leaching. However, the Co-

/MCM-41 shows less leaching [Fig. 3.4 (C) and Fig. 3.5 (C)] compared with Co/MCM-41 (50) and Co-MCM-41 (50).

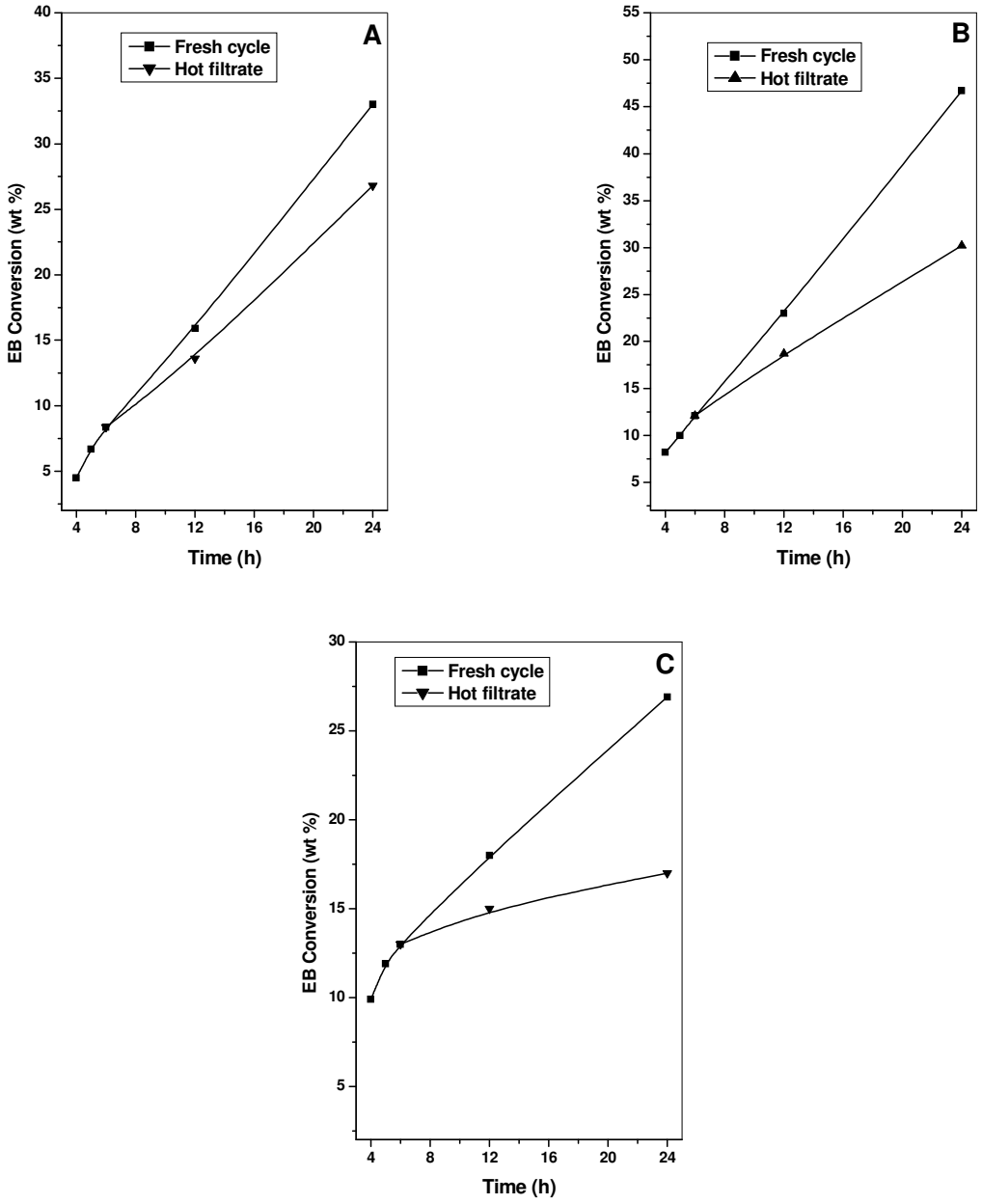

Fig. 3.4. Leaching study over different catalysts in absence of solvent [A] Co/MCM-41 (50), [B] Co-MCM-41 (50) and Co-/MCM-41 (for leaching study, catalyst was removed after 6h and filtrate was used for the further reaction). Reaction conditions are same as mentioned in footnote of Fig. 3.1.

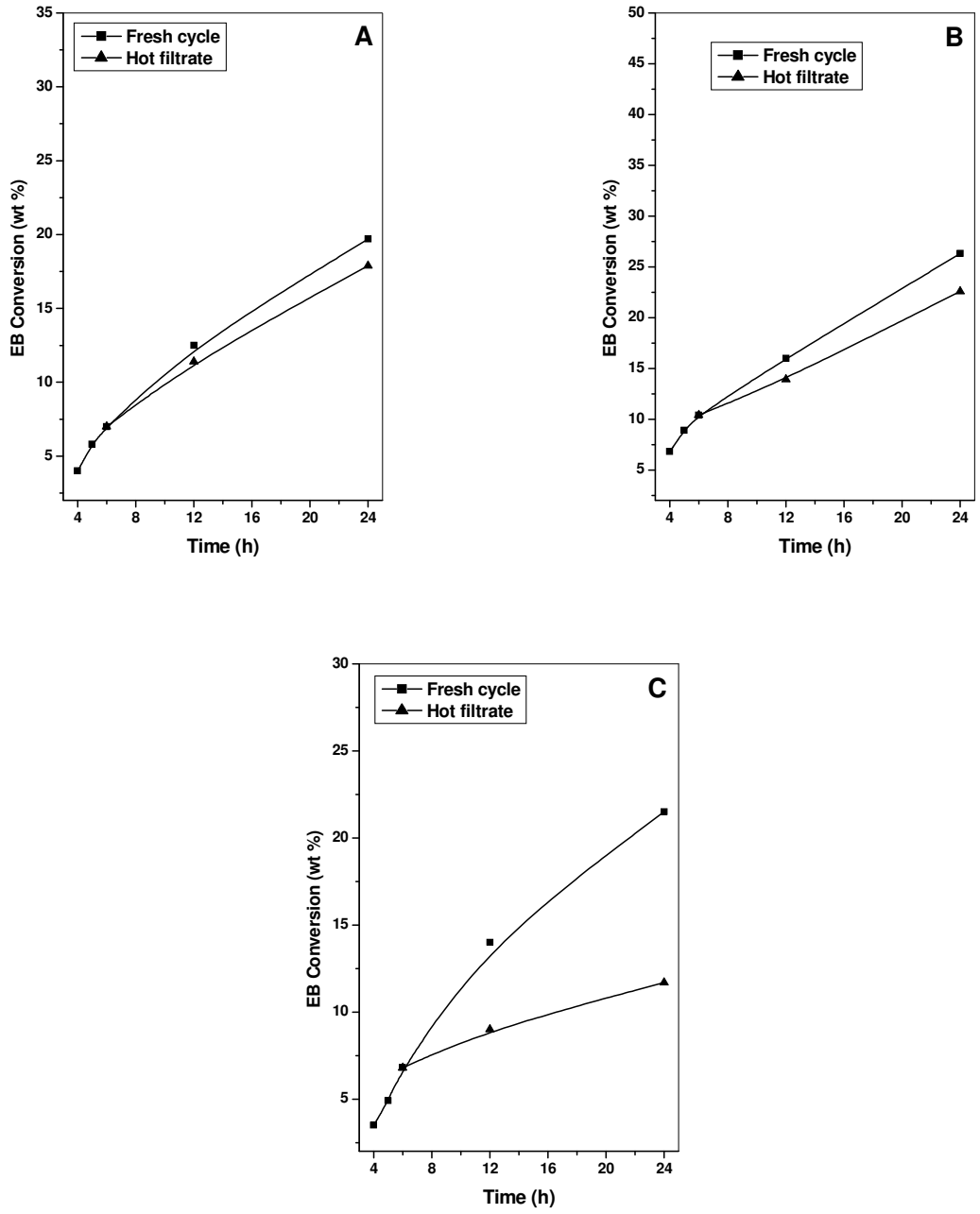

Fig. 3.5. Leaching study over different catalysts in presence of acetonitrile [A] Co/MCM-41 (50), [B] Co-MCM-41 (50) and Co-/MCM-41 (for leaching study, catalyst was removed after 6 h and filtrate was used for the further reaction). Reaction conditions are same as mentioned in footnote of Fig. 3.3.

This can be explained in terms of the dative bond (which is strong) formation between the cobalt and nitrogen (of the spacer) in the immobilized sample. It was observed that the leaching in the ethylbenzene oxidation reaction, when carried out in the solvent (acetonitrile) medium, is more than in the absence of the solvent. This indicates that cobalt species have more affinity for the solvent molecules. Thus it is concluded that cobalt is well heterogenized in the immobilized sample than in incorporated and grafted samples.

Finally taking into account all the above reaction results, the probable mechanism is shown in Scheme 3.2. The oxidation of the ethylbenzene with TBHP is supposed to occur by free radical mechanism, yielding primarily ethylbenzenehydroperoxide [34,35]. The reaction may proceed by two ways (path A and B). Since the secondary radical is more stable than primary radical, path A is more favorable. In the reaction mixture, no products (2-phenyl acetaldehyde and 2- phenyl acetic acid) were detected from path B. BZ and BA are forming as overoxidized products of AP.

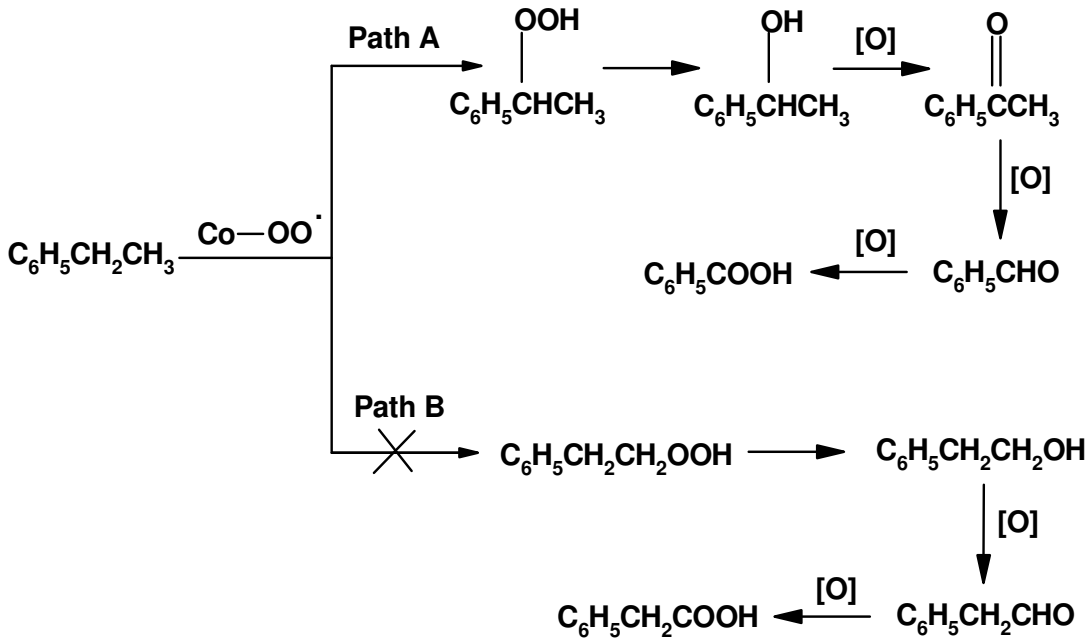

Scheme 3.2. Mechanistic pathway for the formation of different products in the oxidation of ethylbenzene

3.2.3. Oxidation of Ethylbenzene over Cobalt containing HMS

In order to evaluate the catalytic activity of the cobalt containing HMS samples, oxidation reaction of ethylbenzene was carried out as a model reaction. Catalytic results show the formation of three oxidized products viz. benzaldehyde (BZ), acteophenone (AP) and benzoic acid (BA) [Scheme 3.1]. The choice of the oxidant was *tert.* butyl hydroperoxide (TBHP) since aq. hydrogen peroxide (H_2O_2) had not shown any conversion of the ethylbenzene.

In order to probe the role of solvents, series of solvent like CH_3CN, CH_2Cl_2, $(CH_3)_2CO$, C_2H_5OH were used in the present reaction. When solvents were used for the oxidation of ethyl benzene, the conversions are less and follows the order CH_3CN (32.4) > CH_2Cl_2 (29.4) > $(CH_3)_2CO$ (12.8) > C_2H_5OH (0.8) and the selectivity towards the desired product acetophenone follows the order $(CH_3)_2CO$ (39.0) > CH_3CN (36.8) > CH_2Cl_2 (31.2) over the catalyst Co-HMS (100), after 24 h of the reaction (Fig. 3.6B). Interestingly, the conversion was more under solvent free conditions for both the cobalt-containing samples Co-HMS (100) and Co/HMS (100) showed maximum conversion of 49.5 and 39.0 wt %, respectively, after 24 h (Fig. 3.6A, Table 3.2).

The selectivity towards acetophenone was found greater than 59 % in absence of solvent over cobalt containing HMS catalysts. The formation of other products viz. benzaldehyde may arise from the cleavage in the C-C bonds while the presence of benzoic acid may result from the oxidation of benzaldehyde formed. Hence, it is clear that solvent had negative impact over the performance of the cobalt containing catalyst, which may possibly arise from the blocking of the active catalytic sites by the solvent molecules. Moreover, cobalt incorporated HMS samples (Co-HMS) shows a

decrease in conversion with an increase in the cobalt content in the HMS matrix. The decreased conversion obtained for Co-HMS having lower Si/Co ratio may be due to the presence of nanosized cobalt particles that are unable to detect by the UV-Vis and XPS techniques. Thus, the higher catalytic activity of Co-HMS (100) sample shows the well dispersion of cobalt in the framework and the presence of isolated cobalt sites are easily accessible for the substrate. In grafted cobalt samples also the conversion gets decreased with increasing the percentage of cobalt loading. Thus the decreased conversions obtained at higher cobalt loadings can be ascribed to the formation of Co_3O_4 species, irrespective of the synthesis method. Co-/HMS catalyst shows lower conversion (31%) of ethylbenzene, but the selectivity to acetophenone is maximum (82 %).

Table 3.2. Catalytic activity of Co-HMS and Co/HMS for the oxidation of ethylbenzene in absence of solvent

Entry	Catalyst	EB Conv. (wt %)	Selectivity (wt %)		
			BZ	AP	BA
1	HMS	-			
2	Co-HMS (100)	49.5	25.0	60.0	15.0
3	Co-HMS (50)	36.9	21.7	59.2	18.5
4	Co/HMS (100)	39.0	37.2	65.4	14.0
5	Co/HMS (50)	35.0	34.8	63.3	15.0
6	Co-/HMS	31.0	14.0	82.0	4.0

Reaction Conditions: ethylbenzene 1 g, TBHP 1.22 g, catalyst 0.05 g, temperature 80 ^oC; reaction time 24 h (absence of solvent).

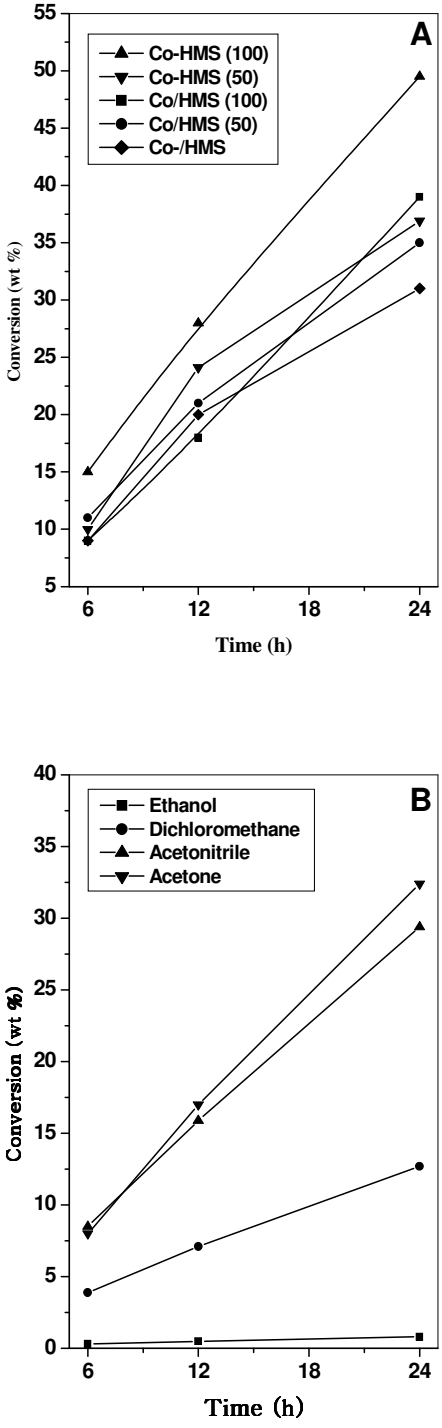

Fig. 3.6. [A] Conversion of ethylbenzene vs. time in solvent free media for different catalyst; [B] Influence of different solvent on activity of the catalyst Co-HMS (100).

The heterogeneity of the catalyst was verified by performing the typical hot filtrate experiments, under solvent free as well as in presence of solvents. The catalyst applied under the reaction condition was removed after 6 h catalytic run and the filtrate was monitored for further reactions. In presence of acetonitrile solvent, the Co-HMS (100) and Co/HMS (100) catalysts show the leaching of active sites and among them the grafted catalyst shows an almost similar conversion like the fresh cycle (Fig. 3.7). This finding is in contradiction to the earlier report, that leached cobalt species are not active in oxidation reactions [36]. However, the immobilized cobalt containing HMS (Co-/HMS) sample is not prone to leaching.

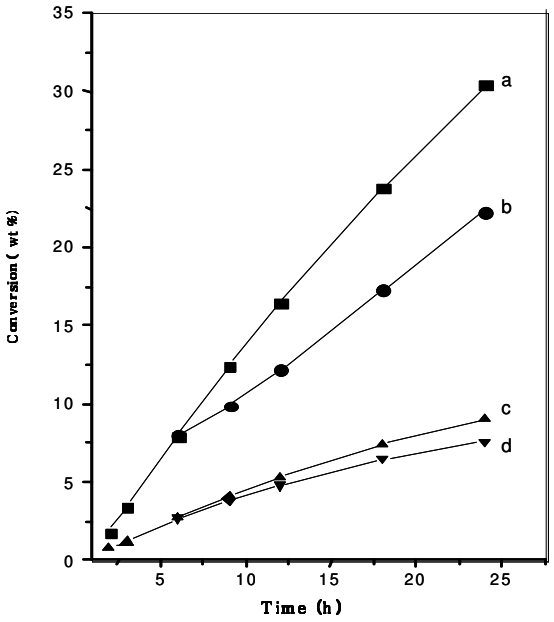

Fig. 3.7. Leaching study: Conversion of ethylbenzene vs. time using acetonitrile as solvent for (a) Co-HMS (100), (b) Co-HMS (100) was removed and filtrate used after 6h, (c) Co/HMS (100), (d) Co/HMS (50) was removed and filtrate used after 6h.

3.3. CATALYTIC OXIDATION OF DIPHENYLMETHANE OVER COBALT CONTAININING MCM-41 AND HMS

3.3.1. Reaction Procedure

Liquid phase oxidation of diphenylmethane was performed in a stirred round bottom flask fitted with a water-cooled condenser using 70-wt % TBHP as an oxidant [Scheme 3.3]. The catalyst (5 wt % with respect to diphenylmethane) was added to the reaction mixture consisting of diphenylmethane (99 %, 1 g, 5.9 mmol), TBHP (70 wt %, 0.76g, 5.9 mmol) and acetonitrile (5 ml) and heated at constant temperature of 80 ^{o}C under magnetic stirring. After certain interval of time, the reaction mixture was cooled to room temperature and catalyst was separated by centrifugation. The products were analyzed by gas chromatograph (Agilent, HP 6890) equipped with a flame ionization detector (FID) and a capillary column (5 µm cross linked methyl silicone gum 0.2 mm x 50 m) and was further confirmed by GC-MS (Shimadzu 200A). Leaching of the metal during the course of reaction was verified by resubmission of the filtrate for further reaction at same reaction conditions.

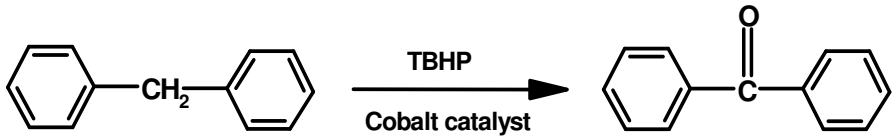

Scheme 3.3. Oxidation of diphenylmethane

3.3.2. Investigation of Catalytic Activity

Oxidation of diphenylmethane was carried out with 70 % *ter.* butyl hydroperoxide as oxidant. Other oxidants, 30 wt % H_2O_2 and 4 wt % NaOCl were also used as oxidant with cobalt catalyst. With H_2O_2 and NaOCl, negligible conversion of diphenylmethane was obtained (1.5 and 2.5 % with H_2O_2 and NaOCl, respectively). Benzophenone is the major product in the oxidation of diphenylmethane. The reaction was studied taking into consideration of temperature, solvent, framework and extraframework cobalt.

The catalytic activity of cobalt incorporated, grafted and immobilized catalysts have been shown in the Table 3.3. It is clear that, selectivity remains almost the same irrespective of catalyst used in the reaction. However, the conversion varies depending upon the different cobalt species. It is found that immobilized cobalt catalyst gives higher conversion followed by grafted and incorporated cobalt catalysts, respectively. The order of activity of different catalysts is as follows: Co-/HMS [33.0 %] > Co-/MCM-41 [29.0 %] > Co/HMS (50) [22.0 %] > Co-HMS (50) ([8.70 %] > Co/MCM-41 (50) [15.5 %] > Co-MCM-41 (50) [15.10 %] > Co-HMS (100) [14.36 %] > Co-MCM-41 (100) [11.50 %] > Co/HMS (100) [9.50 %] > Co/MCM-41 (100) [6.80 %]. It was observed that catalytic activity of immobilized cobalt species is more than grafted and incorporated cobalt species, respectively (Table 3.3). The results also indicate that catalytic activity of cobalt species in HMS is more than MCM-41. It may be due to wormhole like pore structure of HMS with larger pore diameter. The pore structure with wormhole like pore structure is easily accessible to the reactant. Moreover, from the performance of catalyst (prepared by different methods), it seems

that oxidation of diphenylmethane requires more exposure of active cobalt species for the oxidation of diphenymethane.

Table 3.3. Comparison of catalytic performance for the oxidation of diphenylmethane in acetonitrile.

Catalyst	Conversion of diphenylmethane (wt %)	Selectivity to Benzophenone (wt %)
Co-MCM-41 (100)	11.5	100
Co-HMS (100)	14.3	100
Co-MCM-41 (50)	15.1	100
Co-HMS (50)	18.7	100
Co-/MCM-41	29.0	100
Co-/HMS	33.0	100
Co/MCM-41 (100)	6.8	100
Co/HMS (100)	9.5	100
Co/MCM-41 (50)	15.5	100
Co/HMS (50)	22.0	100

Catalyst: 0.05 g, temperature - 80 ^{0}C, diphenylmethane: TBHP = 1:1, time - 12 h, solvent - acetonitrile.

This is why incorporated cobalt (active sites are in the framework) species are less active when compared with grafted and immobilized cobalt species. Moreover, the selectivity remains always high with cobalt catalyst (irrespective of synthesis methods). Thus, it proved that cobalt catalyst is very much selective and can be successfully employed for the oxidation of diphenylmethane.

The reaction temperature have prominent role in the reaction. It is found that conversion of diphenylmethane increases very slightly with the increase of temperature without any change in selectivity to benzophenone (Table 3.4). The temperature above 80 ^{0}C was intentionally avoided because of the decomposition of TBHP at higher temperature.

Table 3.4. Effect of temperature on catalytic performance of Co-/MCM-41.

Temperature (^{o}C)	Conversion of diphenylmethane (wt %)	Selectivity to benzophenone (wt %)
50	21	100
65	26	100
80	29	100

Catalyst: 0.05 g, solvent: acetonitrile, diphenylmethane: TBHP = 1:1, time: 12 h.

The role of solvent is very crucial in the oxidation of diphenymethane and selectivity to benzophenone. For this, the reaction was examined using different solvents like acetonitrile, acetone, ethanol, methanol and dichloromethane. No catalytic activity was found with methanol and ethanol. Table 3.5 shows that with dichloromethane, conversion of diphenylmethane is more. However, the selectivity to benzophenone is low. Further, ortho and para hydroxy derivative of benzophenone were formed from benzophenone when dichloromethane was used as solvent. This results in the decrease of selectivity to benzophenone. In other solvents, selectivity to benzophenone was obtained in the range of 90-100 %. In chlorinated solvent, C─H

bond at ortho and para position of phenyl ring is more weakened and radical hydroxy substitution occurs at ortho and para positions of phenyl ring.

Table 3.5. Effect of solvent on catalytic performance over Co-MCM-41 (50).

Solvent	Conversion of diphenylmethane (wt %)	Selectivity to benzophenone (wt %)
Acetonitrile	13	100
Acetone	10	100
Dichloromethane	22.8	70.2
Isopropyl alcohol	6.3	92

Catalyst - 0.05 g, temperature - 80 ^{0}C, diphenylmethane: TBHP = 1:1, time - 12 h.

The feasibility of oxidation of diphenylmethane was examined in solvent free media. In the absence of solvent, the selectivity to benzophenone reduced to 72 % and some unusual hydroxy derivatives of benzophenone were formed. In benzophenone, phenyl radical is stabilized by resonance. Further, the resonance is extended by C═O group. In solvent free media, it seems that cobalt ion in the transition state stabilize the phenyl radical at ortho and para position via resonance more explicitly and formation of hydroxy substituted derivative of benzophenone becomes more viable. This is not the case when reaction was carried out in presence of solvent except dichloromethane (among the tested solvents). It is conceptualized that there is some mechanism operating to arrest the stabilization of phenyl radical at ortho and para position and subsequently avoiding the formation of hydroxy derivative of benzophenone. However, the mechanism is not yet understood. Table 3.6 shows that the increase in

the conversion of diphenylmethane was observed with increase in the cobalt content in solvent free media. However, the selectivity decreases with increase in the metal content. It was also observed that cobalt immobilized catalyst still remains very selective (more than 95 % selectivity to benzophenone) and decrease in the selectivity to benzophenone is more in grafted and incorporated cobalt catalyst in solvent free media for the oxidation of diphenylmethane. In immobilized cobalt catalyst, the acidity of cobalt reduced due to transfer of electron from the nitrogen (of the spacer group) to cobalt species via formation of dative bond. Thus it seems that more selective (to benzophenone) nature of immobilized catalyst is due decrease of acidity to certain extent. Wang et al reported that in acetic acid (as solvent), cobalt grafted on MCM-41 forms hydroxy derivative of benzophenone [37].

Table 3.6. Oxidation of diphenylmethane in solvent free media.

Catalyst	Conversion of diphenylmethane (wt %)	Selectivity to benzophenone (wt %)
Co-MCM-41 (100)	7.4	89.2
Co-MCM-41 (50)	10.0	85.0
Co/MCM-41 (100)	5.0	82.0
Co/MCM-41 (50)	7.5	77.8
Co-/MCM-41	12.2	100
Co-HMS (100)	11.5	90.0
Co-HMS (50)	13.0	78.3
Co/HMS (100)	8.7	75.9
Co/HMS (50)	10.4	72.0
Co-/HMS	15.0	100

Catalyst - 0.05 g, temperature - 80 ^{0}C, diphenylmethane: TBHP, time - 12 h.

Finally, the leaching of the catalyst was examined by submitting the hot filtrate (after removal of catalyst) for further reaction. From the Fig. 3.8, the immobilized cobalt catalyst functions heterogeneously. Incorporated and grafted cobalt catalysts are prone to leeching. In this case, leaching is due to weak interaction of metal ion with the silica. In immobilized catalyst, cobalt is strongly held to nitrogen of the spacer group via dative bond. This reveals that strong interaction is necessary for leaching resistive catalyst.

It have been shown that oxidation of diphenylmethane took place by radical mechanism [38,39]. It is generally believed that oxidation of benzophenone is initiated via hydrogen abstraction by $C(CH_3)_3^{\cdot}$ followed by formation of diphenyl radical, which subsequently undergo reaction to form benzophenone (Scheme 3.4).

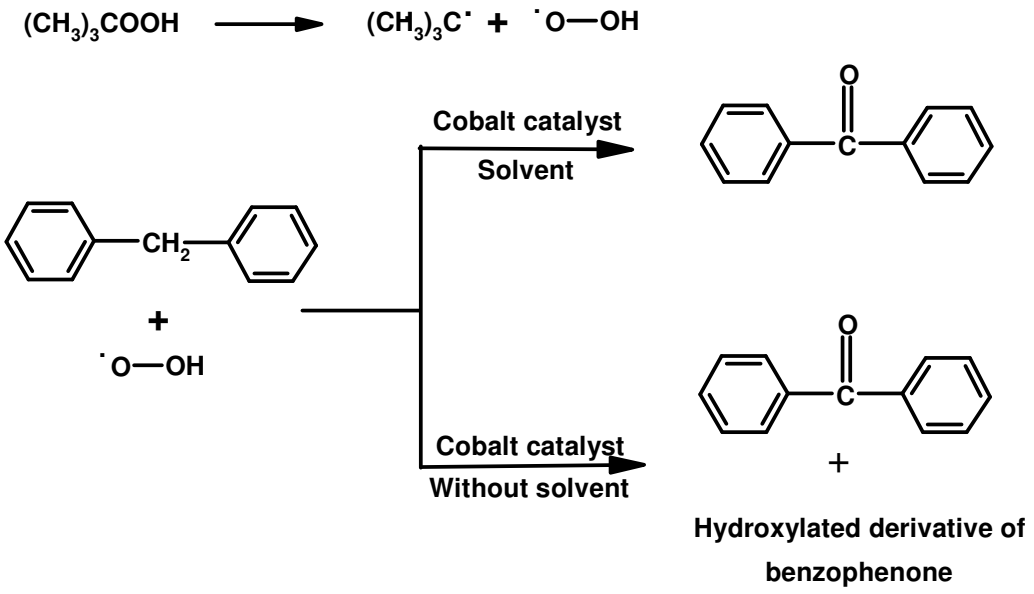

Scheme 3.4. Plausible radical mechanism for oxidation of diphenylmethane

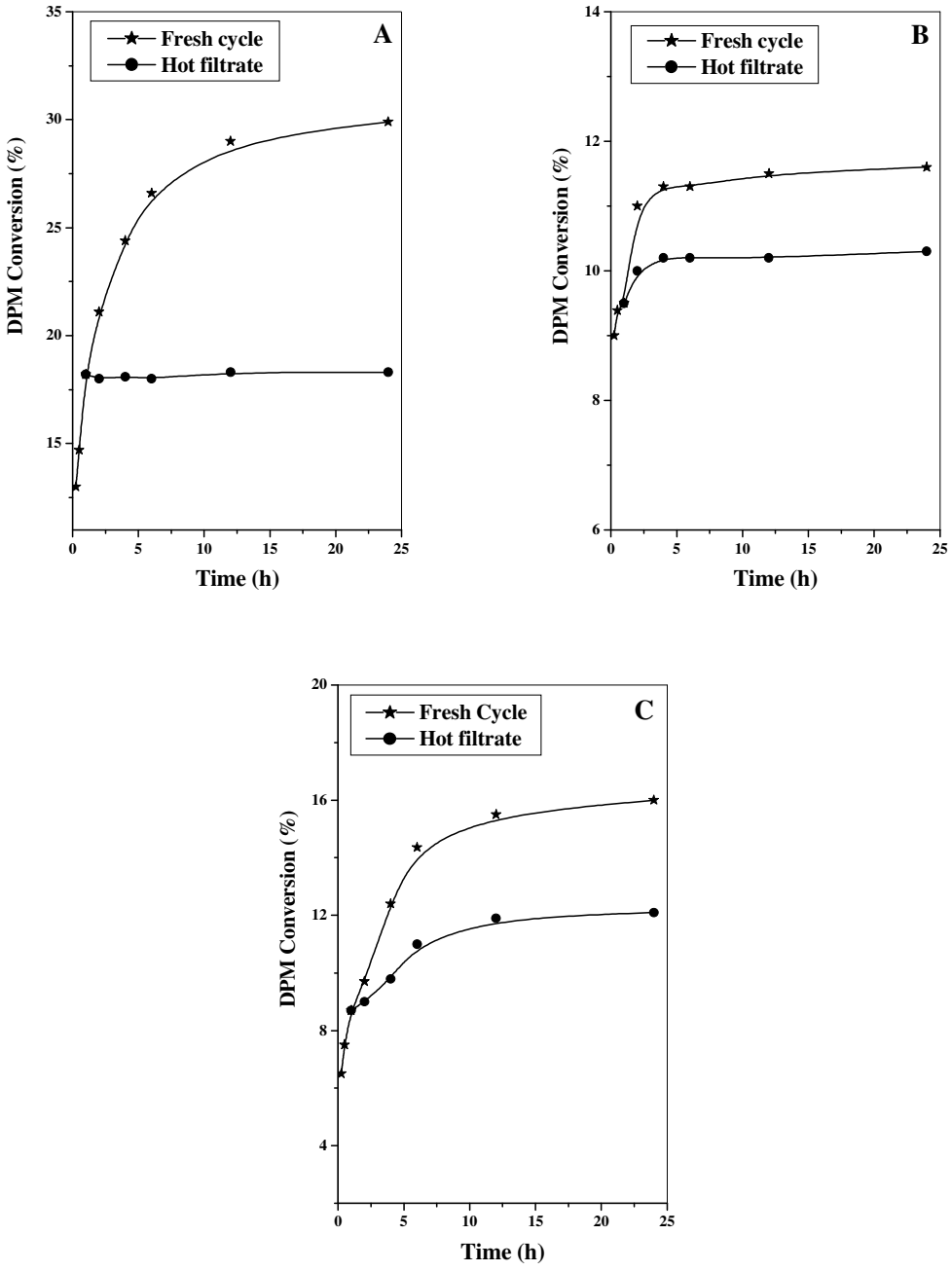

Fig. 3.8. Leaching study over the catalyst [A] Co-/MCM-41, [B] Co-MCM-41 (50) and [C] Co/MCM-41 (50).

References

[1] G. Centi, F. Cavani, F. Trifiro, M.V. Twigg, M.S. Spencer (Eds.), Selective Oxidation by Heterogeneous Catalysis: Recent Developments, Fundamental and Applied Catalysis, Kluwer/Plenum Publishing Corporation, New York and London, 2001.

[2] P. Arpentinier, F. Cavani, F. Trifiro, The Technology of Catalytic Oxidations. 1. Chemical Catalytic and Engineering Aspects, Paris, France, 2001.

[3] G. Centi, S. Perathoner, Selective Oxidation, Section E, Industrial Processes and Relevant Engineering Issues, I.T. Horvath, Encyclopedia of Catalysis, Wiley, New York, 2003.

[4] E.O. Ohsol, Hydrocarbon oxidation, in: J.J. McKetta (Ed.), Encyclopedia of Chemical Processing and Design, vol. 33, Marcel Dekker, New York, 1987, P. 36.

[5] A. Bruckner, U. Bentrup, A. Martin, J. Radnik, L. Wilde, G.-U. Wolf, Stud. Surf. Sci. Catal. 130 A (2000) 359.

[6] D.A. Bulushev, L. Kiwi-Minsker, V.I. Zaikovskii, A. Renken, J. Catal.193 (2000) 145.

[7] F. Konietzni, H.W. Zanthoff, W.F. Maier, J. Catal. 188 (1999) 154.

[8] S. D. Val, M.L. Granados, J.L.G. Fierro, J. Santamaria-Gonzalez, A. Jimenez-Lopez, J. Catal. 188 (1999) 203.

[9] J.S. Yoo, J.A. Donohue, M.S. Kleefish, P.S. Lin, S.D. Elfine, Appl. Catal. A 105 (1993) 83.

[10] J.S. Yoo, C. Choi-Feng, J.A. Donohue, Appl. Catal. A 118 (1994) 87.

[11] J.S. Yoo, Appl. Catal. A Gen. 143 (1996) 29.

[12] G. Centi, S. Perathoner, S. Tonini, Topics Catal. 11 (2000) 195.

[13] G. Centi, S. Perathoner, S. Tonini, Catal. Today 61 (2000) 211.

[14] (a) E. Iglesia, S. C. Reyes, R. J. Modon, S. L. Soled, Adv. Catal. 39 (1993) 221. (b) A. C. Vosloo, Fuel. Process. Technol. 71 (2001) 149.

[15] C. S. Marvel, W. M. Sperry, Organic Syntheses, Collected Volume 1, (1941) P. 95.

[16] N. K. Mal, A. V. Ramaswamy, Appl. Catal. A 143 (1996) 75.

[17] I. Hermans, J. Peeters, P. A. Jacobs, J. Org. Chem. 2007, 72, 3057.

[18] S. Vetrivel, A. Pandurangan, J. Mol. Catal. A 217 (2004) 165.

[19] V. R. Choudhary, J. R. Indurkar, V. S. Narkhede, R. Jha, J. Catal. 227 (2004) 257.

[20] A. Shaabani, A. Bazgir, F. Teimouri, D. G. Lee, Tetrahedron Lett. 43 (2002) 5165.

[21] J. H. Clark, A. P. Kybett, P. Landon, D. J. Macquarrie, K. Martin, J. Chem. Soc., Chem. Commun. (1989) 1355.

[22] J. Muzart, Tetrahedron Lett. 28 (1987) 2131.

[23] J. Muzart, A. N'Ait Ajjou, J. Mol. Catal. 66 (1991) 155.

[24] J. Muzart, Chem. Rev. 92 (1992) 113.

[25] B. M. Choudary, A. D. Prasad, V. Bhuma, V. Swapna, J. Org. Chem. 57, (1992) 5841.

[26] R. A. Sheldon, J. D. Chen, J. Dakka, E. Neeleman, Stud. Surf. Sci. Catal. 83 (1994) 407.

[27] T. K. Das, K. Chaudhari, E. Nandanan, A. J. Chandwadkar, A. Sudalai, T. Ravindranathan, S. Sivasanker, Tetrahedron Lett. 38 (1997) 3631.

[28] A. J. Pearson, G. R. Han, J. Org. Chem. 50 (1985) 2791.

[29] K. Nakayama, M. Hamamoto, Y. Nishiyama, Y. Ishii, Chem. Lett. (1993) 1699.

[30] Y. Ishii, S.Y. Fujibayashi, K. Nakayama, M. Hamamoto, S. Sakaguchi, Y. Nishiyama, J. Mol. Catal. 110 (1996) 105.

[31] P. S. Singh, K. Kosuge, V. Ramaswamy, B.S. Rao, Applied Catalysis A: General 177 (1999) 149.

[32] J. M. Thomas, R. Raja, J. Organo. Chem. 689 (2004) 4110.

[33] I. L. Finar, Organic Chemistry, Vol. 1, 6 th edition, 617

[34] J.D. Chen, R.A. Sheldon, J. Catal. 154 (1995) 1.

[35] S.H. Jhung, Y.S. Uh, H. Chan, Appl. Catal. 62 (1990) 61.

[36] W. A. Carvalho, M. Wallau, U. Schuchardt, J. Mol. Catal. A, 144 (1999) 91.

[37] F. Chang, W. Li, F. Xia, Z. Yan, J. Xiong, J. Wang, Chem. Letter 11 (2005) 1540.

[38] R. L. Brutchey, I. J. Drake, A. T. Bell, T. D. Dilley, Chem. Commun. (2005) 3736.

[39] Y. Ogata, H. Tezuka, T. Kamei, J. Org. Chem. 34 (1969) 845.

4.1. Introduction

Ordered mesoporous silica has been emerged as an area of intense research in catalysis and material research [1-3]. The narrow and controllable pore size distribution, relatively large pore openings, large surface areas and greater absorption capacity are the significant properties of mesoporous material in catalysis [4]. The active sites can be created using different types of methods like synthesis, post synthesis and immobilization. The metal containing molecular sieves find wide application in oxidation, reduction and acidic reactions. Zirconia catalysts are finding widespread use due to their moderate acidity and their oxidizing capability [5,6]. Zirconium has been introduced into the framework of ordered (MCM-41 and MCM-48) and disordered (HMS) mesoporous silicas [7-16]. These solids combine high surface area (usually higher than 800 m^2/g) and size selectivity, but the synthetic procedures used severely affect the catalytic performances of the resulting materials. An important condition for having very active supported zirconia catalysts lies in site isolation: the Zr atoms must be isolated and well dispersed throughout the silica network, thus avoiding the formation of ZrO_2 clusters [17].

In this chapter, synthesis and characterization of zirconium containing MCM-41 and HMS were studied in detail.

4.2. Synthesis and Characterization of Zirconium containing MCM-41

4.2.1. Experimental

The starting materials and their sources were fumed silica (99 %, Aldrich), zirconium *ter.* butoxide (99.95 %, Lancaster), cetyltrimethylammonium bromide (98 %, Loba Chemie), trimethoxy propyl amine silane and sodium hydroxide (Merck). All the chemicals were used without further purification.

4.2.1.1. Synthesis

4.2.1.1.1. Synthesis of hexagonal mesoporous molecular sieves MCM-41

Fumed silica and cetyl trimethyl ammonium bromide (CTMABr) were used as silica source and surfactant, respectively. In a typical synthesis, CTMABr was dissolved in Sodium hydroxide (NaOH) solution. To this, fumed silica was added slowly and stirred for 6 h. The molar gel composition was as follows

$$1\ SiO_2: 0.19\ CTMABr: 0.4\ NaOH: 78\ H_2O$$

Finally pH of the gel was maintained at 10.9 using dil. HCl. The gel was transferred to glass bottle (autoclavable) and kept in oil bath maintained at 100 ^{o}C for 48 h. Mixture was filtered, washed several times with distilled water under vacuum and dried at 100 ^{o}C. As synthesized materials was calcined at 500 ^{o}C for 12 h.

4.2.1.1.2. Synthesis of Zirconium substituted MCM-41 (Zr-MCM-41)

Zr-MCM-41 was synthesized by direct hydrothermal method with Si/Zr ratio of 100 and 50. Fumed silica was added slowly to the mixture of NaOH and CTMABr with constant stirring. After 1 h, calculated amount of Zirconium (IV) *ter.* butoxide was added and stirring was allowed for another 5 h. The molar gel composition was

$$1\ SiO_2: x\ Zr(O^tBt)_4: 0.19\ CTMABr: 0.4\ NaOH: 120\ H_2O$$

Where 'x' is the calculated amount of Zirconium (IV) *ter.* butoxide for different Si/Zr ratios. The pH of the gel was maintained at 10.5. The gel was transferred to autoclavable bottle kept in oil bath maintained at 100 ^oC for three days. Finally, it was filtered, washed several times with distilled water and dried in air at 100 ^oC for 12 h. As synthesized material was calcined as described earlier. The materials were designated as Zr-MCM-41 (100) and Zr-MCM-41 (50) for Si/Zr ratio of 100 and 50, respectively.

4.2.1.1.3. Synthesis of zirconium-grafted MCM-41 (Zr/MCM-41)

Zirconium (IV) *ter.* butoxide (0.064 and 0.128 g for 1.5 and 3 wt % of zirconium loading respectively) was dissolved in anhydrous toluene (50 ml). To this, 1 g of MCM-41 was added and refluxed at 100 ^oC for 12 h with constant stirring. Solvent was removed at its boiling temperatures using rotavapor. The samples were dried and calcined at 500 ^oC to remove the organic matter. They were designated as Zr/MCM-41 (100) and Zr/MCM-41 (50) for 1.5 and 3-wt % loading of zirconium, respectively.

4.2.1.1.4. Synthesis of zirconium immobilized on MCM-41 (Zr-/MCM-41)

Equal moles of trimethoxy propyl amine silane and Zirconium (IV) *ter.* butoxide (0. 12 g Zirconium (IV) *ter.* butoxide and 0.06 g trimethoxy propyl amine silane) were mixed in 100 ml toluene at room temperature for 6 h. After half an hour, 1 g of MCM-41 was added to the solution. The resulting solution was kept in oil bath maintained at 100 ^{0}C for 10 h with constant stirring. Solvent was removed at its boiling temperatures using rotavapor and the samples were dried at 70 ^{0}C. Sample was designated as Zr-/MCM-41.

4.2.1.2. Characterization

Powder X-ray diffraction pattern of the samples were recorded on a Rigaku D max III VC Ni filtered Cu Kα radiation, λ = 1.54 Å between 1 and 10 (2θ angle) with a scanning rate of 1^o/min. The specific surface area, total pore volume and average pore diameter were measured by the N_2 adsorption desorption method using NOVA 1200 (Quanta Chrome) instrument. The samples were activated at 300 ^{o}C for 3 h under vacuum and then adsorption desorption was conducted by passing nitrogen over samples which was kept under liquid nitrogen. Pore size distribution was obtained by applying BJH pore analysis method to the desorption branch of nitrogen adsorption isotherm. SEM micrograph of the zirconium containing samples were obtained on JEOL-JSM 520 scanning microscope while the TEM images were performed on a JEOL-TEM 1200 EX instrument with 100 kV accelerating voltage to probe the mesoporosity of the material. Zirconium content in the samples was determined by atomic absorbance analysis using Perkin Elmer 11013 spectrometer after dissolution

of the samples in HCl-HF solution. Diffuse reflectance UV-Vis spectra of the powder samples were recorded in the range 200-800 nm on Shimadzu UV 2101 PC spectrometer equipped with a diffuse reflectance attachment, using $BaSO_4$ as the reference.

4.2.2. Results and Discussion

4.2.2.1. Powder X-ray diffraction

Fig. 4.1 shows the XRD diffraction pattern of calcined zirconium containing MCM-41 materials in the range 1-10 degree of 2θ angle. The X-ray powder diffraction patterns are typical of MCM-41 type materials and show (100), (110), (200) and (210) diffraction peaks in agreement with the literature [1,2]. The presence of higher order reflection peaks indicate well-defined long-range mesoporous structural order. Physicochemical properties of these mesoporous materials are summarized in Table 4.1. For pure MCM-41, the main (100) reflection peak was observed at 2θ angle of 2.5 degree. In zirconium incorporated MCM-41 sample, this peak was appeared at slightly less 2θ angle than for pure MCM-41 (Table 4.1), which subsequently results in the increase in the value of d spacing and unit cell parameter (a_0).

The unit cell parameter (a_0) was calculated using the formula $a_0 = 2d/\sqrt{3}$. The increase in the a_0 value is due to incorporation of zirconium in the framework of MCM-41 (Zr-O and Si-O bond lengths are 1.71160 and 1.5090 Å, respectively) [18-20]. Moreover, the a_0 value increases with the increase in the zirconium content. For Zr-MCM-41 (100) and Zr-MCM-41 (50), the a_0 values are 42.63 and 44.3 Å, respectively, which is higher than pure MCM-41 (the corresponding value for MCM-

41 was observed at 40.80 Å). This fact reveals the successful incorporation of zirconium in the mesoporous silica framework.

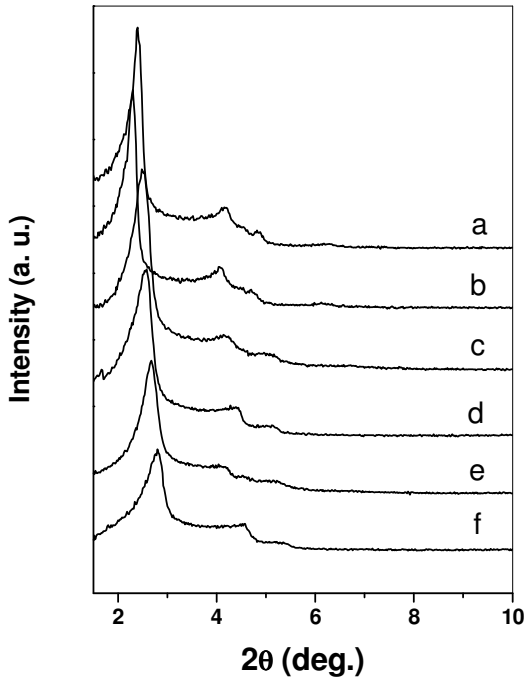

Fig. 4.1. X-ray diffraction patterns of zirconium containing MCM-41: (a) Zr-MCM-41 (100), (b) Zr-MCM-41 (50), (c) MCM-41, (d) Zr/MCM-41 (100), (e) Zr/MCM-41 (50) and (f) Zr-/MCM-41.

Furthermore, the incorporation of zirconium in the framework does not affect the mesoporous hexagonal structural ordering as evidenced from the presence of higher order reflection peaks in the XRD patterns of incorporated samples. Thus, retaining the hexagonal structure. The a_0 value decreased in the zirconium grafted and immobilized MCM-41 samples when it is compared with pure MCM-41 (Table 4.1). This is obvious because of the presence of the zirconium on the framework (through spacer in case of immobilization) of MCM-41. However, the decrease in the a_0 value

of immobilized sample is more than grafted one [a_0 value for Zr-/MCM-41 is 36.39 Å; for Zr/MCM-41 (100) and Zr/MCM-41 (50) are 39.8 and 38.16 Å, respectively. Both values are comparatively less than for pure MCM-41]. No characteristic peaks belonging to crystalline zirconium oxide related compound has been observed in the higher angle XRD.

Table 4.1. Physico-chemical properties of zirconium containing MCM-41.

Catalyst	Si/Zr [a] (molar ratio)	2θ angle (degree)	d-spacing (Å)	a_0 [b] (Å)	S_{BET} [c] (m^2g^{-1})	D_p [d] (Å)
MCM-41	-	2.50	35.30	40.8	1010	31.0
Zr-MCM-41 (100)	108	2.39	36.92	42.6	980	32.1
Zr-MCM-41 (50)	55	2.30	38.36	44.3	940	33.5
Zr/MCM-41 (100)	98	2.56	34.47	39.8	905	30.2
Zr/MCM-41 (50)	51	2.67	33.05	38.1	835	29.3
Zr-/MCM-41	60	2.80	31.51	36.4	715	n. d.

[a] Zirconium content estimated by AAS analysis.

[b] Unit cell parameter values calculated using $a_0 = 2d_{100}/\sqrt{3}$.

[c] S_{BET} is the surface area calculated by BET method.

[d] D_p is the average pore diameter.

n. d.- not determined

4.2.2.2. N_2 sorption isotherms

N_2 adsorption-desorption isotherms and BJH pore size of zirconium containing mesoporous MCM-41 are shown in Fig. 4.2 [21]. All isotherms showed type IV character, with completely reversible nature, which is typical for uniform mesoporous MCM-41 [22]. The isotherms exhibit a sharp inflection in the range of 2.5-3.5 of

relative pressure (P/P_o) because capillary condensation of N_2 within the mesopores suggesting a narrow pore size distribution [1,2]. The steep rise in the isotherm shifts slightly toward higher relative pressure with the incorporation of zirconium (Fig. 4.2A). The hysterisis loop was not observed with the introduction of zirconium in the framework showing no distortion in the structure. The isotherms for MCM-41 and zirconium grafted MCM-41 are almost the same with no any difference in the position of inflection point. For the zirconium immobilized MCM-41 samples, sharpness diminished in the isotherms and shifts towards low relative pressure because of the spacer group. BET surface areas, pore volume and pore diameters are reported in Table 4.1. Highest BET surface area of 1010 m^2g^{-1} was observed for the pure MCM-41 sample. The BET surface area decreased with increasing zirconium content. For incorporated samples, Zr-MCM-41 (100) and Zr-MCM-41 (50), surface area was found to be 980 m^2g^{-1} and 940 m^2g^{-1}, respectively. However, for grafted and immobilized samples, decrease in BET surface area is remarkable (Table 4.1). The pore size distribution curves are very sharp showing a very narrow pore size distribution (Fig. 4.2B). The more pore volume was observed with the zirconium incorporated MCM-41 samples.

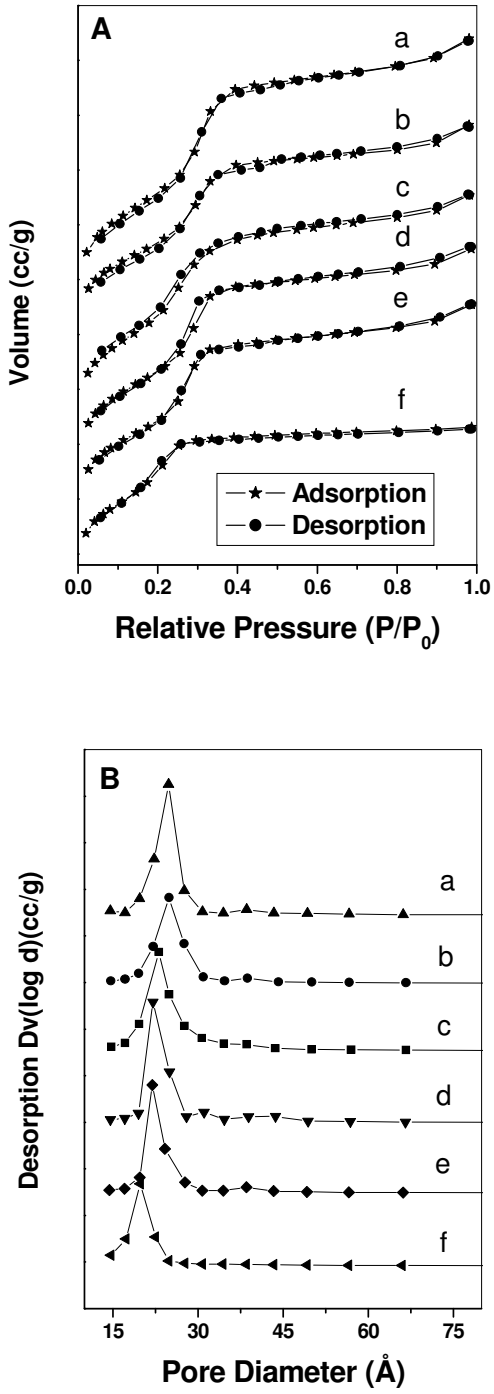

Fig. 4.2. [A] N_2 sorption isotherms and [B] BJH pore size distribution curves of zirconium containing MCM-41: (a) Zr-MCM-41 (100), (b) Zr-MCM-41 (50), (c) pure MCM-41, (d) Zr/MCM-41 (100), (e) Zr/MCM-41 (50) and (f) Zr-/MCM-41.

4.2.2.3. FT-IR spectroscopy

Fig. 4.3 shows the FT-IR spectra of MCM-41 and zirconium containing MCM-41 in the range of 4000-400 cm^{-1}. Absorption band at 960 cm^{-1} seen in the spectra is attributed to stretching vibration of Si-O-Si and Si-O-Zr bonds [23]. The intensity of the peak at 960 cm^{-1} is increasing with the zirconium content in zirconium incorporated MCM-41 samples, which is taken as the proof for the incorporation of zirconium in the framework.

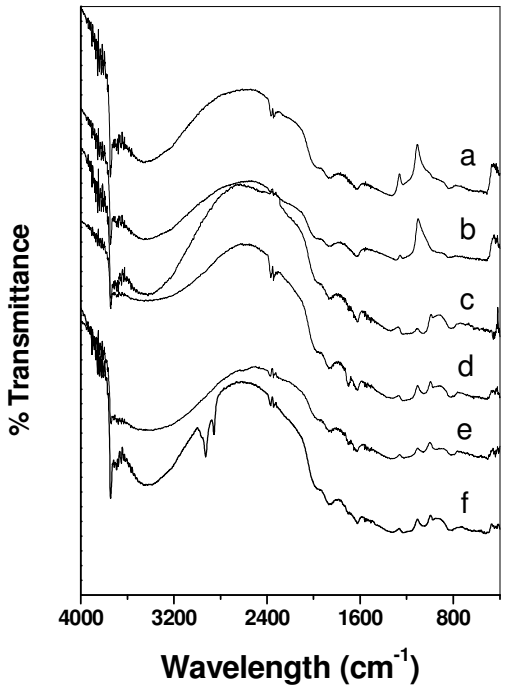

Fig. 4.3. FT-IR spectra of zirconium containing MCM-41: (a) Zr-MCM-41 (100), (b) Zr-MCM-41 (50), (c) pure MCM-41, (d) Zr/MCM-41 (100), (e) Zr/MCM-41 (50) and (f) Zr-/MCM-41.

The bands around 1080 and 1228 cm^{-1} are associated to the internal and external asymmetric Si-O stretching modes. This band can be interpreted in terms of the

overlapping of both Si-O-Si and Si-O-Zr bond vibrations [24]. The broad bands in the hydroxyl region are attributed to surface silanol with hydrogen bonded OH groups. A sharp absorption band at 3748 cm^{-1} is ascribed to free Si-OH groups. It is to be noted that the area under this band was found more in zirconium incorporated MCM-41 samples indicating that additional area may be due to free Zr-OH groups. In the Zr-/MCM-41 sample, the sharp bands at 2927 and 2854 cm^{-1} due to asymmetric and symmetric stretching vibration of C-H bond confirms the successful functionalisation of 3-amino propyl trimethoxy silane on the wall of MCM-41 [23-25].

4.2.2.4. Microscopic images

The morphology and the long-range order were investigated by SEM and TEM. Fig. 4.4 Shows the SEM and TEM of MCM-41 and Zr-MCM-41 (100). From the XRD results, it is clear that that morphology is hexagonal since high reflection peaks are present (characteristic of hexagonal structure). However the SEM and TEM show the morphology, which seems like spherical with uniform particle size. Reports claim that it is due transformation of hexagonal to spherical morphology (in spite of high reflection peaks in the XRD) [26]. TEM images clearly indicate that most of the particles are aggregated in Zr-MCM-41.

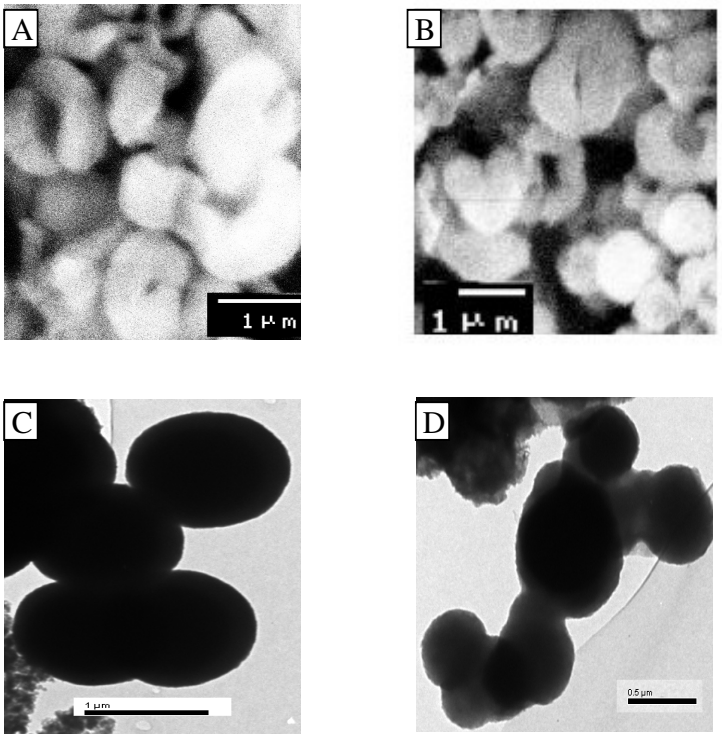

Fig. 4.4. SEM and TEM picture of MCM-41 and Zr-MCM-41 (100).

4.2.2.5. UV-Vis spectroscopy

DR UV–Vis spectra of zirconium containing MCM-41 samples are shown in the Fig. 4.5. Zirconium containing mesoporous silica absorb at 212 nm [27,29]. The absorption edge of zirconium is due to $O^{2-} \rightarrow Zr^{4+}$ charge transfer transitions in a tetrahedral coordination. In ZrO_2 where there is fully connectivity of Zr-O-Zr linkage, the LMCT shifts to lower energy value [39]. The intense absorbance edge in range of 200-212 nm is indicative of tetrahedral zirconium in the framework of amorphous silica framework. No characteristic peak at 230 nm featuring the presence of bulk zirconia was observed. In grafted and immobilized samples, weak absorption observed

in the energy range of 200-210 nm, suggesting few zirconium in the tetrahedral coordination. Moreover, the absorptions in the range 229-240 nm are prominent, suggesting the presence of Zr-O-Zr linkages. In addition to this, the absorption features around 275, 330 and 375 nm are observed. In absence of reliable data, it is difficult to know about these features.

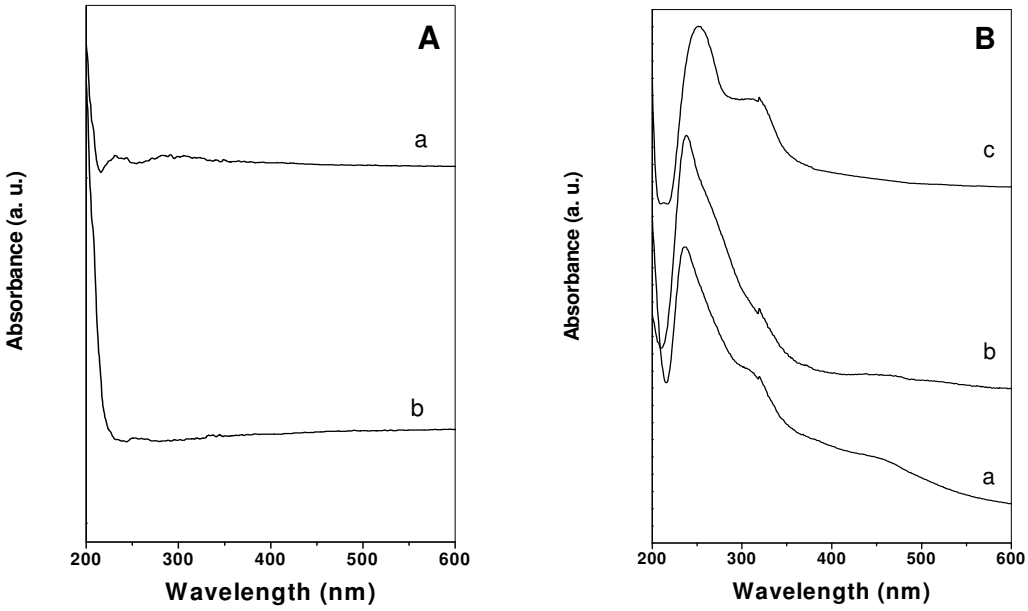

Fig. 4.5. UV-vis spectra of zirconium containing MCM-41: [A] (a) Zr-MCM-41 (100), (b) Zr-MCM-41 (50), [B] (a) Zr/MCM-41 (100), (b) Zr/MCM-41 (50) and (c) Zr-/MCM-41.

4.3. Synthesis and Characterization of Zirconium containing HMS

4.3.1. Experimental

The starting materials were ethyl silicate (40 %, Indoplast), hexadecyl amine (95 %, Lancaster), zirconium (IV) *ter.* butoxide (99.95 %, Lancaster), trimethoxy propyl amine silane (99 %, Aldrich), absolute ethyl alcohol (Merck), and sodium hydroxide (Merck). All the chemicals were used without further purification.

4.3.1.1. Synthesis

4.3.1.1.1. Synthesis of hexagonal mesoporous molecular sieves (HMS)

Ethyl silicate (ES) and hexadecylamine (HA) were used as silica source and surfactant, respectively. First, surfactant solution was prepared and it was heated at 60 ^{0}C (because of partial miscible nature of HA in water) for half an hour to form uniform mixture. To this, TEOS in ethyl alcohol was added gently with constant stirring for 4 h. The pH of the gel was maintained in between 5.2 to 5.5 with dil. HCl. The final molar gel composition was as follows

$$1SiO_2: 0.14HA: 8.1EtOH: 84H_2O$$

The solution was transferred to glass bottle and kept at room temperature for 48 h. It was filtered, washed with copious amount of water and dried at 100 ^{o}C. It was calcined at 510 ^{o}C for 12 h in air.

4.3.1.1.2. Synthesis of zirconium substituted hexagonal mesoporous molecular sieves HMS (Zr-HMS)

The procedure followed for synthesis of Zr-HMS was same as mentioned above. In a typical synthesis, mixture zirconium (IV) *ter.* butoxide (0. 62 g and 0.31 g for Si/Zr 50 and 100, respectively) and 12 g of ES in absolute ethanol was added dropwise to surfactant solution (2.8 g of HA) with constant stirring for 4 h. The pH of the gel was maintained at 5.2. The gel was transferred to a glass bottle and kept at room temperature for 48 h. The final molar gel composition was same as mentioned above. Finally, it was filtered, washed several times with distilled water and dried at 100 ^{0}C. Calcination was carried out at 510 ^{o}C for 12 h in air. The template free samples were designated as Zr-HMS (50) and Zr-HMS (100), respectively.

4.3.1.1.3. Synthesis of zirconium-grafted HMS (Zr/HMS)

Zirconium (IV) *ter.* butoxide (0.064 and 0.128 g for 1.5 and 3 wt % of zirconium loading, respectively) was dissolved in anhydrous toluene. To this, 1 g of HMS was added and refluxed at 100 ^{o}C for 12 h with constant stirring. Solvent was removed at its boiling temperatures using rotavapor. The samples were dried and calcined at 450 ^{o}C to remove the organic matter. They were designated as Zr/HMS (100) and Zr/HMS (50) for 1.5 and 3 wt % loading of zirconium, respectively.

4.3.1.1.4. Synthesis of zirconium immobilized on HMS (Zr-/HMS)

Equal moles of trimethoxy propyl amine silane and Zirconium (IV) *ter.* butoxide (0.12 g of Zirconium (IV) *ter.* butoxide and 0.06 g of trimethoxy propyl amine silane) were mixed in 100 ml toluene at room temperature for 6 h. After half an hour, 1 g of HMS was added to the solution. The resulting solution was refluxed for

12 h with constant stirring. Solvent was removed as mentioned above. Sample was designated as Zr-/HMS.

4.3.1.2. Characterization

Powder X-ray diffraction pattern of the samples were recorded on a Rigaku D max III VC Ni filtered Cu Kα radiation, λ = 1.54 Å between 1 and 10 (2θ angle) with a scanning rate of 1^{o}/min. The specific surface area, total pore volume and average pore diameter were measured by the N_2 adsorption desorption method using NOVA 1200 (Quanta Chrome) instrument. The samples were activated at 300 ^{o}C for 3 h under vacuum and then adsorption desorption was conducted by passing nitrogen over samples which was kept under liquid nitrogen. Pore size distribution was obtained by applying BJH pore analysis method to the desorption branch of nitrogen adsorption isotherm. SEM micrograph of the zirconium containing samples were obtained on JEOL-JSM 520 scanning microscope while the TEM images were performed on a JEOL-TEM 1200 EX instrument with 100 kV accelerating voltage to probe the mesoporosity of the material. Zirconium content in the samples was determined by atomic absorbance analysis using Perkin Elmer 11013 spectrometer after dissolution of the samples in HCl-HF solution. Diffuse reflectance UV-Vis spectra of the powder samples were recorded in the range 200-800 nm on Shimadzu UV 2101 PC spectrometer equipped with a diffuse reflectance attachment, using $BaSO_4$ as the reference.

4.3.2. Results and Discussion

4.3.2.1. Powder X-ray diffraction

Powder X-ray diffraction of zirconium containing HMS samples were shown in Fig. 4.6. The diffraction peak was observed in 2θ range of 2-3 degree (observed for the mesoporous material as observed by Mobil researchers) [1,2,31-33]. XRD peak of pure HMS and zirconium containing HMS display only main (100) reflection peak and thus lacks in higher order reflection peaks (110), (200), (210) etc. Absence of higher order reflection peaks are indicative of deviation from the hexagonal structure. However, Tanev et al pointed out that electron diffraction pattern is congruent with the hexagonal structure [31]. Furthermore, it is clearly seen from the XRD pattern that (100) reflection peak is slightly broad when it is compared with main reflection peak in MCM-41. The broadness arises from the fact that it has pores in the slightly varying range. This like broad peak is mostly observed for the porous structure with wormhole like morphology. The broad nature of the peak results in the slight loss of uniformity in the pore size dimension. The 2θ angle and unit cell parameter of pure HMS, Zr-HMS, Zr/HMS and Zr-/HMS samples were shown in the Table 5.1. Zirconium incorporated HMS shows slight shift towards less 2θ angle than pure HMS, which subsequently results in the increase of unit cell parameter. It was observed that the increase in value of the unit cell parameter is increasing with the increase of zirconium content. Increase in the unit cell parameter in zirconium incorporated HMS indicate successful incorporation of zirconium in the framework of HMS. This leads to the decrease of unit cell parameter value in the zirconium grafted and immobilized HMS samples from the original values of HMS. Furthermore, it is found that decrease in the

value of unit cell parameter is related to the quantity of zirconium on the framework or pores in the grafted and immobilized samples. Higher angle XRD pattern shows the absence of microcrystals of ZrO_2 in zirconium incorporated HMS samples since no peaks related to ZrO_2 domain was found.

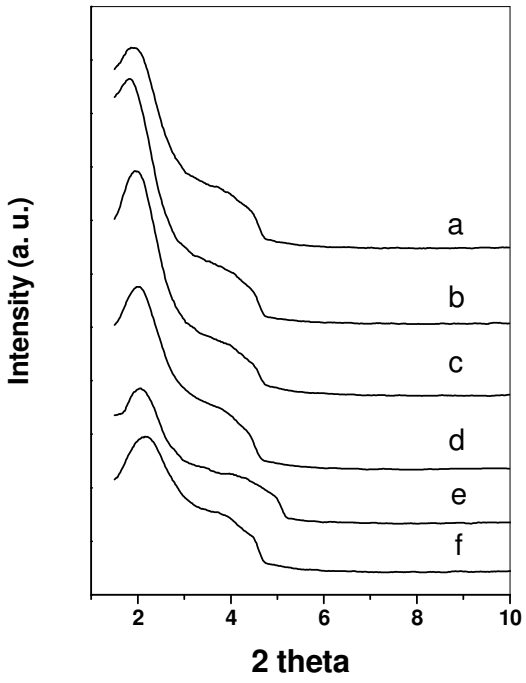

Fig. 4.6. Power X-ray diffraction pattern of zirconium containing HMS: (a) Zr-HMS (100), (b) Zr-HMS (50), (c) HMS, (d) Zr/HMS (100), (e) Zr/HMS (50) and (f) Zr-/HMS.

Table 4.2. Physico-chemical properties of zirconium containing HMS samples prepared by different methods.

Catalyst	Si/Zr [a] (molar ratio)	2θ angle (degree)	d-spacing (Å)	a_0 [b] (Å)	S_{BET} [c] (m^2g^{-1})	D_p [d] (Å)
HMS	-	1.98	44.57	51.48	828	41.5
Zr-HMS (100)	103	1.94	45.49	52.54	767	42.7
Zr-HMS (50)	58	1.83	48.23	55.70	725	44.0
Zr/HMS (100)	106	2.09	42.23	48.77	702	40.2
Zr/HMS (50)	54	2.15	41.05	47.41	630	39.0
Zr-/HMS	58	2.25	39.23	45.31	579	n. d.

[a] Zirconium content estimated by AAS analysis.

[b] Unit cell parameter values calculated using $a_0 = 2d_{100}/\sqrt{3}$.

[c] S_{BET} is the surface area calculated by BET method.

[d] D_p is the average pore diameter.

n. d. – not determined.

4.3.2.2. N_2 Sorption Measurements

N_2 adsorption desorption isotherms and BJH pore size distribution curve of zirconium containing HMS samples are shown in the Fig. 4.7. All the isotherms are typical of mesoporous material [1,2]. The isotherms exhibit steep rise in the adsorption of N_2 in the range 0.3-0.5 of P/P_0 (relative pressure). All the isotherms are almost reversible with no any hysterisis loop showing the uniformity of the pores. The nature of the isotherms is of type IV (according to the IUPAC classification) [21-22]. The steep rise in the adsorption desorption isotherms is due to the capillary condensation of the N_2 in the mesoporous channels [2b].

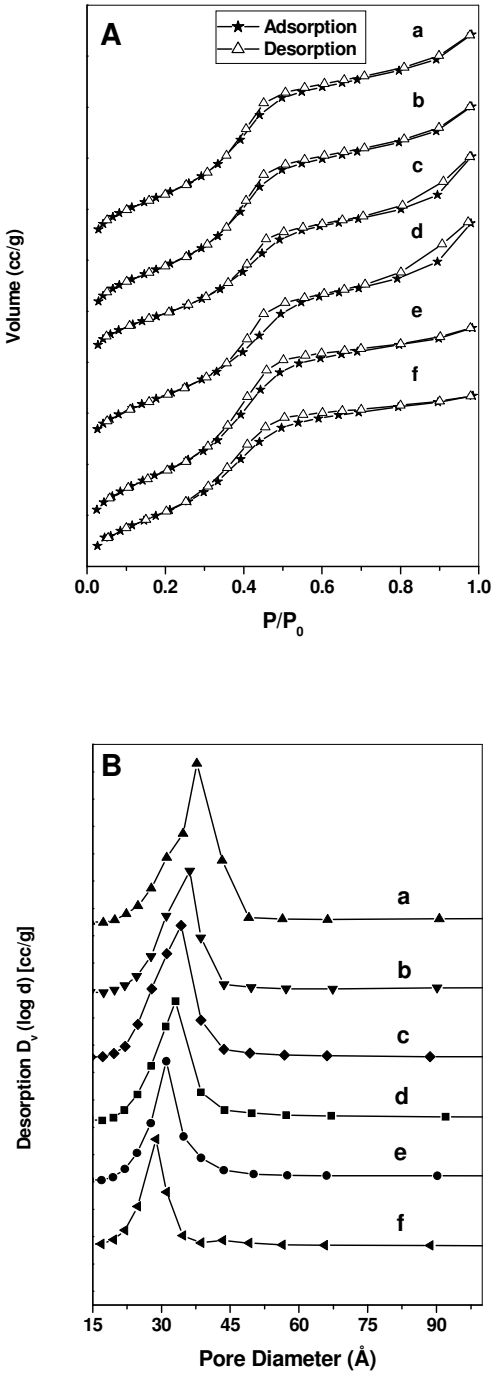

Fig. 4.7. [A] N_2 adsorption desorption isotherms and [B] BJH pore size distribution curve of zirconium containing HMS: (a) Zr-HMS (100), (b) Zr-HMS (50), (c) HMS, (d) Zr/HMS (100), (e) Zr/HMS (50) and (f) Zr-/HMS.

In addition to this hysterisis loop was observed at the higher value of relative pressure. Tanev et al argued the presence of such hysterisis loop due to textural mesoporosity, which made HMS material distinguishable from other mesoporous materials [31]. It is clear from the Table 4.2 that BET surface area is more for pure HMS samples (828 m^2g^{-1}). The incorporation of the zirconium ion in the framework of the HMS results into decrease of surface area. This clearly indicates that zirconium is uniformly dispersed. However, the decrease in the BET surface area was observed for the grafted and immobilized samples indicating the zirconium on the wall of framework. The BJH pore size distribution curves are shown in the Fig. 4.7. All the curves are sharp and are indicative of uniformly ordered mesoporous structure. The more decrease in the pore size was observed for the zirconium immobilized samples suggesting the successful immobilization of zirconium species via spacer group.

4.3.2.3. FT-IR Spectroscopy

The FT-IR spectra of zirconium incorporated, grafted and immobilized HMS samples are shown in Fig. 4.8. The broad band at 3600-3350 is due to free silanol groups, which are hydrogen bonded to each other. In addition, the band at 3750 cm^{-1} is due to free -OH groups linked with Si and Zr. Two bands at around 1082 and 1228 cm^{-1} associated to internal and external asymmetric Si–O stretching modes as well as two bands (800 and 457 cm^{-1}) assigned to symmetric stretching and tetrahedral bending of Si-O bonds, respectively, were observed [34, 35].

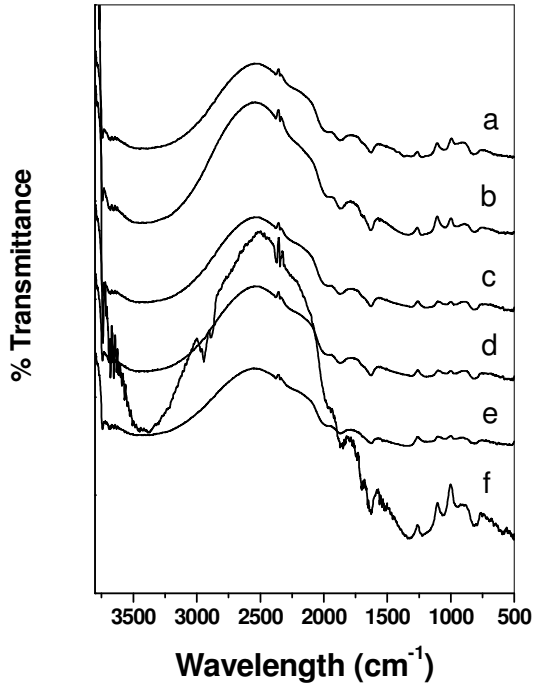

Fig. 4.8. FT-IR spectra of zirconium containing HMS: (a) Zr-HMS (100), (b) Zr-HMS (50), (c) HMS, (d) Zr/HMS (100), (e) Zr/HMS (50) and (f) Zr-/HMS.

The band at 962 cm^{-1} is attributed to Si-O-Si and Si-O-Zr symmetric stretching [23,24,36,37]. However, the intensity of this band is increasing with the increase in metal content in zirconium incorporated HMS samples. This is taken as the proof for the incorporation of zirconium in framework of HMS. For the zirconium immobilized HMS sample, spectra show the C-H stretching frequency at 2960 and 2850 cm^{-1} [25]. This shows the successful linking of tri-methoxy amino propyl silane on the silica support. In addition, the peak at 3300 cm^{-1} due to N-H stretching vibration was observed [25].

4.3.2.4. Microscopic Images

The SEM pictures of Zr-HMS (50) and Zr/HMS (50) were shown in Fig. 4.9. It is clear that most of the particles are agglomerated via cross-linking of mesoporous wall. For pure HMS or metal containing HMS, agglomeration of the particles was reported earlier and this causes distortion in the hexagonal structure [38]. The spherical nature of particles as clearly seen from the figure is quite due to the distortion in the hexagonal structure. This gives rise to wormhole like morphology to this material.

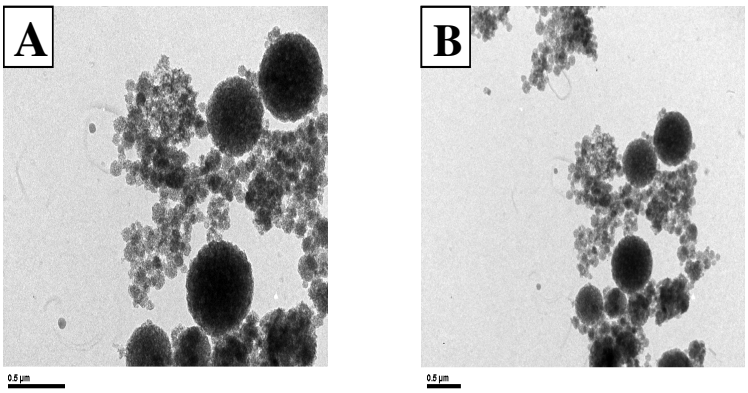

Fig. 4.9. [A] SEM pictures of Zr-HMS (50) and [B] Zr/HMS (50)

4.3.2.5. UV-Vis spectroscopy

UV-Vis spectroscopy used to find the presence of isolated zirconium ions incorporated in the framework of silica framework. Zirconium containing mesoporous silica absorb at 212 nm [27,29]. The absorption edge of zirconium is due to $O^{2-} \rightarrow Zr^{4+}$ charge transfer transitions in a tetrahedral coordination. In ZrO_2 where there is fully connectivity of Zr-O-Zr linkage, the LMCT shifts to lower energy [39].

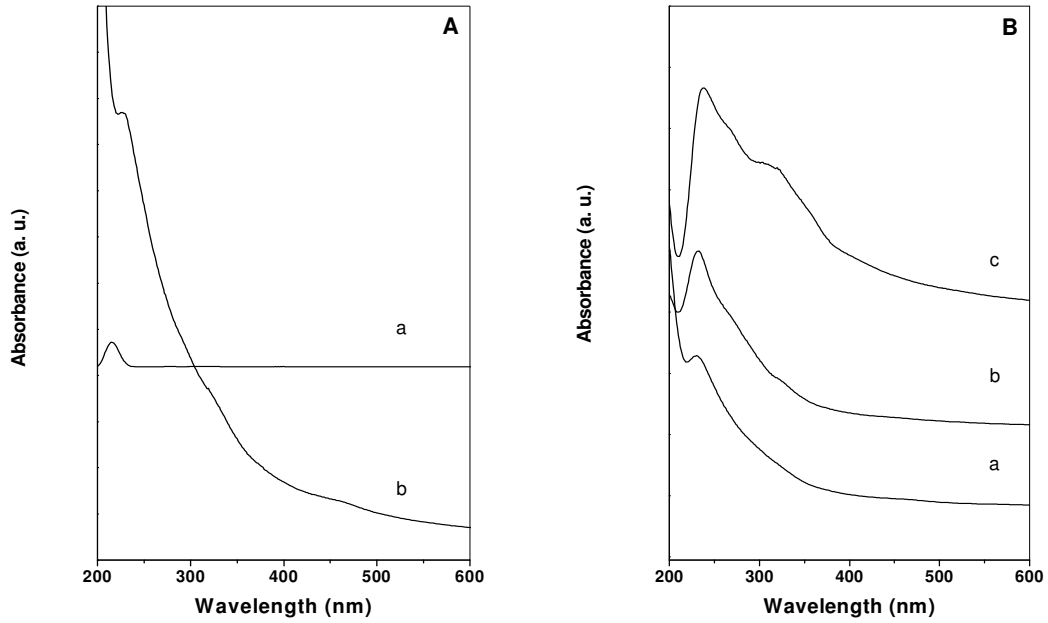

Fig. 4.10. UV-Vis spectra of zirconium containing HMS: [A] (a) Zr-HMS (100) and (b) Zr-HMS (50); [B] (a) Zr/HMS (100), (b) Zr/HMS (50) and (c) Zr-/HMS.

Zr-HMS (100) sample shows absorption peak at 214 nm indicating that zirconium ion is in the framework of mesoporous silica walls (Fig. 4.10A). With the increasing zirconium content in zirconium substituted sample [Zr-HMS (50)], absorption in low energy range, 230-350 nm, was found. There is no well defined peak at 230 nm indicating the absence of bulk zirconia. In grafted and immobilized samples, weak absorption observed in the energy range of 200-210 nm, suggesting less zirconium in the tetrahedral coordination (Fig. 4.10B). Moreover, the absorptions in the range 229-240 nm are prominent, suggesting the presence of Zr-O-Zr linkages. In addition to this, the absorption features around 275, 330 and 375 nm are observed. However, there are no reports for the assignment of these features.

References

[1] C. T. Kresge, M. E. Leonowicz, W. J. Roth, J. C. Vartuli, J. S. Beck, Nature 359 (1992) 710.

[2] J. S. Beck, J. C. Vartuli, W. J. Roth, M. E. Leonowicz, C. T. Kresge, K. D. Schmitt, C. Chu, D. H. Olson, E. W. Sheppard, S. B. McCullen, J. B. Higgins, J. L. Schenkler, J. Am. Chem. Soc. 114 (1992) 10834.

[3] S. Biz, M. L. Occelli, Catal. Rev. Sci. Eng. 40 (1998) 329.

[4] A. Corma, Chem. Rev. 97 (1997) 2373.

[5] K. Tanabe, M. Misono, Y. Ono, H. Hattori, Stud. Surf. Sci. Catal. 51 (1989) 1.

[6] K. Tanabe, T. Yamaguchi, Catal. Today 20 (1994) 185; T. Yamaguchi, Catal. Today 20 (1994) 199.

[7] X. X. Wang, F. Lefebvre, J. Patarin, J. M. Basset, Microporous and Mesoporous Materials 42 (2001) 269.

[8] K. Chaudhari, R. Bal, D. Srinivas, A.J. Chandwadkar, S. Sivasanker, Microporous and Mesoporous Mater. 50 (2001) 209.

[9] M. L. Occelli, S. Biz, A. Auroux, Appl. Catal. A 183 (1999) 231.

[10] D. J. Jones, J. Jimenez-Jimenez, A. Jimenez-Lopez, P. Maireles-Torres, P. O. Pastor, E. Rodriguez-Castellon, J. Roziere, Chem. Commun. 1997, 431.

[11] M. S. Morey, G. D. Stucky, S. Schwarz, M. Froba, J. Phys. Chem. B 103 (1999) 2037.

[12] A. Tuel, S. Gontier, R. Teissier, Chem. Commun. (1996) 651.

[13] S. Gontier, A. Tuel, Appl. Catal. A, 143 (1996) 125.

[14] Tuel, A. Microporous Mesoporous Mater. 1999 (27) 151.

[15] M. Selvaraj, P.K. Sinha, K. Lee, I. Ahn, A. Pandurangan, T.G. Lee, Microporous and Mesoporous Mater. 78 (2005) 139.

[16] J. E. Haskouri, S. Cabrera, C. Guillem, J. Latorre, A. Beltran, Daniel Beltran, M. D. Marcos, P. Amoros, Chem. Mater. 14 (2002) 5015.

[17] C. Flego, L. Carluccio, C. Rizzo, C. Perego, Catal. Commun. 2 (2001) 43.

[18] J. El Haskouri, S. l. Cabrera, C. Guillem, J. Latorre, A. Beltran, D. Beltran, M. D. Marcos, P. Amoros, Chem. Mater. 14 (2002) 5015

[19] M. Selvaraj, P. K. Sinha, K. Lee, I. Ahn, A. Pandurangan, T. G. Lee, Microporous and Mesoporous Mater. 78 (2005) 139

[20] M. K. Dongare, D. P. Sabde, R. A. Shaikh, K. R. Kamble, S. G. Hegde, Catal. Today 49 (1999) 267.

[21] E. P. Barrette, L. G. Joyner, P. P. Halenda, J. Am. Chem. Soc. 73 (1951) 373.

[22] S. Bruanaur, L. S. Deming, W. S. Deming, E. J. Teller, Am. Chem. Soc. 62 (1940) 1723.

[23] X. J. Chen, Q. Li, R. Xu, F. Xiao, Angew. Chem. Int. Ed. Engl. 34 (1995) 2694.

[24] A. Jentys, N. H. Pham, H. Vinek, J. Chem. Soc., Faraday. Trans. 92 (1996) 3287.

[25] C. Zhang, W. Zhou, S. Liu; J. Phys. Chem. B 109 (2005) 24319.

[26] A.D. Badiei, L. Bonneviot, Inorg. Chem. 37 (1998) 4142.

[27] S. Gontier, A. Tuel, Appl. Catal. A: General 143 (1996) 125.

[28] A. Tuel, S. Gontier, R. Teissierb, Chem. Commun. (1996) 651.

[29] J. Liu, S. Liao, G. Jiang, X. Zhang, L. Petrik, Microporous and Mesoporous Mater. 95 (2006) 306.

[30] A. Tuel, Microporous and Mesoporous 27 (1999) 151.

[31] P. T. Tanev, M. Chibwe, I. J. Pinnavaia, Nature, 368 (1994) 324.

[32] P. T. Tanev, T. J. Pinnavaia, science 267 (1995) 865.

[33] W. Zhang, M. Froba, J. Wang, P. T. Tanev, J. Wong, T. J. Pinnavaia, J. Am. Chem. Soc. 118 (1996) 9164.

[34] M. Boccuti, K. Rao, A. Zecchina, G. Leofanti, G. Petrini, Stud. Surf. Sci. Catal. 48 (1989) 133.

[35] A. Thangaraj, R. Kumar, S. Mirajkar, P. Ratnasamy, J. Catal. 130 (1991) 1.

[36] K. Li, C. Lin, Catal. Today 97 (2004) 257.

[37] M. Guidotti, N. Ravasio, R. Psaro, G. Ferraris, G. Moretti, J. Catal. 214 (2003) 242.

[38] T. R. Pauly, T. J. Pinnavaia, Chem. Mater. 13 (2001) 987.

[39] M. S. Moray, G. D. Stucky, S. Schwarz, M. Froba, J. Phys. Chem. B 103 (1999) 2037.

5.1. Introduction

Oxidation of aniline is an important reaction. Many industrial routes have been searched to prepare the azo compound, but most of them are hazardous in nature. The products from this reaction are highly useful in various industries. The nitroso and azoxy compounds are used as intermediates, in vulcanization of rubber, stabilization of halogenated materials and as antioxidant in lubricating ions. Azoxybenzenes are employed as dyes, reducing agents, chemical stabilizers and polymerization inhibitors. Some derivatives of azoxybenzenes are used as liquid crystals in electronic display and therapeutic medicines [1]. Because of these value added products, oxidation of aniline assumes significant role in the industry. Since then several catalysts were used (both homogeneous and heterogenous). Oxidation of aniline in homogeneous medium is reported over transition metal complexes of vanadium [2], iron [3] and molybdenum complexes [4]. In the heterogeneous medium, various types of molecular sieves [5-7] and mesoporous silica containing nanometric dispersed titanium oxide [8] have been reported to effectively catalyze the oxidation of aniline to azoxybenzene. Stoichiometric oxidants such as MnO_2 were used in the oxidation of aniline [9].

Styrene oxide is commercially important intermediate used in the synthesis for fine chemicals, pharmaceuticals and other value added products from the epoxidation of styrene [10]. Their selective synthesis is a subject of considerable academic and industrial interest. Conventionally, two methods practiced for its synthesis, namely dehydrochlorination of styrene chlorohydrin with a base or oxidation of styrene using stoichiometric amount of organic peracids such as peracetic acid and *m*-chlorobenzoic acid [11]. Both these methods require hazardous chemicals and show poor selectivity

for styrene epoxide, thus leading to the generation of undesirable products. The use of peracid is not a clean method being equivalent amounts of acid waste is produced. The safety while handling peracids is also a matter for concern. There is utmost need for the development of new epoxidation methods, which use safer oxidants and produce little waste. The use of hydrogen peroxide is an attractive option both on environmental and economic grounds. It is cheap, readily available and gives water as the only byproduct. Titanium containing silicates are widely studied catalyst for the epoxidation reactions. One of the most widely studied catalysts is TS-1 [12,13]. However, the main drawback is its small pore size dimension, which is not fit for the entry of bulky substrate and formation of phenyl acetaldehyde as the major product [14,15]. To overcome the steric limitation of TS-1, other large pore size titanium containing silicates have been developed [16]. For bulky substrates however, steric effects play an important role.

The present chapter outlines the potential application of zirconium containing MCM-41 and HMS for the liquid phase oxidation of aniline and styrene.

5.2. Reaction Procedure

Oxidation reactions of aniline (99.5 % purity, Aldrich) were performed in a round bottom flask fitted with a water condenser. The reaction mixture of the aniline (1 g, 10 mmol), equimolar amount of H_2O_2 (30 wt %, 1.14 g, 10 mmol) and 10 ml acetonitrile to which catalyst (5 wt % with respect to substrate) was added and heated at constant temperature 80 ^oC under magnetic stirring. Oxidation of styrene was performed in a stirred round bottom flask fitted with a water-cooled condenser. The catalyst (5 wt % with respect to styrene) was added to the reaction mixture consisting of styrene (99 %, 1.1 g, 10.5 mmol), H_2O_2 (30 wt %, 1.16 g, 10.5 mmol) and acetonitrile (10 ml) and heated at constant temperature of 75 ^oC under magnetic stirring. After certain interval of time, the reaction mixture was cooled to room temperature and catalyst was separated by centrifugation. The products were analyzed by gas chromatograph (Agilent, HP 6890) equipped with a flame ionization detector (FID) and a capillary column (5 µm cross linked methyl silicone gum 0.2 mm x 50 m) and was further confirmed by GC-MS (Shimadzu 200A). Leaching of the metal during the course of reaction was verified by resubmission of the filtrate after some interval of time for further reaction at same reaction conditions.

5.3. Investigation of Catalytic properties

5.3.1. Oxidation of aniline over zirconium containing MCM-41

The catalytic activity of zirconium containing mesoporous MCM-41 (prepared by different methods) was investigated for the liquid phase oxidation of aniline. The possible products formed from the oxidation reaction of aniline viz. nitrosobenzene (NSB), nitrobenzene (NB), azobenzene (AZO) and azoxybenzene (AZY) were shown in Scheme 5.1. The catalyst was studied under different temperatures and solvents for the oxidation of aniline. It was also studied with oxidants like hydrogen peroxide (H_2O_2, 30 wt %) and *ter.* butyl hydroperoxide (TBHP, 70 wt %).

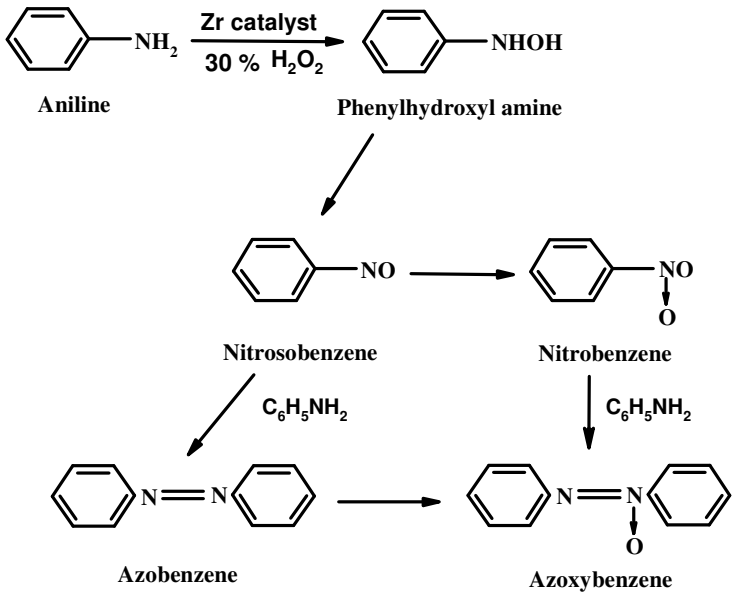

Scheme 5.1. Oxidation of aniline

Effect of temperature

The oxidation of aniline was studied in the temperature range of 60-80 ^{0}C over the catalyst, Zr-MCM-41 (50), with H_2O_2 (30 %) as oxidant in acetonitrile medium. Temperature more than 80 ^{0}C was intentionally avoided since it causes the decomposition of H_2O_2 and reduces the activity of the catalyst. Table 5.1 summarizes the catalytic activity of Zr-MCM-41 (50) with different temperatures.

Table 5.1. Effect of temperature on the performance of the catalyst [Zr-MCM-41 (50)] in oxidation of aniline.

Temperature (^{0}C)	Conversion of aniline (wt %)	Selectivity (wt %)			
		NSB	NB	AZO	AZY
60	6	-	-	-	100
70	21.7	-	-	-	100
80	35.4	-	-	2	98

Time – 24 h, NSB - nitrosobenzene, NB - nitrobenzene, AZO - azobenzene, AZY - azoxybenzene, Solvent - acetonitrile, aniline - 1 g, H_2O_2 - 1.14 g, catalyst amount - 0.05 g.

It was observed that at 60 ^{0}C, catalytic activity is very low (6 % conversion of aniline). At 70 ^{0}C, its catalytic activity was found good (21.7 % conversion of aniline). However, at 80 ^{0}C, the activity of the catalyst was significant (35.4 % conversion of aniline). It is clear from the Table 5.1, at low temperature AZY is only the product. But, at higher temperature (80 ^{0}C), other product (AZO) was also formed (though the amount is low) in addition to AZY. It is well known that AZO and AZY are formed

from the reaction of NSB and aniline in a consecutive step (discussed later). It seems that at low temperature, the rate of formation of NSB is low and entirely used for the formation of AZY. It seems that at higher temperature, overoxidation of AZO into AZY not occurred completely and certain quantity of AZO was identified.

Effect of solvent

As the reaction is carried out in the liquid phase the catalyst performance is very much influenced by the nature of the solvent. The activity of the catalyst for the oxidation of aniline was studied with different solvents such as acetonitrile, acetone, ethanol, methanol and dichloromethane. Table 5.2 indicates that with acetonitrile solvent, the activity and selectivity of the catalyst [Zr-MCM-41 (50)] is found highest and minimum with dichloromethane.

Table 5.2. Effect of solvent on the performance of catalyst [Zr-MCM-41 (50)].

Solvent	Conversion of aniline (wt %)	Selectivity (wt %)			
		NSB	NB	AZO	AZY
Acetonitrile	35.4	-	-	2	98
Acetone	13.5	-	80	6.2	13.8
Ethanol	15.2	-	-	13.2	86.8
Methanol	14.4	-	-	4	96
Dichloromethane	4	28	-	-	72

Time - 24 h, NSB - nitrosobenzene, NB - nitrobenzene, AZO - azobenzene, AZY- azoxybenzene, aniline - 1 g, H_2O_2 - 1.14 g, catalyst amount - 0.05 g, solvent amount - 10 ml, temperature - 80 ^{0}C.

In acetone, ethanol and methanol, it presents nearly the same activity. However, the product distribution is substantially different because of the different polarities of the solvents [5,17]. The conversion of aniline in different solvents follows the order: acetonitrile (35.4 %) > ethanol (15.2 %) > methanol (14.4 %) > acetone (13.5 %) > dichloromethane (4 %). Selectivitywise (AZY), the order is methanol (96 %) > acetonitrile (94 %) > ethanol (86.8 %) > dichloromethane (71.8 %) > acetone (13.8 %). It is important to note that catalytic activity for the oxidation of aniline in particular solvent depends on the different metals used as catalyst (under similar condition). Yet the reason for higher activity of the catalyst in acetonitrile medium is not clearly understood, but there is a common view about formation of peroxyimidates by reaction of HO_2^- with nitriles [18]. This peroxyimidates generates O_2 very slowly. Still, it is unknown how the acidity or basicity and polarity of the solvent affect the interaction of the aniline and H_2O_2 at catalytically active zirconium sites.

Effect of oxidant

The effect of oxidant in the oxidation of aniline was studied with different oxidants Viz. H_2O_2 and TBHP over Zr-MCM-41 (50). Table 5.3 shows that there is huge difference in the catalytic activity with H_2O_2 and TBHP. Conversion of aniline with H_2O_2 is 35.4 % while with TBHP 3 % only. Furthermore, with TBHP, NSB and AZO are the main products. This is in accordance with the reports by Neelam et al with pillared layer titanium catalyst with TBHP as oxidant [19]. But, in case of H_2O_2, AZY is the main product (although NSB, NB and AZO are formed in minute fraction). The low reactivity of the TBHP may be due to low electrophilic character of Zr–$OOC(CH_3)_3$ as compared to Zr–OOH. Indeed, Corma et al pointed out the low activity

of titanium catalyst with TBHP (as compared to H_2O_2) in oxidation of cyclohexene is due to low electrophilic character of Ti–$OOC(CH_3)_3$ [20]. This specifies the magnificent effect of oxidant on the activity of catalyst and product distribution in the oxidation of aniline.

Table 5.3. Effect of oxidants on the performance of catalyst [Zr-MCM-41 (50)].

Oxidant	Conversion of aniline (wt %)	Selectivity (wt %)			
		NSB	NB	AZO	AZY
H_2O_2	35.4	-	-	2	98
TBHP	3	42	-	58	-

Time - 24 h, NSB - nitrosobenzene, NB - nitrobenzene, AZO - azobenzene, AZY - azoxybenzene, aniline - 1 g, H_2O_2 - 1.14 g, TBHP - 1.22 g, catalyst - 0.05 g, solvent - acetonitrile (10 ml), temperature - 80 ^{0}C.

Effect of different zirconium species and its content

Table 5.4 outlined the activity of catalysts. It is clear that whatsoever the zirconium species AZY (selectivity to AZY more than 93 %) is the major product from the oxidation of aniline with H_2O_2 as oxidant in acetonitrile medium. The conversion of aniline over the different catalysts is in the order: Zr-MCM-41 (50) [35.4 %] > Zr/MCM-41 (50) [23.4 %] > Zr-/MCM-41 [22 %] > Zr-MCM-41 (100) [21 %] > Zr/MCM-41 (100) [15.5 %].

Table 5.4. Catalytic activity of incorporated, grafted and immobilized zirconium catalyst in acetonitrile medium for oxidation of aniline.

Catalyst	Conversion of aniline (wt %)	Selectivity (wt %)			
		NSB	NB	AZO	AZY
Zr-MCM-41 (100)	21	-	-	6	94
Zr-MCM-41 (50)	35.4	-	-	2	98
Zr/MCM-41 (100)	15.5	-	1.5	-	98.5
Zr/MCM-41 (50)	23.4	-	-	-	100
Zr-/MCM-41	22	-	-	-	100

Time - 24 h, NSB - nitrosobenzene, NB - nitrobenzene, AZO - azobenzene, AZY - azoxybenzene, aniline - 1 g, H_2O_2 - 1.14 g, catalyst - 0.05 g, temperature - 80 ^{0}C.

It was found that conversion of aniline increases with increase in the zirconium content in the catalyst. The conversion of aniline of 35.4 % was obtained over Zr-MCM-41 (50) while Zr-MCM-41 (100) gives 21 %. The same thing was observed with grafted zirconium [15.5 and 23.4 % conversion of aniline for Zr/MCM-41 (100) and Zr/MCM-41 (50), respectively; Table 5.4]. It seems that increase in the zirconium content is accompanied with the increase in the selectivity to AZY. For incorporated zirconium catalyst, the selectivity to AZY improves from 94 to 98 % as the zirconium content increases. At the same time, the selectivity to AZO reduced and other products (NSB and NB) were not identified. In case of Zr/MCM-41 (50) and Zr-/MCM-41, AZY is only the product. Thus, it is concluded that increase in the zirconium content have the effect of increase in catalytic activity and selectivity to AZY. It is assumed that AZO and AZY are formed from the NSB and phenylhydroxylamine (P^H, not

found in the reaction mixture). However, the mechanism of forming AZY is very complex [21].

For diffusion study, the oxidation of aniline was carried out over the zirconium containing MCM-41 in solvent free media (Table 5.5). No reports were found for the oxidation of aniline in solvent free media. It is important to note that aniline and H_2O_2 are highly immiscible so vigorous stirring is needed to expose more boundary surface at interface of two phases. In perspective of activity of catalyst, zirconium-containing MCM-41 shows more activity in solvent free media than in solvent (Table 5.4 and 5.5).

This indicates that reaction occurs at the interface of two immiscible liquids phase. The order of activity of different catalysts in solvent free media was found same as observed in the acetonitrile medium. It was observed that effect of phenomenon of diffusion limitation was felt on the distribution of products (NSB, NB, AZO and AZY in the solvent free medium for oxidation of aniline. However, the selectivity to AZY in solvent free media was decreased remarkably. It seems that in solvent free medium once the NSB formed (from the phenylhydroxylamine), NB formation by further oxidation of NSB is favorable (although selectivity is less). This can be explained in terms of diffusion limitation. AZO and AZY being the bulky molecules face the problems of diffusion in solvent free medium and results in the decrease of selectivity to AZY. Leaching study shows that zirconium species were well heterogenized in immobilized catalyst in oxidation of aniline (Fig. 5.1). However, slight leaching was observed in incorporated and grafted catalyst.

Table 5.5. Catalytic activity of different catalysts in solvent free media for the oxidation of aniline.

Catalyst	Conversion of aniline (wt %)	Selectivity (wt %)			
		NSB	NB	AZO	AZY
Zr-MCM-41 (100)	25.8	17	12	9.6	61.4
Zr-MCM-41 (50)	37	2.9	20.6	4.1	72.4
Zr/MCM-41 (100)	18	6.7	1.5	8.8	83
Zr/MCM-41 (50)	27	3.8	3.2	8	85
Zr-/MCM-41	36.4	2.2	6	10.8	81

Time - 24 h, NSB - nitrosobenzene, NB - nitrobenzene, AZO - azobenzene, AZY - azoxybenzene, aniline - 1 g, H_2O_2 - 1.14 g, catalyst - 0.1 g, temperature - 80 ^{0}C.

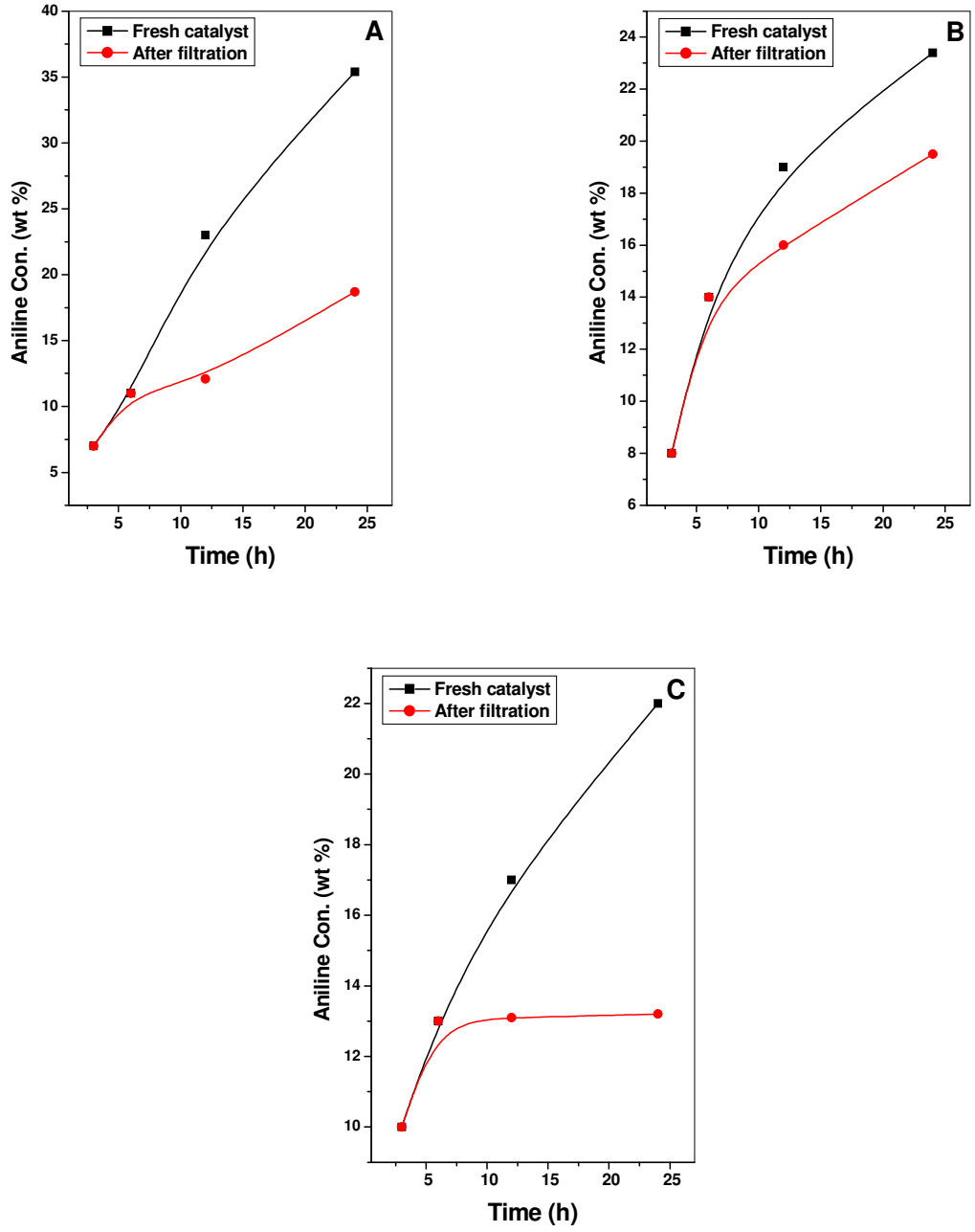

Fig. 5.1. Leaching study of different catalysts in presence of acetonitrile for the oxidation of aniline [A] Zr-MCM-41 (50), [B] Zr/MCM-41 (50) and [c] Zr-/MCM-41 (for leaching study, catalyst was removed after 6 h and filtrate was used for the further reaction).

5.3.2. Oxidation of aniline over zirconium containing HMS

The catalytic activity of zirconium containing mesoporous HMS was investigated for the liquid phase oxidation of aniline. The products formed from the oxidation of aniline were nitrosobenzene (NSB), nitrobenzene (NB), azobenzene (AZO) and azoxybenzene (AZY) [Scheme 5.1]. Oxidation of aniline can be studied with oxidant either H_2O_2 or TBHP. However, the results with H_2O_2 are more impressive than with TBHP. Liquid phase oxidation of aniline was carried out in solvent and without solvent (Table 5.6 and 5.7) at 80 ^{0}C. The blank reaction (without the catalyst) was carried out under similar conditions. But, the conversion of aniline obtained was 2.5 % only with poor selectivity to AZY (60 %).

Table 5.6. Catalytic activity of incorporated grafted and immobilized zirconium catalyst in acetonitrile for the oxidation of aniline.

Catalyst	Conversion of aniline (wt %)	Selectivity (wt %)			
		NSB	NB	AZO	AZY
Zr-HMS (100)	27.0	-	-	4.2	95.7
Zr-HMS (50)	42.2	-	-	1	99
Zr/HMS (100)	16.9	-	-	-	100
Zr/HMS (50)	28.2	-	-	-	100
Zr-/HMS	33	-	0.8	1	98.2
Blank	2.1	5	12	23	60

Time - 24 h, NSB - nitrosobenzene, NB - nitrobenzene, AZO - azobenzene, AZY - azoxybenzene, aniline - 1 g, H_2O_2 - 1.14 g, catalyst - 0.05 g, temperature - 80 ^{0}C.

Table 5.7. Catalytic activity of different catalysts in solvent free media for the oxidation of aniline.

Catalyst	Conversion of aniline (wt %)	Selectivity (wt %)			
		NSB	NB	AZO	AZY
Zr-HMS (100)	25.7	1.0	2.5	7.0	89.5
Zr-HMS (50)	36.3	-	3.4	4.7	91.9
Zr/HMS (100)	17.2	0.7	1.3	5.0	93.0
Zr/HMS (50)	27.9	-	2.0	4.1	93.9
Zr-/HMS	38.1	1.4	3.6	6.1	88.9

Time - 24 h, NSB - nitrosobenzene, NB - nitrobenzene, AZO - azobenzene, AZY - azoxybenzene, aniline - 1 g, H_2O_2 - 1.14 g, catalyst - 0.1 g, temperature - 80 ^{0}C.

It has been found that conversion of aniline is increasing with the increase of zirconium content irrespective of other parameters (synthesis method, whether carried out in solvent or absence of solvent, etc.). Nevertheless, the conversion of aniline over TS-1 catalyst was not increased as pointed out by Tuel et al [21]. Over Zr-HMS (100) catalyst, NSB (3.4 % selectivity) was identified along with AZO and AZY. However, it was disappeared over Zr-HMS (50). Also, the selectivity to AZO was found decreased. Scheme 5.1 makes it clear that NSB is consumed for the formation of AZO, after condensation with aniline, which in turn further oxidized to AZY. This explains the fall of selectivities to NSB and AZO over Zr-HMS (50) when it is compared with Zr-HMS (100). From Table 5.7, it is explicitly seen that over zirconium grafted HMS catalyst oxidation of aniline gives only AZY without any identification NSB and AZO. Yet the exact reason behind 100 % selectivity to AZY over zirconium grafted

HMS is not known. Zirconium immobilized HMS catalyst offers very good conversion of aniline (33 %) with high selectivity of 98.2 % to AZY. Over these zirconium catalysts, the oxidation of NSB to NB has not been observed. Over immobilized catalyst, it was formed partially. The reason may be that zirconium catalyst is mildly acidic that can facilitate the condensation of NSB with the aniline. Thus, it is concluded that increase in the zirconium content have the effect of increase in catalytic activity and selectivity to AZY. It is assumed that AZO and AZY are formed from the NSB and phenylhydroxylamine.

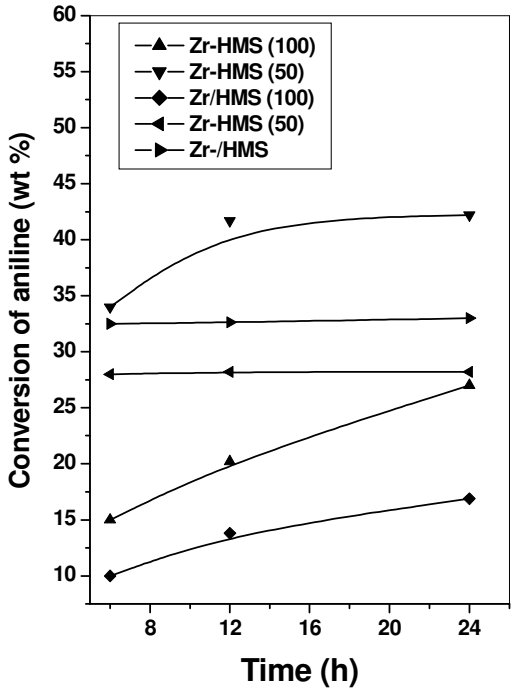

Fig. 5.2. Conversion of aniline Vs time over zirconium containing HMS in acetonitrile.

Fig. 5.2 indicates that the catalyst is prone to deactivation. However, after 6 h, the conversion of aniline over Zr/HMS (50) and Zr-/HMS remains almost constant. The deactivation of the catalyst with the progress of the reaction may be caused due to

adsorption of the products on the surface and thereby blocking the active zirconium sites. The mechanism of forming AZY is very complex [21,22].

For diffusion study, the oxidation of aniline was carried out over the zirconium containing HMS in solvent free media (Table 5.7). No reports were found for the oxidation of aniline in solvent free media. It is important to note that aniline and H_2O_2 are highly immiscible and vigorous stirring is needed to expose more boundary surface at interface of two phases. It was observed that effect of phenomenon of diffusion limitation was felt on the distribution of products (NSB, NB, AZO and AZY in the solvent free medium for oxidation of aniline. The selectivity to AZY in solvent free media was decreased remarkably. It seems that in solvent free medium once the NSB is formed (from the phenylhydroxylamine), NB formation by further oxidation of NSB is favorable. In this case, formation of AZO seems substantial since its overoxidation to AZY was slightly altered by diffusion limitation.

5.3.3. Oxidation of Styrene over Zirconium containing MCM-41

Liquid phase epoxidation of styrene was carried out over zirconium containing MCM-41 catalysts with 30 % H_2O_2 oxidant. Styrene oxide (SO) and benzaldehyde (BZ) were the two main products in the oxidation of styrene (Scheme 5.2). The other products viz. phenylacetaldehyde (PA), phenyl acetic acid and benzoic acid were found under certain reaction conditions.

Table 5.8 shows the performance of zirconium containing MCM-41 catalysts in acetonitrile medium. When H_2O_2 was used, only SO and BZ were identified. However, with TBHP, PA was also reported in addition to the above two mentioned products.

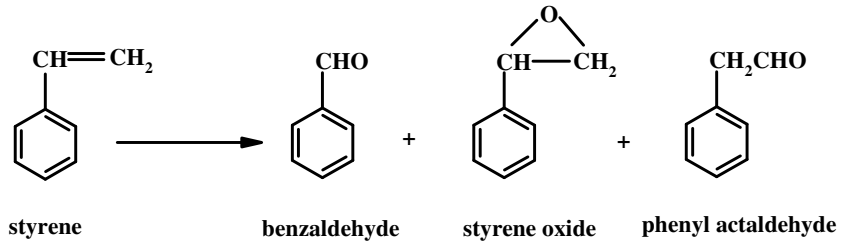

Scheme 5.2. Oxidation of styrene

It is found that catalytic activity of zirconium containing MCM-41 is increased with the increase in the zirconium content. Subsequently, the selectivity to SO decreased. Table 5.8 shows the catalytic activity is in the order Zr-MCM-41 (50) > Zr-/MCM-41 > Zr/MCM-41 (50) > Zr-MCM-41 (100) > Zr/MCM-41 (100). However, with TBHP its order is Zr-MCM-41 (50) > Zr/MCM-41 (50) > Zr-/MCM-41 > Zr-MCM-41 (100) > Zr/MCM-41 (100). This clearly suggests that, incorporated zirconium species are more active in the oxidation of styrene than grafted and

immobilized species. The formation of PA when TBHP was used is quite interesting. It seems that once styrene oxide formed undergoes rearrangement reactions to form PA [13-15].

Table 5.8. Catalytic activity of zirconium containing MCM-41 in acetonitrile medium for liquid phase oxidation of styrene.

Catalyst	Oxidant	STY conv. (Wt %)	Product distribution (wt %)		
			SO	BZ	PA
Zr-MCM-41 (100)	H_2O_2	8	38.2	61.8	-
Zr-MCM-41 (50)	H_2O_2	14.4	23.7	76.3	-
Zr/MCM-41 (100)	H_2O_2	4.9	36.8	63.2	-
Zr-MCM-41 (50)	H_2O_2	9.2	32.1	67.8	-
Zr-/MCM-41	H_2O_2	11	30	70	-
Zr-MCM-41 (100)	TBHP	9.9	32	50	18
Zr-MCM-41 (50)	TBHP	18.6	27.2	43.5	29.3
Zr/MCM-41 (100)	TBHP	8.2	30.1	51.1	18.8
Zr-MCM-41 (50)	TBHP	15	24	44	32
Zr-/MCM-41	TBHP	12.9	33	52	15

STY - styrene, SO - styrene oxide, BZ - benzaldehyde, PA - phenyl acetaldehyde, Reaction condition: catalyst amount - 0.05 g, temperature – 75 ^{0}C, solvent - acetonitrile, styrene: oxidant - 1:1, time - 6 h.

Furthermore, the cleavage at the double bond of styrene takes place to form BZ [23]. Dumitriu et al proposed the formation of BZ by cleavage of SO also [24]. The decrease in the selectivity to SO with increasing zirconium content is more probably due to its tendency to form BZ. It appears that being TBHP is having bulky $C(CH_3)_3$

group, probably it exerts steric hindrance for the styrene to reach at the catalytic active sites or partially inhibiting the cleavage of SO to form BZ. This results in the decrease of selectivity to BZ. However the mechanism of cleavage and rearrangement of styrene oxide is controversial. With TBHP, these two reactions (cleavage and rearrangement of styrene oxide) are competitive to each other and the formation of PA occurs is supposed to occur at the cost of BZ (probably the cleavage of styrene oxide).

In the absence of solvent, the oxidation of styrene with H_2O_2 suffers from the decomposition of hydrogen peroxide and leads to very poor performance of the catalyst [25]. Incorporated and immobilized zirconium species in the absence of solvent leads to very low selectivity of SO (Table 5.9). However, the extraframework species gives only BZ. Phenylacetaldehyde was not identified in the oxidation of styrene in absence of solvent.

It seems that very low selectivity may arise from the acidity of the zirconium in the absence of solvent, responsible for the decomposition of H_2O_2 [26]. With TBHP, even in absence of solvent, remarkable conversion was found but the disadvantage is that overoxidation products of benzaldehyde and phenylacetaldehyde to benzoic acid and phenyl acetic acid are formed, respectively.

Role of solvent is one of the important features in the oxidation of styrene for better selectivity to styrene oxide. Among the solvents: acetonitrile, acetone, dimethylformaide, ethanol, methanol, dichloromethane studied, catalytic activity was observed in acetonitrile and acetone only (Table 5.10). However, it does not seem correlation of the role of polarity of the solvent with the catalytic activity in case of zirconium catalyst with H_2O_2 for the oxidation of styrene. Still, it is unclear why these

zirconium catalysts are more active in acetonitrile solvent. Probably, acetonitrile may be partly neutralizing the acidity of the zirconium species.

Table 5.9. Catalytic activity of zirconium containing MCM-41 in solvent free media for liquid oxidation of styrene.

Catalyst	Oxidant	STY conv. (Wt %)	Product distribution (wt %)			
			SO	BZ	PA	Others
Zr- MCM-41 (100)	H_2O_2	1.2	7	93		
Zr- MCM-41 (50)	H_2O_2	2.3	4	96		
Zr/ MCM-41 (100)	H_2O_2	0.8	-	100		
Zr/ MCM-41 (50)	H_2O_2	1.9	-	100		
Zr-/ MCM-41	H_2O_2	0.8	5	95		
Zr- MCM-41 (100)	TBHP	10	26	45	14	15
Zr- MCM-41 (50)	TBHP	15	21	41.5	17	20.5
Zr/ MCM-41 (100)	TBHP	19	25	53	11	11
Zr/ MCM-41 (50)	TBHP	23	19	45	11.9	24.1
Zr-/ MCM-41	TBHP	17	25	52.5	24.5	8

STY - styrene, SO - styrene oxide, BZ - benzaldehyde, PA - phenyl acetaldehyde, Reaction condition: catalyst amount - 0.05 g, temperature – 75 ^{0}C, styrene: oxidant - 1:1, time - 6 h.

The oxidation of styrene is mostly carried out with high molar ratio of styrene:H_2O_2 (1:3). From the Table 5.11, it is clear that catalytic activity increased, but selectivity to styrene oxide decreased. However, the reaction suffers from the overoxidation of benzaldehyde and phenylacetaldehyde to form benzoic acid and phenyl acetic acid, respectively. These overoxidation products were not observed when 1:1 ratio of

styrene:H_2O_2 used. Moreover, it is observed that with 1:3 ratio of styrene:H_2O_2 has effect on the decrease of selectivity to styrene oxide.

Table 5.10. Effect of different solvent on the performance of the catalyst [Zr-MCM-41 (50)] in oxidation of styrene.

Solvent	STY conv. (Wt %)	Product distribution (wt %)		
		SO	BZ	PA
Acetonitrile	14.4	23.7	76.3	-
Acetone	8.5	20	80	-

STY - styrene, SO - styrene oxide, BZ - benzaldehyde, PA - phenyl acetaldehyde, Reaction condition: catalyst amount - 0.05 g, temperature – 75 ^{0}C, solvent - acetonitrile, styrene:H_2O_2- 1:1, time - 6 h.

Table 5.11. Catalytic activity of zirconium containing MCM-41 in acetonitrile medium for liquid oxidation of styrene with 1:3 ratio of styrene:H_2O_2.

Catalyst	STY conv. (Wt %)	Product distribution (wt %)			
		SO	BZ	PA	Others
Zr-MCM-41 (100)	12.5	19.3	70.6	2.4	12.3
Zr-MCM-41 (50)	20	15	64.1	5.9	23
Zr/MCM-41 (100)	7.5	17	66.3	2.7	14
Zr-MCM-41 (50)	13	11	60.9	3.1	25
Zr-/MCM-41	15.8	22	63	2	13

STY - styrene, SO - styrene oxide, BZ - benzaldehyde, PA - phenyl acetaldehyde, Reaction condition: catalyst amount - 0.05 g, temperature – 75 ^{0}C, solvent - acetonitrile, time - 6 h.

Fig. 5.3 shows that zirconium immobilized catalyst in the styrene oxidation (Zr-/MCM-41) behaves heterogeneously since no leaching was observed. Zr-MCM-41 (50) and Zr/MCM-41 (50) shows slight leaching.

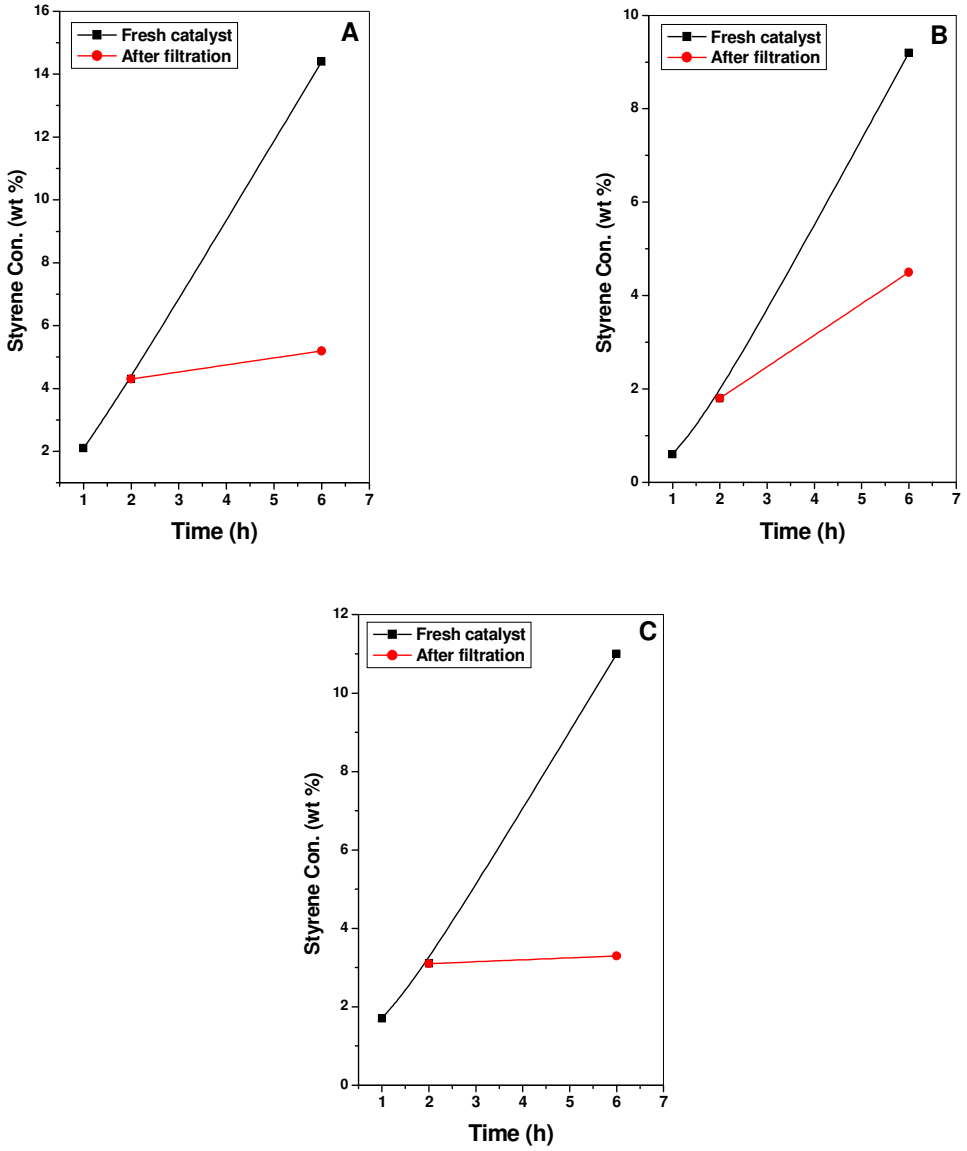

Fig. 5.3. Leaching study of different catalysts in presence of acetonitrile for the oxidation of styrene [A] Zr-MCM-41 (50), [B] Zr/MCM-41 (50) and Zr-/MCM-41 (for leaching study, catalyst was removed after 2 h and filtrate was used for the further reaction).

5.3.4. Oxidation of Styrene over Zirconium containing HMS

Liquid phase epoxidation of styrene was carried out over zirconium containing HMS catalysts with 30 % H_2O_2 oxidant. Styrene oxide and benzaldehyde are the two main products in the oxidation of styrene (Scheme 5.2). The other products viz. phenylacetaldehyde, phenyl acetic acid and benzoic acid were found with certain reaction conditions.

Table 5.12 summarized the catalytic activity of the zirconium containing HMS in acetonitrile (with H_2O_2 and TBHP) for the oxidation of styrene at 80 ^{0}C. It has been observed that nature of the oxidant has effect on the product distribution in styrene oxidation. The catalytic activity was found increasing with the increase of zirconium content (whether it is incorporated or grafted species). However, this trend is accompanied with decrease in selectivity to SO. Among the incorporated, grafted and immobilized zirconium species, zirconium in the framework was observed catalytically more active. With H_2O_2, styrene oxide (SO) and benzaldehyde (BZ) are the only products. In acetonitrile with H_2O_2, the order of catalytic activity of zirconium containing HMS was Zr-HMS (50) > Zr-/HMS > Zr-HMS (100) > Zr/HMS (50) > Zr/HMS (100). The highest conversion of styrene (19.5 %) with H_2O_2 was obtained over Zr-HMS (50) with 27.8 % selectivity to SO. The highest selectivity to SO was found over incorporated zirconium catalyst followed by immobilized and grafted zirconium catalyst, respectively.

Table 5.12. Catalytic activity of zirconium containing HMS in acetonitrile medium for liquid phase oxidation of styrene.

Catalyst	Oxidant	STY conv. (Wt %)	Product distribution (wt %)		
			SO	BZ	PA
Zr-HMS (100)	H_2O_2	12.2	33	67	-
Zr-HMS (50)	H_2O_2	22	21	79	-
Zr/HMS (100)	H_2O_2	5.5	19	81	-
Zr/HMS (50)	H_2O_2	9.8	13	87	-
Zr-/HMS	H_2O_2	14.5	23	77	-
Zr-HMS (100)	TBHP	11	30	55	15
Zr-HMS (50)	TBHP	19.8	20	36	27
Zr/HMS (100)	TBHP	9.5	28	52	20
Zr/HMS (50)	TBHP	14	21	42	37
Zr-/HMS	TBHP	16	27	48	25

STY - styrene, SO - styrene oxide, BZ - benzaldehyde, PA - phenyl acetaldehyde, Reaction condition: catalyst amount - 0.05 g, temperature – 75 ^{0}C**,** solvent - acetonitrile, styrene: oxidant - 1:1, time - 6 h.

However, it depends on the metal e.g. framework niobium ions located in the framework have been found more active for the formation of BZ than extraframework species [27], Iron species in the framework of MCM-41 were more active for the epoxidation of styrene in compare with extraframework species [23]. Oxidation of styrene using TBHP as oxidant results in formation of PA (which was not observed with H_2O_2), in addition to SO and BZ. Furthermore, the selectivity PA was found increasing with the zirconium content and it is highest over the grafted zirconium catalyst. It seems that PA formation occurs more at the cost of BZ.

The oxidation of styrene with H_2O_2 at the same temperature but in absence of solvent over zirconium catalyst materialized into very low conversion of styrene (Table 5.13). Low conversion of styrene is attributed to rapid decomposition of H_2O_2 because of acidic sites accompanied with the zirconium. BZ shows dominance with this reaction condition. Moreover, the oxidation of styrene with TBHP in absence of solvent over zirconium catalyst ushers good conversion (even more than that carried out in acetonitrile under similar condition, Table 5.12 and 5.13). In this case, no such rapid decomposition of TBHP was found in absence of solvent.

Table 5.13. Catalytic activity of zirconium containing HMS in solvent free media for liquid oxidation of styrene.

Catalyst	Oxidant	STY conv.	Product distribution (wt %)			
		(Wt %)	SO	BZ	PA	Others
Zr-HMS (100)	H_2O_2	1.4	9.3	90.7		
Zr-HMS (50)	H_2O_2	2.9	7.6	92.4		
Zr/HMS (100)	H_2O_2	0.8	-	100		
Zr/HMS (50)	H_2O_2	1.6	-	100		
Zr-/HMS	H_2O_2	2.5	7	93		
Zr-HMS (100)	TBHP	18	27	47	13	13
Zr-HMS (50)	TBHP	28	21	41	15	23
Zr/HMS (100)	TBHP	20.0	22.4	48.5	19	10.1
Zr/HMS (50)	TBHP	25.6	18.2	40	13.1	28.7
Zr-/HMS	TBHP	20.0	22	41	26.5	10.5

STY - styrene, SO - styrene oxide, BZ - benzaldehyde, PA - phenyl acetaldehyde, Reaction condition: catalyst amount - 0.05 g**,** temperature – 75 ^{0}C, styrene: oxidant - 1:1, time - 6 h.

Reaction mechanism for the formation of styrene oxide

We have shown the plausible mechanism for the formation of SO via free radical mechanism (Scheme 5.3). The formation of BZ from styrene can occur by two different ways. One possible pathway is the oxidation of the side chain, which causes breaking of the C═O to form the BZ. Other way to form BZ from styrene is by epoxidation reaction to form SO which further forms BZ in the presence of peroxide. Two different pathways may occur parallel. It is not understood why SO rearranges to PA when TBHP was used as oxidant. But, it seems that $\dot{C}(CH_3)_3$ formed from TBHP might be useful in the ring opening of the SO and thus facilitating the rearrangement of SO to PA. The rearrangement of SO was observed over TS-1 catalyst with H_2O_2 [15]. However, it is worth to mention that electronic effect of titanium and zirconium played in the reaction may be different.

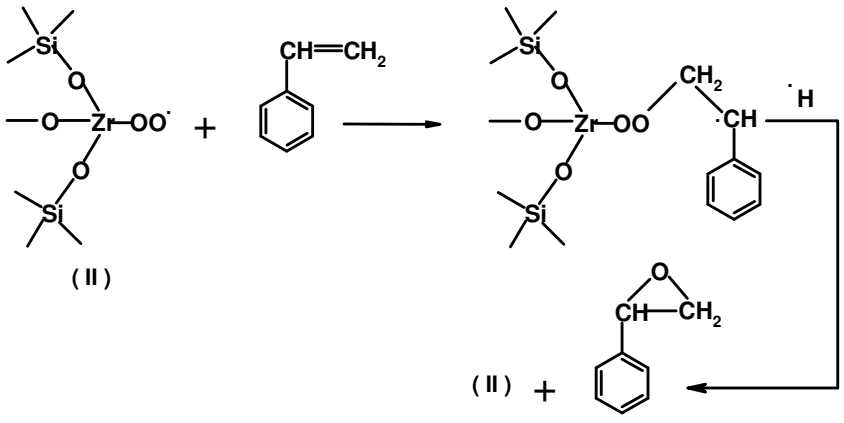

Scheme 5.3. Plausible mechanism of formation of styrene to styrene oxide by radical mechanism

5.4. References

[1] S. Sakuae, T. Tsubakino, Y. Nishiyama, Y. Ishii, J. Org. Chem. 58 (1993) 3633.

[2] R.A. Sheldon, J. Dakka, Catalysis Today 19 (1994) 215.

[3] H. Huang, D. Sommerfeld, B.C. Dunn, C.R. Lloyd, E.M. Eyring, J. Chem. Soc., Dalton Transactions 8 (2001) 1301.

[4] S. Tollari, M. Cuscela, F. Porta, Chem. Commun. 19 (1993) 1510.

[5] S.B. Waghmode, S.M. Sabne, S. Sivasankar, Green Chemistry 3, (2001) 285.

[6] T. Selvam, A.V. Ramaswamy, Catalysis Letters 31, (1995) 103.

[7] T. Selvam, A.V. Ramaswamy, J. Chem. Soc., Chem Commun. 10 (1994) 1215.

[8] A. Tuel, L.G. Hubert-Pfalzgraf, J. Catal. 217 (2003) 343.

[9] O.H. Wheeler, D. Gonzalez, Tetrahedron 20 (1964) 189.

[10] (a) K. Bauer, D. Garbe, H. Surburg, Common Fragrance and Flavor Materials, Wiley-VCH, New York/Weinheim, 1997; (b) G. Sienel, R. Rieth and K. T. Rowbottom, Ullmann's Encyclopedia of Organic Chemicals, Wiley-VCH, Weinheim, 1999; (c) J.T. Lutz, M. Grayson, D. Eckroth, G.J. Bushey, C.I. Eastman, A. Klingsberg, L. Spiro (Eds.), Kirk-Othmer Encyclopedia of Chemical Technology, vol. 9, third ed., Wiley, New York, 1980, 251.

[11] D. Swern, Organic Peroxides, ed. D. Swern, Wiley Interscience, New York, 1971, vol. 2.

[12] S.B. Kumar, S.P. Mirajkar, G.C.G. Pais, P. Kumar, R. Kumar, J. Catal. 156 (1996) 163.

[13] J.S. Reddy, U.R. Khire, P. Ratnasamy, R.B. Mitra, J. Chem. Soc. Chem.

Commun. 1234 (1992).

[14] C.V. Rode, U.N. Nehete, M.K. Dongare, Catal. Commun. 4 (2003) 365.

[15] S.C. Laha and R. Kumar, J. Catal. 204 (2001) 64.

[16] (a) T. Blasco, M.A. Camblor, A. Corma, P. Esteve, A. Martinez, C. Prieto, S. Valencia, J. Chem. Soc. Chem. Commun. (1996) 2367; (b) A. Corma, Chem. Rev. 97 (1997) 2413; (c) W. Zhang, M. Froba, J. Wang, P.T. Tanev, J. Wong, T.J. Pinnavaia, J. Am. Chem. Soc. 118 (1996) 9164.

[17] S. Gontier, A.Tuel, Applied Catalysis. A: General 118 (1994) 173.

[18] (a) K. B. Wiberg, J. Am. Chem. Soc. 77 (1955) 2519; (b) G. B. Payne, P. H. Deming, P. H. Williams, J. Org. Chem. 26 (1961) 659; (c) G. Laus, J. Chem. Soc., Perkin Trans. 2 (2001) 861.

[19] N. Jagtap, V. Ramaswamy, Applied Clay Science 33 (2006) 89.

[20] A. Corma, P. Esteve, A. Martinez, S. Valencia, J. Catal. 152 (1995) 18.

[21] S. Gontier, A. Tuel, J. Catal. 157 (1995) 124.

[22] S. Gontier, A. Tuel, Appl. Catal. A: 143 (1996) 125.

[23] Y. Wang, Q. Zhang, T. Shishido, K. Takehira, J. Catal. 209 (2002) 186.

[24] V. Huleaa, E. Dumitriu, Appl. Catal. A: General 277 (2004) 99.

[25] V.R. Choudhary, N.S. Patil, S.K. Bhargav, Catal. Lett. 89 (2003) 1.

[26] J. Zhuang, D. Maa, Z. Yan, X. Liu, X. Han, X. Bao, Y. Zhang, X. Guo, X. Wang, Appl. Catal. A 259 (2004) 1.

[27] V. Parvulescu, C. Constantin, B.L. Su, J. Mol. Catal. A 202 (2003) 171.

6.1. Summary

The present thesis gives an account of

(1) Syntheses of cobalt and zirconium containing mesoporous silica, MCM-41 and HMS.

(2) Characterization of these metal containing mesoporous silica materials.

(3) Potential catalytic application of these materials in selective oxidation and epoxidation reaction.

Chapter 1 presents general introduction pertaining to different types of mesoporous silica materials and various physico-chemical aspects of mesoporous silica materials. The different characteristic properties of these materials, formation mechanism, synthesis parameters, various routes of introducing the metal in mesoporous silica, characterization and application as supports for different catalytically active transformations are discussed in brief.

Chapter 2 describes the synthesis of cobalt containing MCM-41 and HMS by direct substitution method, grafting method and by immobilization method with different cobalt content. The catalysts are characterized by powder XRD, N_2 sorption isotherms, SEM and TEM, XPS, FT-IR and UV-Vis spectroscopy.

Chapter 3 describes the catalytic potential of cobalt containing MCM-41 and HMS for the liquid phase oxidation of ethylbenzene and diphenylmethane using aqueous hydrogen peroxide (H_2O_2) and ter. Butyl hydroperoxide (TBHP) as oxidant. The reactions are studied with different reaction parameters like temperature, solvents, oxidants etc.

Chapter 4 describes the synthesis of zirconium containing MCM-41 and HMS by direct substitution method, grafting method and by immobilization method with different zirconium content. The materials are characterized by powder XRD, N_2 sorption isotherms, SEM and TEM, FT-IR and UV-Vis spectroscopy.

Chapter 5 describes the catalytic application of zirconium containing MCM-41 and HMS for the oxidation of aniline and styrene using hydrogen peroxide (H_2O_2) and ter. Butyl hydroperoxide (TBHP) as oxidant. The role of different catalytic species and the effect of solvents on the distribution of products are studied in detail.

6.2. Conclusion

6.2.1. Synthesis and Characterization

- Powder XRD diffraction pattern of the metal (cobalt and zirconium) containing mesoporous MCM-41 and HMS confirms mesoporous structure of the materials. The shift of (100) peak to lower 2θ angle (than pure MCM-41 and HMS) in metal substituted MCM-41 and HMS reveals the incorporation of metal in the framework. The lack of higher order reflection peak in XRD pattern after immobilization indicates the reduction in the ordering of the mesoporous channels.
- Mesoporosity of the metal (cobalt and zirconium) containing mesoporous MCM-41 and HMS materials were also confirmed from steep rise in the adsorbed volume (of N_2 gas) in the N_2 sorption isotherms.
- Increasing intensity of the band at 960 cm^{-1}, with the increase of metal content, in the FT-IR spectra of the metal (cobalt and zirconium) substituted MCM-41

and HMS is indicative of incorporation of the metal ion in the framework of mesoporous silica. In immobilized samples, the presence of peak at 2927 and 2854 cm^{-1} indicate the successful linking of trimethoxy propyl amine silane on the wall of silica.

- ❖ The morphology of the metal (cobalt and zirconium) containing MCM-41 was observed distorted hexagonal. Metal (cobalt and zirconium) containing HMS showed wormhole like morphology.
- ❖ Mainly, tetrahedral and octahedral Co(II) was found present in the cobalt containing MCM-41 and HMS as evidenced from the UV-Vis spectra of the materials. However, in the grafted and immobilized samples, octahedral Co(II) species are predominant. In zirconium substituted MCM-41 and HMS, the absorption around 210 nm indicate the presence of tetrahedral Zr (IV) suggesting the incorporation of zirconium. The assignment of the absorptions in the range of 240-350 nm in the UV-Vis spectra of zirconium containing samples is subject to debate because of absence of reliable data, however, it may be due to presence of polymeric zirconium (Zr-O-Zr).

6.2.2. Catalysis

Oxidation of Ethylbenzene

- ❖ Oxidation of ethylbenzene shows good performance in solvent free media using TBHP as oxidant over cobalt containing mesoporous MCM-41 and HMS.

- In solvent free media, the selectivity to acetophenone was found more than in solvent media.
- Higher ratio of TBHP:Ethylbenzene does not result in increase of catalytic activity.
- Among the solvent studied for the oxidation of ethylbenzene, performance of the cobalt containing MCM-41 and HMS was found good with acetonitrile.
- The immobilized cobalt catalyst was found highly selective to acetophenone.
- Leaching study shows that immobilized cobalt catalyst is less prone for leaching.

Oxidation of Diphenylmethane

- Cobalt containing MCM-41 and HMS are active in the oxidation of diphenylmethane using TBHP as oxidant.
- With acetonitrile as solvent, the conversion of diphenylmethane was found more with 100 % selectivity to benzophenone.
- In solvent free media, conversion of diphenylmethane has been reduced. Also, the selectivity to benzophenone was decreased due to the formation of side products like hydroxylated derivative of benzophenone.
- The catalytic activity of cobalt immobilized on MCM-41 and HMS was found significant than grafted and incorporated cobalt catalyst.
- Cobalt grafted and incorporated catalyst shown leaching. Immobilized cobalt catalyst has been found stable for leaching.

Oxidation of Aniline

- Zirconium containing MCM-41 and HMS has performed well in the oxidation of aniline using aq. H_2O_2 as oxidant with azoxybenzene as the major product.
- With TBHP, the activity of the catalyst was found insignificant.
- In absence of solvent, though the catalytic activity increased, it has adverse effect on the selectivity to azoxybenzene.
- Highest conversion of aniline and selectivity (more than 94 %) has been found in acetonitrile.
- Incorporated zirconium catalyst was found more active than grafted and immobilized zirconium catalyst.

Oxidation of styrene

- The catalytic activity of the zirconium containing MCM-41 and HMS in oxidation of styrene was found restricted by the acidity associated with these catalysts.
- With H_2O_2 as oxidant, only styrene oxide and benzaldehyde were identified. However, with TBHP, phenylacetaldehyde (the rearranged product of styrene oxide) was formed in addition to styrene oxide and benzaldehyde.
- In solvent free media, the decomposition of H_2O_2 has been main problem which result into negligible catalytic activity of zirconium containing MCM-41 and HMS.
- With 1:3 ratio of styrene:H_2O_2, conversion of aniline has increased with subsequent decrease in selectivity to styrene oxide.

List of Publications

1. Characterization and catalytic activity of cobalt containing MCM-41 prepared by direct hydrothermal, grafting and immobilization methods

   Shrikant S. Bhoware and A.P. Singh

   Journal of Molecular Catalysis A: Chemical, 266 (2007) 118

2. Cobalt-containing hexagonal mesoporous molecular sieves (Co-HMS): Synthesis, characterization and catalytic activity in the oxidation reaction of ethylbenzene **Shrikant S. Bhoware,** S. Shylesh, K.R. Kamble and A.P. Singh

   Journal of Molecular Catalysis A: Chemical, 255 (2006)123.

3. Oxidation of ethylbenzene and diphenyl methane over ordered mesoporous M-MCM 41 (M = Ti, V, Cr): Synthesis, characterization and structure-activity correlations

   R.K. Jha, S. Shylesh, **S.S. Bhoware** and A.P. Singh

   Microporous and Mesoporous Materials, 95 (2006) 154.

List of Manuscripts Communicated

1. Oxidation of aniline styrene over zirconium containing HMS With Wormhole like pore structure **(communicated)**

   Shrikant S. Bhoware, K. R. Kamble and A.P. Singh

2. Zirconium Containing Mesoporous MCM-41 for the Liquid Phase Oxidation of Aniline and Styrene **(communicated)**

   Shrikant S. Bhoware, K. R. Kamble and A.P. Singh

Contributions to National/International Symposia/Conferences

1. Synthesis of silica functionalised sulphonic acid groups for acid catalyzed reactions

   S. Shylesh, S. Parambadath, **S. S. Bhoware** and A. P. Singh

   6th National Symposium in Chemistry, Indian Institute of Technology, Kanpur, 2 February **2004** (***Poster Presentation***)

2. Hydrothermal synthesis of metal substituted mesoporous M-MCM-41: Comparative study over Ti-MCM-41, V-MCM-41 and Cr-MCM-41

   S. S. Bhoware, **S. Shylesh**, K. R. Kamble and A. P. Singh

   17th National Symposium in Catalysis, Central Salt and Marine Chemical Research Institute, Bhavnagar, India, January **2005** (***Oral presentation***)